CESIUM CARBONATE CATALYZED EFFICIENT SYNTHESIS OF NAPHTHOCHROMENES UNDER MICROWAVE IRRADIATION

B. D. Rupnar,[a] V. P. Pagore,[a] S. U. Tekale,[b] S. U. Deshmukh,[a] S. B. Ubale,[a] Sunita B. Shinde [c] and R. P. Pawar*[a]

Cesium carbonate catalyzed three-component condensation reaction of an aldehyde, malononitrile and α-naphthol or β-naphthol proceeded rapidly in ethanol to afford corresponding naphthochromenes in high yield under microwave irradiation.

*Corresponding Authours
    Fax: +91 0240 2334430
    Tel.: +91 240 2334577
    E-Mail: rppawar@yahoo.com
[a]   Department of Chemistry, Deogiri College, Station Road, Aurangabad (MS) India 431 005.
[b]   Department of Chemistry, Muktanand College Gangapur, Aurangabad (MS) India.
[c]   Department of Chemistry, MGM College of Engineering, Kamothe, New Mumbai (MS) India.

Introduction

Organic transformations involving benign reaction media are of considerable interest in synthesis; especially multicomponent condensation reactions (MCR) in which two or more steps are completed without isolation of any intermediate.[1] Microwaves have been emerged as extensively useful non-conventional energy source for performing organic synthesis. Microwave assisted reactions have received great importance due to their simplicity in operation, short reaction time, enhanced rate of reaction and better yields with high purity as compared to conventional heating[2] reactions.

Chromene is an important class of heterocyclic compounds as they are the main constituents of many natural products. Its derivatives are widely used as cosmetics, pigments[3] and potential biodegradable agrochemicals.[4] Fused chromenes are biologically active compounds showing a wide range of activities such as antimicrobial,[5] antiviral,[6] mutagenicitical,[7] sex pheromonal,[8] antitumoral[9] and CNS activities.[10] Compound EPC2407 (Fig-1) is currently inphase I/II clinical trials as vascular targeting anticancer agentand apoptosis inducer for the treatment of advanced solid tumors.[11] Some other chromene derivatives like etoposide, teniposide, andetopophos are currently in clinical use for the treatment of various malignancies.[12] Thus, the synthesis of 4H-chromene derivatives has recently attracted great interest. Various methods have been reported for synthesizing 4H-chromenes derivatives.

Chromenes are generally prepared by multicomponent condensation of aromatic aldehyde, active methylene derivatives and activated phenol or naphthol in presence of various base using acetonitrile or ethanol as a solvent under conventional heating.[13-16] Recently, we synthesized 4H-chromene derivatives by condensing barbituric acid, aldehyde and malononitrile using yttrium oxide in aqueous methanol as a catalyst system efficiently.[17]
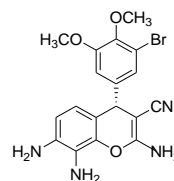

Figure 1. Structure of EPC2407

Cesium carbonate has been widely used as a strong base in organic synthesis due to its ease of handling, low hygroscopicity[18], and high solubility in organic solvents as compared to alkali metal hydroxides. In recent years, cesium carbonate has found extensive applications as an excellent base in variety of synthetic transformations[19-28] and has received even industrial acceptance. Its basic strength is shown by the fact that it is the base of choice for reactions that are too sensitive towards strong bases or reactions that require a "Balanced base," stronger than other carbonates and weaker than hydroxides and alkoxides[29]. It is compatible with a variety of functional groups.

Experimental

Materials and instruments

All starting materials and chemical reagents were purchased from SD Fine Chemical Company and used without further purification. Melting points were determined in open capillaries using Electrothermal Mk3 apparatus. Infrared (IR) spectra in KBr pellets were recorded using a Perkin-Elmer FT-IR spectrometer. ^{1}H NMR spectra were recorded on an 400 MHz FT-NMR spectrometer in CDCl₃ or DMSO-d6 as a solvent and chemical shift values were recorded in units   δ (ppm) relative to tetramethylsilane (Me₄Si) as an internal standard.

Table 1. Three-component condensation reaction

Entry	R	Naphthol	M.p., ^{0}C	Lit. M.p., ^{0}C	Time, min.	Yield, %
a	P-Cl	α - naphthol	234-237	231-232	2	92
b	P-NO$_2$	α - naphthol	242-245	239-241	1.5	94
c	m-NO$_2$	α - naphthol	209-211	210-212	2.5	93
d	H	α - naphthol	207-210	211-212	2.5	89
e	p-Br	α - naphthol	237-240	241-243	3	91
f	p-F	α - naphthol	225-228	230-232	2.5	92
g	p-OCH$_3$	α - naphthol	184-186	182-183	4	90
h	p-OH	α - naphthol	238-240	241-245	4.5	89
i	m-OH	α - naphthol	245-247	250-253	4.5	84
j	p-Cl	β - naphthol	210-211	206-208	4	90
k	p-NO$_2$	β - naphthol	182-184	185-186	4	91
l	p-Br	β - naphthol	244-246	242-244	4.5	88
m	p-F	β - naphthol	236-239	233-235	5	89
n	H	β - naphthol	281-283	280	4.5	90

The microwave irradiation was carried out in a scientific microwave oven (CATA-4R-Model No. QW-99, India makes), 2450 MHz Frequency, with power output of 140-700 W.

General procedure for the synthesis of naphthochromenes

A mixture of aromatic aldehyde (1 mmol), malononitrile (1 mmol), α-naphthol or β-naphthol (1 mmol) and cesium carbonate (10 mol %) in ethanol (5 mL) was mixed properly and irradiated under microwave oven at the power of 140W for a period 2-5 min (Table 1). The progress of reaction was monitored by thin layer chromatography (ethyl acetate: hexane 4:1). After completion of reaction (2-5 min), the reaction mass was cooled at room temperature and poured over cold water. The obtained solid was filtered, washed with water, and crude solid was recrystallized from hot ethanol to afford an analytically pure compound 4a–n. The products were confirmed by comparisons with authentic samples, IR, ^{1}H NMR and melting points.
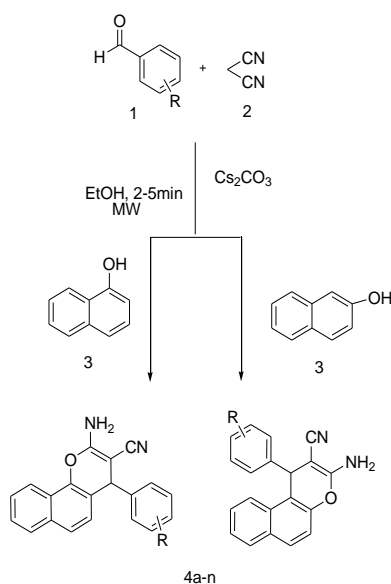
Scheme 1.

Result and discussion

In this article, we described a simple and high yielding protocol for the synthesis of naphthochromenes involving three-component one-pot condensation of aldehyde1(1 mmol), malononitrile 2 (1 mmol) and α-naphthol or β-naphthol 3 (1 mmol) using cesium carbonate in ethanol (5 ml) under microwave condition (scheme 1). In order to determine the mole % of catalyst, we have carried out model reaction of p-NO$_2$ benzaldehyde, malononitrile and α-naphthol with different amount of catalyst and found the optimum catalyst loading of cesium carbonate to be 10 mol %. By decreasing the amount of catalyst to 5 mol % the yield of product 4a was reduced; however, by increasing the amount of catalyst from 10 to 15 mol %, no appreciable change in the yield of product was observed.

Next, in order to investigate the substrate scope of the reaction, a variety of substituted benzaldehydes were used employing the present optimized reaction conditions. The yield and reaction were found to be fairly equal and good (Table 1). Spectral data of some selected compounds shown below

4H-Naphtho[1,2-b]pyran-3-carbonitrile-2-amino-4-(4-chloro-phenyl) (Table 1, entry a):

IR (KBr): 3437, 3348, 3242, 2961, 2862, 2220, 1644, 1593, 1520, 1460, 1390, 1275, 1185, 1035, 881, 850, 764 cm^{-1}; ^{1}H NMR (DMSO-d$_6$, 400 MHz): 4.8 (1H, s) C-H, 6.89 (2H, s) N-H, 7.0 (1H,d) Ar-H, 7.2 (2H, d) Ar-H, 7.35 (2H, d) Ar-H, 7.50 (3H, m) Ar-H, 7.84 (1H, d) Ar-H, 8.1 (1H, d) Ar-H.

4H-Naphtho[1,2-b]pyran-3-carbonitrile-2-amino-4-(4-fluoro-phenyl) (Table 1, entry f):

IR (KBr): 3440, 3350, 3244, 2960, 2858, 2222, 1646, 1591, 1524, 1461, 1391, 1280, 1181, 1033, 883, 847, 763 cm^{-1}; ^{1}H NMR (DMSO-d$_6$, 400 MHz): 4.8 (1H, s) C-H, 6.9 (2H, s) N-H, 7.0 (1H,d) Ar-H, 7.1 (2H, d) Ar-H, 7.4 (2H, d) Ar-H, 7.5 (3H, m) Ar-H, 7.8 (1H, d) Ar-H, 8.2 (1H, d) Ar-H.

Conclusion

In conclusion, naphthochromenes were successfully synthesized by using cesium carbonate catalyst under microwave radiation from aldehydes, malononitrile and a naphthol. The promising points for the present methodology are clean reaction procedure, short reaction times, simplicity in operation and catalyst with high catalytic activity.

Acknowledgment

References

[1] Li, C. J., *Chem. Rev.*, **2005**, *105*, 3095.

[2] Carpenter, R. D., Lam, K. S., Mark, J. K., *J. Org. Chem.*, **2007**, *72*, 284.

[3] Ellis, G. P., Weissberger, A., Taylor, E. C., *John Wiley: New York, Chapter II.*, **1977**, 11-139.

[4] Hafez, E. A. A., Elnagdi, M. H., Elagemey, A. G. A., El- Taweel, F. M. A. A., *Heterocycles*, **1987**, *26*, 903.

[5] Khafagy, M. M., Abd El-Wahab, A. H. F., Eid, F. A., El- Agrody, A. M., *Farmaco.*, **2002**, *57*, 715.

[6] Martinez-Grau, A., Marco, J. L., *Bioorg. Med. Chem. Lett.*, **1997**, *7*, 3165.

[7] Hiramoto, K., Nasuhara, A., Michikoshi, K., Kato, T., Kikugawa, K., *Mutation Res.*, **1997**, *395*, 47.

[8] Bianchi, G., Tava, A., *Agric. Biol. Chem.*, **1987**, *51*, 2001.

[9] Mohr, S. J., Chirigos, M. A., Fuhrman, F. S., Pryor, J. W., *Cancer Res.*, **1975**, *35,* 3750.

[10] Eiden, F., Denk, F., *Arch. Pharm. Weinheim Ger. (Arch. Pharm.).,* **1991**, *324*, 353.

[11] http://www.epicept.com/Products_/Product_Pipeline/Cancer/EPC 2407/ @2012 EpiCept Corporation.

[12] Meresse, P., Dechaux, E., Monneret, C., *Curr. Med. Chem.,* **2004**, *11*, 2443.

[13] Abdel-Latif, F. F., *Indian J. Chem.*, **1990**, *29B,* 664.

[14] Elagamy, A. G. A., El-Taweel, F. M. A., *Indian J. Chem.,* **1990**, *29B,* 885.

[15] Elagamy, A. G. A., El-Taweel, F. M. A., Khodeir, F. M. N., Elnagdi, M. H., *Bull. Chem. Soc. Jpn.,* **1993 ,** *66* , 464.

[16] Bioxham, J., Dell, C. B., Smith, C. W., *Heterocycles,* **1994**, *38,* 399.

[17] Bhagat, D. S., Katariya, M. V., Patil, C. S., Deshmukh, S. U., Shisodia, S. U., Pandule, S. S., Pawar, R. P., *Eur. Chem. Bull.,* **2015**, *4(10)*, 450

[18] Xie, W.. Zhao, M., Cui, C., *Organometallics.*, **2013**, *32(24)*, 7440.

[19] Cuny, G. D., *Tetrahedron Lett.*, **2003**, *44*, 8149.

[20] Parrish, J. P., Dueno, E. E., Kim, S., Jung, K. W., *Synth.Commun.,* **2000**, *30(15)*, 2687.

[21] Dueno, E. E., Chu, F., Kim, S., Jung, K. W., *Tetrahedron Lett.,* **1999**, *40*, 1843.

[22] Salvatore, R. N., Nagle, A. S., Jung, K. W., *J. Org. Chem.*, **2002**, *67*, 674.

[23] Flessner, T., Doye, S., *J. Prakt. Chem.*, **1999**, *341*, 186**.**

[24] Littke, A. F., Fu, G. C., *J. Org. Chem.,* **1999**, *64*, 10.

[25] Grasa, G. A., Singh, R., Stevens, E. D., Nolan, S. P., *J. Organomet. Chem.,* **2003**, *687*, 269.

[26] Littke, A. F., Fu, G. C., *Angew. Chem. Int. Ed.,* **1998**, *37*, 3387.

[27] Batey, R. A., Shen, M., Lough, J. *Org. Lett.,* **2002**, *4*,1411.

[28] Eckhardt, M., Fu, G. C., *J. Am. Chem. Soc.,* **2003**, *125*, 13642.

[29] Ulaganathan, S., Chandran, R., Ramakrishnan, U., *Curr. Chem. Lett.,* 2012, 1, 123.

A POLYMER-ORGANOCLAY NANOCOMPOSITE FOR SIMULTANEOUS REMOVAL OF CHROMIUM(VI) AND ORGANIC DYES

Adel A. El-Zahhar[a,b]

Synthesis of polyacrylonitrile (PAN)-organoclay nanocomposite was studied through grafting of PAN onto organophilic kaolinite. The organophilic kaolinite was prepared by treatment of kaolinite with different ratios of hexadecylethyldimethylammonium (HDEDMA) to kaolinite. The chemical grafting polymerization of acrylonitrile (AN) onto organophilic kaolinite was performed. The synthesized polymer-organoclay nanocomposite was studied for simultaneous adsorption of Cr(VI) and methylene blue dye (MB) from aqueous solutions. The results of Cr(VI) or the dye adsorption revealed that the adsorbed amounts increased with increasing HDETMA concentration. The removal percentage of Cr(VI) reached more than 98 % if individually studied, while 96 % was obtained when competing with dye. Also the adsorption of Cr(VI) was potentially influenced by its concentration in solution. The isothermal studies were performed using Langmuir and Freundlich models. The maximum calculated adsorption capacity was found to be 127 mg g^{-1} and 68 mg g^{-1} for Cr(VI) and methylene blue, respectively for individual adsorption, while in simultaneous adsorption their adsorption capacity was not affected by the other.

Corresponding Authors
    Tel: +966583186281
    E-Mail: adelelzahhar@yahoo.com
[a]   Chemistry Department, College of Science, KKU, P.O. 9004, Abha 61321, KSA
[b]   Nucl. Chem. Dept., Atomic Energy Authority, P.C.13759,Cairo,Egypt

Introduction

Clays are used in many scientific applications and technological fields, due to their natural availability and the capacity for the chemical and physical modifications. Clays are characterized by their high platelet aspect ratio, swelling ability and some features that make clays very desirable in the industrial and scientific applications.[1] Clays contain inorganic cations in their basal spacing, which make them hydrophilic in nature. This nature renders clays ineffective adsorbents for hydrophobic and aliphatic compounds.[2] The inorganic ions present in the clay can be effectively replaced by organic cationic surfactant molecules through cation-exchange reactions. This replacement leads to expansion of the interlayer spacing which leads to an increase in the basal spacing. As a result, the swelling percentage and the potential thermodynamical interactions increase significantly with increasing basal spacing. The unique properties of unmodified and modified clay, renders these materials finding industrial applications, additives, as thickeners in coating products, glues, plastisols, drilling fluids[3] and for wastewater treatment,[4] and other technological applications.[5-8] In recent years, clays have find use in the field of materials science such as solid phase polymeric nanocomposites.[9] Polymer clay composites have been accepted major importance due to their major criteria for utilization in some advanced technology. The high surface area of polymer clay composites (reached 750-800 m^2 g^{-1}), due to exfoliation degree of polymer composite enhance the physicochemical properties of the produced composites.[10] The low coast and characteristics of unmodified and modified clay minerals also lead to unique superior applications for the produced composite.[11] Clay minerals of layered structure, e.g. montmorillonite, bentonite and etc. have exchangeable hydrated cations (Na$^+$ and Ca^{2+}), these ions are responsible for the advanced adsorption properties of these materials.[12] In this connection, the use of organically modified clays for polymer clays nanocomposite preparation has started in the early 1990's.[13,14] The modification of clay includes the exchange of amine salts with the exchangeable cations in the clay with varied amine structure and concentration.[15] Different research papers were published dealing with organically modified clay polymer composites for different applications.[16,17] The organic modification is essential for the compatibility of polymer with clay, which leads to a decrease in the surface energy and increase the surface compatibility.

Experimental

Materials

All chemicals were used as received without purification. Kaolinite was purchased from Sigma-Aldrich, acrylonitrile (AN) was obtained from Merck Co., hexadecylethyldimethyl ammonium bromide (HDEDMA) was obtained from Aldrich Chemical Company Inc. and potassium peroxysulphate was provided by Merck. All other chemicals were of reagent grade and were used without further purification.

Preparation of polymer organo-clay composite

Organically modified kaolinite was prepared as the following process: appropriate weight of kaolinite clay was pre-dried, pre-wetted with distilled water, then mixed with NaCl and HDEDMA solutions at different mixing ratios to

yield different concentrations of amines, from 0 % to 100 % of the cation exchange capacity The mixtures were agitated for 24 h, centrifuged washed, dried at 80 ºC, activated for 1 h at 105 °C in oven, and mechanically ground.

The polymer clay composite was prepared as: in a three-neck round bottomed flask equipped with a magnetic stirrer and a reflux condenser, HDEDMA–kaolinite, acrylonitrile, and initiator potassium peroxysulphate were placed in DMF. The flask was purged by nitrogen for 20 min, heated and magnetically stirred at 90–95 °C for 8 h. Then the reaction mixture was transferred into another flask and extracted with CH_2Cl_2 for 72 h. The produced polyacrylonitrile – organokaolinite (PAN-OK) composite was then dried at 40 °C for 24 h.

Sorption studies of Cr(VI) and MB using PAN-OK

The adsorption of Cr(VI) was studied using PAN-OK through mixing 0.05 g of the dry composite with 25 ml of chromium solution of different concentration with agitation for the appropriate time. The concentration of Cr(VI) was measured before and after equilibrium using a UV-spectrometer and 1,5-diphenylcarbazide at λ_{max} = 540 nm.

The adsorption of methylene blue (MB) dye was performed by immersing the 0.05 g of composite adsorbent into 25 mL of dye solution with varied concentration. All adsorption experiments were examined through a batch method on a stirrer with a constant speed at 120 rpm. The amount of adsorbed MB was evaluated using a UV spectrometer at λ_{max} = 590 nm.

The amount adsorbed Cr(VI) or MB at equilibrium (q_t, mg g^{-1}) was calculated using following as:

$$q_t = \frac{V(C_0 - C_t)}{m} \qquad (1)$$

where,

C_0 is the initial concentration (mg L^{-1}),

C_t is the equilibrium concentration in the solution at time t, (mg L^{-1}),

V is the volume of solution used (L), and

m is the weight of composite (g).

Results and Discussions

Characterization of PAN-OK composite material:

The IR spectrum reveled that, absorption bands appeared at 2980 cm^{-1} and 1450 cm^{-1} that can be attributed to the stretching of the aliphatic C–H bonds, 3632 cm^{-1} for OH groups, 2927 cm^{-1} and 2855 cm^{-1} for the amine group of surfactant, 2246 cm^{-1} for C≡N groups of the polymer moiety, the band at 1040 cm^{-1} for Si–O of clay moiety and the strong band at 1000–1160 cm^{-1} is likely due to siloxane (Si–O–Si) bond. X-ray diffraction patterns of PAN grafted organoclay showed a strong peak at 2θ = 3.43° and 5.14° indicating that the interlayer *d*-spacing of the clay was slightly decreased due to grafting of polymer onto the clay surface.

Sorption of MB and Cr(VI) on PAN-OK composite:

The adsorption of both MB and Cr(VI) was studied individually and in presence of each other using the prepared PAN-OK composite.

Effect of pH on the adsorption of MB and Cr(VI) using PAN-OK composite:

The removal of Cr(VI) and MB from aqueous solutions was studied individually using PAN-OK at different pH and the results are given in Figure 1. The results show that the amount adsorbed of Cr(VI) increases greatly with increasing pH and reached its maximum value (23mg/g) at pH 6-7. At pH 7 the more stable species of Cr(VI) is CrO_4^{2-}, while pH lower than 7 a larger dichromate ($Cr_2O_7^{2-}$) ion is formed, the smaller CrO_4^{2-} is more easy to be adsorbed at pH 7 than $Cr_2O_7^{2-}$.[18] At pH higher than 7 the hydrolyzed species of Cr(VI) are formed and the adsorption of Cr(VI) is decreased.
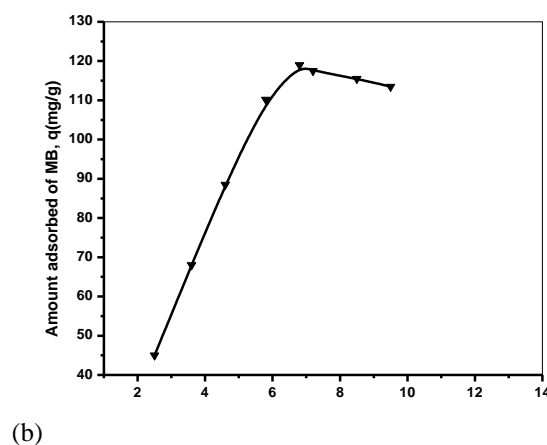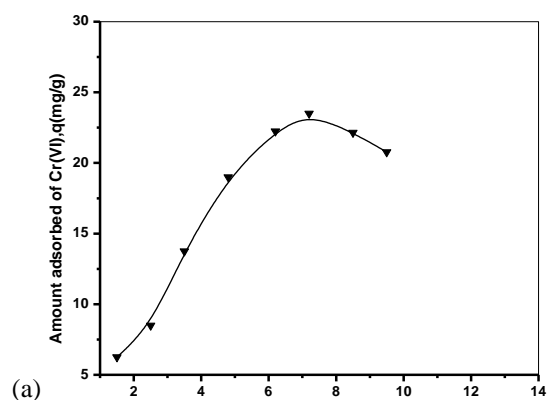

(a)

(b)

Figure 1. Effect of pH on the adsorption of Cr(VI) and MB on PAN-OK (0.05 g of composite, 25 mL of solution, 1 h, [Cr]=50 (a) or 250 (b) mg L^{-1}, respectively.

Concerning the effect of pH on the adsorption of MB using PAN-OK, the amount adsorbed of MB on the PAN-OK increased with increasing pH within the range 2-7. At pH higher than 7 the amount adsorbed of MB on PAN-OK is decreased. This finding could be explained on the bases of protonation of adsorbent active sites at low pH. The dependence of adsorption on pH reflects the participation of ion exchange in the adsorption process.[18]

Effect of HDEDMA concentration on adsorption of MB and Cr(VI)

The adsorption of both MB and Cr(VI) individually on PAN-OK was studied as a function of HDEDMA concentration adsorbed onto kaolinite. The results in Figure 2 and Figure 3 show that the adsorbed amount of Cr(VI) and MB increased with increasing the concentration of HDEDMA in the clay. This observation could be due to increasing the surface active sites on the composite adsorbent with increasing HDEDMA concentration.
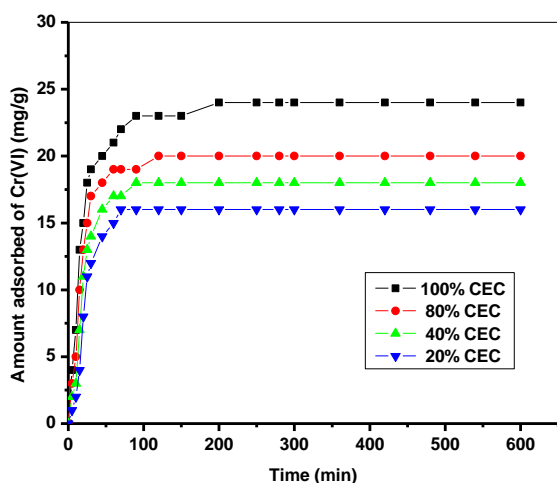

Figure 2. Effect of HEDMA concentration on the adsorption of Cr(VI) onto PAN-OK composite; wt-0.05 g, vol-25 mL, pH-6.8 [Cr]-50 mg L^{-1}
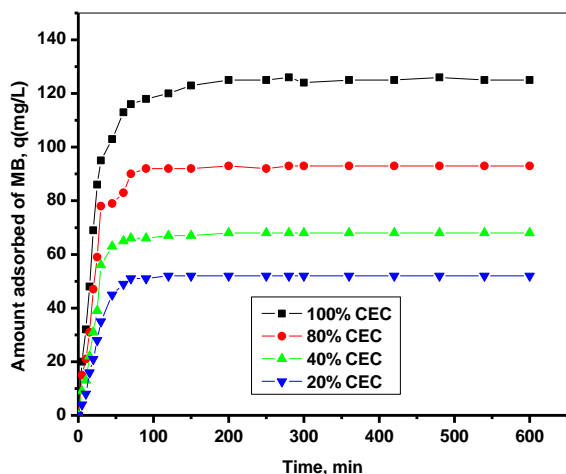

Figure 3. Effect of HEDMA concentration on the adsorption of MB onto PAN-organoclay composite; wt-0.05 g, vol-25 mL, pH-6.8 [MB]-250 mg L^{-1}

Effect of initial concentration of Cr(VI) or MB

The equilibrium sorption capacity for both Cr(VI) and MB individually was studied as a function of their initial concentration in the aqueous solution with measuring their equilibrium concentration. The results in Figure 4 and Figure 5 show the sorption isotherm curves for adsorption of both Cr(VI) and MB, respectively. The shapes of these figures show slight deviation from linearity, with increasing the curvature at higher concentrations. This observation indicates ''non-cooperative sorption''. This type of sorption occurs when the sorbate–sorbent interaction is more powerful than sorbate–sorbate interaction. The Cr(VI) or MB molecules have high affinity to interact with the sorbent surface groups than to each other (forming cluster).
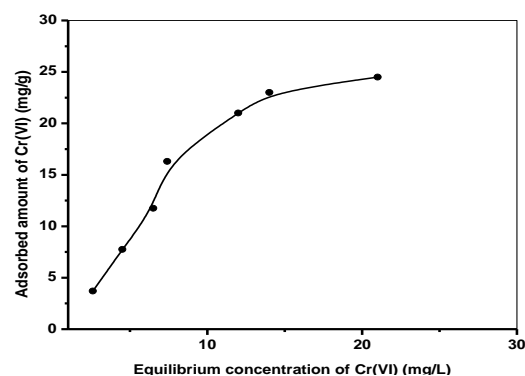

Figure 4. Adsorption isotherm of Cr(VI) onto PAN-organoclay composite; wt, 0.05 g, vol. 25 pH 6.8, time 60 min, temp. 25 °C.
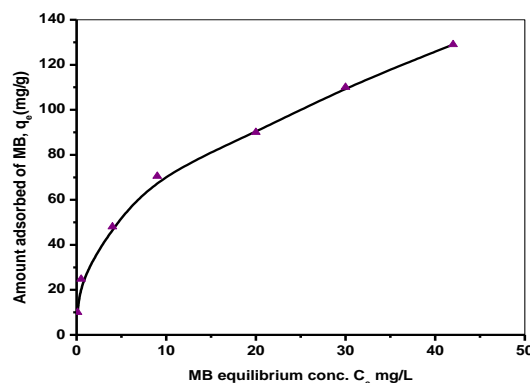

Figure 5. Adsorption isotherms of MB dye onto PAN-organoclay composite; wt, 0.05 g, vol. 25 pH 6.8, time 60 min, temp. 25 °C

Adsorption Isotherms

The results in Figures 4 and 5 show the measured adsorption capacity with the equilibrium concentration of Cr(VI) and MB on PAN-OK. These results reflect that the adsorption capacity of MB is significantly higher than that of Cr(VI), indicating the potential removal of MB using PAN-OK and the higher affinity of MB to PAN-OK than Cr(VI). This finding could be explained on the basis of the strong interaction of MB with the surface groups as it usually coordinated to the surface hydroxyl groups.[19,20]

Langmuir and Freundlich models were used to fit the adsorption data to correlate the adsorption models and the experimental adsorption equilibrium data. In this concern the experimental data for adsorption of both Cr(VI) and MB on PAN-OK were fitted to Langmuir and Freundlich isotherms equations. Langmuir isotherm model could be applied to homogeneous adsorption system, while Freundlich isotherm model could describe the heterogeneous systems, which is an empirical equation and is not limited to the creation of the monolayer.

Langmuir isotherm model equation is represented as:

$$\frac{C_e}{Q_e} = \frac{1}{Q_{max} K_L} + \frac{C_e}{Q_{max}} \qquad (2)$$

where

Q_e is the equilibrium concentration of Cr(VI) or MB on the adsorbent (mg g^{-1}),
C_e is the equilibrium concentration of Cr(VI) or MB in solution (mg L^{-1}),
Q_{max} is the maximum monolayer adsorption capacity of adsorbent material (mg g^{-1}),
and K_L is the Langmuir adsorption constant (L mg^{-1}).

The value of Langmuir constant K_L is an indication to the affinity between adsorbate and adsorbent, while the reciprocal of the K_L value describe the concentration when the adsorption capacity reached to half its maximum value. When C_e/Q_e plotted vs. C_e it gives a straight line with slope equal to $1/Q_{max}$ and intercept equal to $1/Q_{max}K_L$.[21] The values of Langmuir constants were calculated from the plot of C_e/Q_e vs C_e, and are presented in Table 1.

Freundlich isotherm model equation is represented as:

$$Q_e = K_F C_e^n \qquad (3)$$

where

K_F (L g^{-1}) is the Freundlich constants, indicating the adsorption capacity and
$1/n$ is a constant indicating the adsorption intensity.[22]

When the value of $1/n$ is smaller than 1, it reflects a favorable adsorption and high sorption capacity. While if $1/n$ is higher than 1, it reflects unfavorable adsorption with lower adsorption capacity. The values of Freundlich constants were obtained from the plot of ln Q_e vs ln C_e, where K_F was calculated from the intercept and $1/n$ was calculated from the slope of the linear plot. The calculated values were given in Table 1.

The values listed in Table 1 reflect that the correlation coefficients with respect to Langmuir isotherm model is higher than that with respect to Freundlich for Cr(VI)-PAN-OK and MB-PAN-OK systems. Also the K_L values reflects the higher affinity Cr(VI). The values of Q_{max} are comparable with the experimental values. The values of $1/n$ reflect a favourable adsorption with respect to Cr(VI) and MB with PAN-OK.

Table 1. Langmuir and Freundlich isotherm constants for the adsorption system of Cr(VI)-PAN-OK and MB-PAN-OK

	Langmuir			**Freundlich**		
	Q_{max}, mg g^{-1}	K_L, L mg^{-1}	R^2	$1/n$	K_F	R^2
Cr(VI)	33.56	0.1368	0.993	0.930	1.90	0.960
MB	133.15	0.196	0.977	0.408	28.10	0.996

Effect of temperature

The adsorption of Cr(VI) and MB on the PAN-OK was studied at different temperature (25-55 °C) using the optimized conditions. The obtained results revealed that the amount adsorbed of Cr(VI) on PAN-OK increases with increasing temperature reflecting enhanced adsorption of Cr(VI) with temperature.
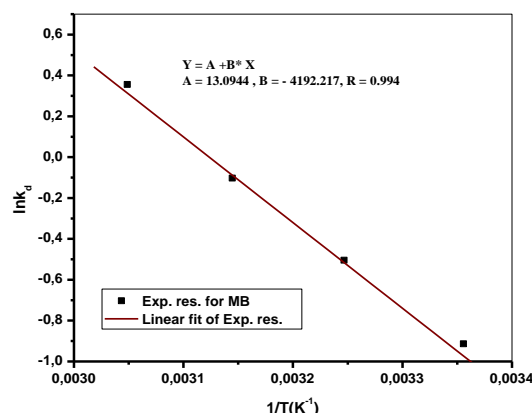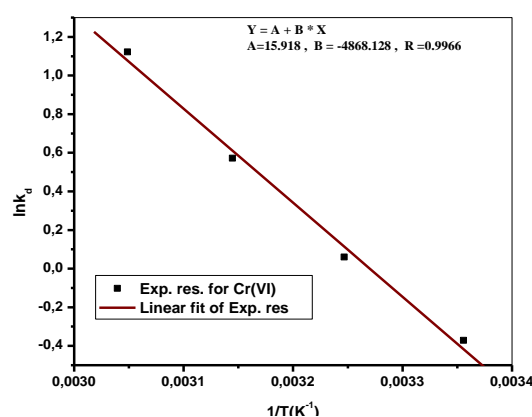

Figure 6. Van't Hoff plots for adsorption of Cr(VI) and MB on PAN-OK

Table 2. Thermodynamic parameters for the adsorption systems of Cr(VI)-PAN-OK and MB-PAN-OK

Adsorption system	ΔH kJ mol^{-1}	ΔS J mol^{-1} K^{-1}	ΔG kJ mol^{-1}	R^2
Cr(VI)-PAN-OK	40.47	132.34	1.033	0.996
MB-PAN-OK	34.85	108.86	2.41	0.994

The similar results were observed with respect to MB, reflecting better sorption at higher temperature. This observation could be due to creation of some new active sites on the sorbent surface. The thermodynamic parameters for adsorption of Cr(VI) and MB on PAN-OK were calculated by applying van't Hoff equation (4) and plotting of $\ln K_d$ vs. $1/T$ (Figure 6).

$$\ln K_d = \frac{\Delta S}{R} \frac{\Delta H}{RT} \qquad (4)$$

$$\Delta G = \Delta H - T\Delta S \qquad (5)$$

Competitive adsorption

The sorption results in Figures 7 and 8 show the simultaneous sorption of Cr(VI) and MB onto PAN-organo-kaolinite. It is clear that the sorption of Cr(VI) is not affected by the presence of MB, and also the sorption of MB not affected by the presence of Cr(VI).
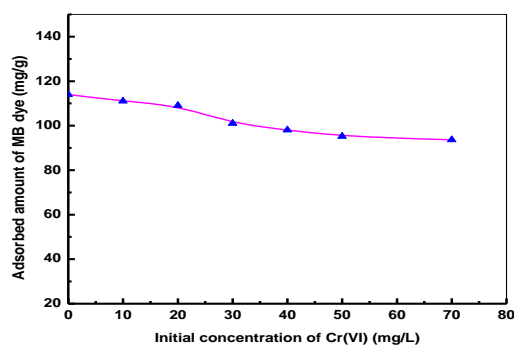

Figure 7. Competitive adsorption of MB in presence of different concentrations of Cr(VI); wt-0.05 g, vol-25 mL, pH-6.8, time 60 min, temp.-25 °C, [MB]-250 mg L^{-1}
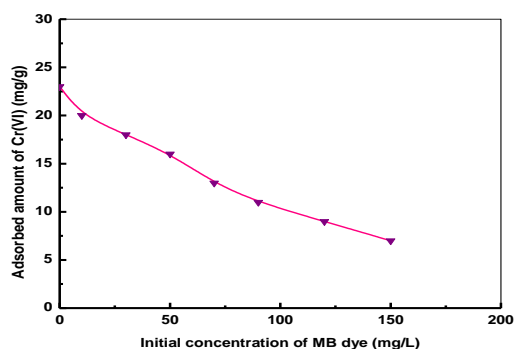

Figure 8. Competitive adsorption of Cr(VI) in presence of different concentrations of MB; wt-0.05 g, vol-25 mL, pH-6.8, time 60 min, temp.-25 °C, [Cr]-50 mg L^{-1}

References

[1] Xi, Y., Frost, R. L., He, H., Kloprogge,T. and Bostrom, T., *Langmuir*, **2005,** *21,* 8675-8680.

[2] Giannelis, E. P., *Adv. Mater.*, **1996,** *8*, 29-35.

[3] Lan, T., Kaviratna,P.D. and Pinnavaia,T.J., *Chem. Mater.*, **1995,** *7*, 2144-2150.

[4] Beall, G.W., *Applied Clay Sci.*,**2003,** *24*, 11-20.

[5] Zadaka, D., Mishael, Y. G., Polubesova, T., Serban, C. and Nir, S., *Applied Clay Sci.*, **2007,** *36*, 174-181.

[6] Lagaly, G., *Solid State Ion.*, **1986,** *22*, 43-51.

[7] Konta, J., *Appl. Clay Sci.*, **1995,** *10*, 275-335.

[8] Murray, H. H., *Appl. Clay Sci.*, **2000,** *17*, 207-221.

[9] Ruiz-Hitzky, E. and Van, A. M., *Clay Mineral and Organoclay-Polymer Nanocomposites*. In: Handbook of Clay Science, F. Bergaya, B. K. G. Theng and G. Lagaly (Eds.) (**2006**), Vol. *1*, Elsevier, Amsterdam, ISBN: 0080441831, pp: 583-621.

[10] Pavlidou, S. and Papaspyrides, C. D., *Prog. Polym. Sci.*, **2008,** *32*, 1119-1198.

[11] Phang, I. Y., Liu, T., Mohamed, A., Pramoda, K. P., Chen, L., Shen, L., Chow, S. Y., He, C., Lu, X. and Hu, X., *Polym. Int.*, **2005,** *54*, 456-464.

[12] Olad, A., *Polymer/Clay Nanocomposites, Advances in Diverse Industrial Applications of Nanocomposites*, Dr. Boreddy Reddy (Ed.), (2011) InTech, ISBN: 978-953-307-202-9.

[13] Kojima, Y., Usuki, A., Kawasumi, M., Okada, A., Kurauchi, T. And Kamigaito, O., *J. Polymer Sci.,Part A: Polymer Chem.*, **1993,** *31*, 1755-1758.

[14] Alexandre, M. and Dubois, P., *Mater. Sci. Eng.*, **2000,** *28*, 1-63.

[15] Fornes, T. D., Yoon, P.J., Hunter, D.L., Keskkula, H. and Paul, D.R., *Polymer*, **2002,***43*, 5915-5933.

[16] Stretz, H. A., Paul, D. R., Li, R., Keskkula, H. and Cassidy, P. E., *Polymer*, **2005,** *46*, 2621-2637.

[17] Shah, R. K., Kim, D. H. and Paul, D. R., Polymer, **2007,** 48, 1047-1057.

[18] Swarnakar, V., Agrawal, N. and Tomar, R., *Int. J. Sci. Eng. Res.,* **2011,** *2*(5), 1-9.

[19] Wang, C. C., Juang, L. C., Hsu, T. C., Lee, C. K., Lee, J. F. and Huang, F. C., *J. Colloid Interf. Sci.*, **2004,** *273*(1), 80-86.

[20] Li, D., Zhao, W., Sun, X., Zhang, J., Anpo, M. and Zhao, J., *Dyes Pigments*, **2006,** *68*(1), 33-37.

[21] Kaewprasit, C., Hequet, E., Abidi, N. and Gourlot, J. P., *J. Cotton. Sci.*, **1998,** *2*(4), 164-173.

[22] Özcan, A. S. and Özcan, A., *J. Colloid Interf. Sci.*, **2004,** *276*(1), 39-46.

DETERMINATION OF BIOACTIVE COMPOUND CONTENT AND ANTIOXIDANT ACTIVITY OF THE LEBANESE *ERYNGIUM CRETICUM* L.

Saeed Zeidan,[a] Akram Hijazi,[a,b]* Hassan Rammal,[a,b,c] Ali Al Bazzal,[a,c] Hussein Annan,[a] and Abd Al- Ameer N. Al-Rekaby[d]

Polyphenolic compounds are bioactive substances widely distributed in the plant kingdom. They act as natural antioxidants and their presence contributes to the color, flavor, and aroma of food. Therefore, they are considered dietary antioxidants with interesting benefits to health. In this article the extraction of total phenolics, total flavonoids and antioxidants activity from *Eryngium creticum* was determined after obtaining the plant extracts by conventional and non-conventional extraction techniques. Also this study aims to determine the bioactive constituents present in *E. creticum* extracts by using GC-MS method. The results obtained show that microwave assisted extraction is the best technique used for the extraction of phenolic compounds and flavonoids from *E. creticum* giving a yield of 34.46 µg mL^{-1} and 21.05 µg mL^{-1} respectively. However, the antioxidants activity, evaluated by the DPPH assay was low in all the extraction techniques. Also the results showed the presence of 9 fatty acid derivatives, most of them have therapeutic effects on human health. These results explain the use of *E. creticum* in traditional medicine to treat various diseases.

* Corresponding Authors
    Tel: 0096171905768
    E-Mail: hijazi_akram@hotmail.com
[a] Doctoral School of Science and Technology, Research Platform for Environmental Science (PRASE), Lebanese University, Lebanon
[b] Laboratory of Materials and Phytochemistry, Lebanese University, Faculty of sciences.
[c   xFaculty of Agriculture and Veterinary Science, Lebanese University, Lebanon
[d] Al Mustansiriya University, College of Science, Department of Biology, Irak

Introduction

Oxidative stress is involved in the pathology of cancer, arteriosclerosis, malaria and rheumatoid arthritis, and could play a role in neurodegenerative diseases and aging processes. Antioxidants perform multiple functions, including the defense against oxidative damage and cell signaling. One major function of antioxidants in the biological system is to prevent the cellular components' damage by the reactive oxygen species.[1]

Bioactive compounds in plants are produced as secondary metabolites. These compounds are called so because they are related to substances that exert an effect on living tissues, and are dedicated to help the plants to increase their overall ability to survive and overcome local challenges 2. The bioactive compounds are ubiquitous in nature. They have been identified and isolated from diverse sources within the living organisms. For decades, organic extracts from various origins have been widely used in the traditional medicine, as well as in the food industry, and are considered to be generally safe. [2]

Eryngium creticum, a perennial plant belonging to the family Umbellifereae, is considered a medicinal plant due to its antioxidant properties.[3] The latter is characterized by the presence of a wide variety of phenolic acids and flavonoids.

In addition to its ability to act as an efficient free radical scavengers, its natural origin is an advantage to all customers, unlike other synthetic antioxidants whose use is being restricted due to its carcinogenicity.[5] *E. creticum* has also showed an antioxidant property through inhibiting lipid peroxidase in the liver of rat. This plant was traditionally used as a diuretic (emmenagogue). Roots and seeds that are immersed in water, are drunk to treat kidney stones, infections, skin diseases, and tumors. It is also an antidote, in which it is used for treating snake bites. Moreover, *E. creticum* has an antifungal activity, as well as a hypoglycemic role in which the deduction from the aerial part of this plant showed a significant reduction in the concentration of blood sugar. Also, this plant has shown an anti-inflammatory, as well as an anti-microbial, activity and was also used for the treatment of poisoning, anemia and infertility.[4,5] Finally, its was recently demonstrated that Lebanese *E. creticum* has an antitumor activity on cervical cancer (HeLa) cell line. [6,7]

This study aims to determine the following: the total phenolic content (TPC), the total flavonoid content (TFC), the antioxidant activity, the esterified fatty acids, the humidity, the ach content, and the alkaloid content of the Lebanese *Eryngium creticum*. In addition, it aims to establish a comparison between the conventional and non-conventional extraction techniques for the total amount of phenols, flavonoids, and antioxidant activity obtained.

Materials and Methods

Plant collection and preparation of the powder

Fresh plants were gathered from Rowiest Al Ballout (Mount Lebanon) on February 2014. Then, plants were well-cleaned and washed with water, and kept to "shade dry" under the room temperature away from the sunlight. After being dried, the collected plants are grinded (using a

grinder) until we obtain a powder form that is preserved in a black container, away from light, heat, and moisture for later use.

Preparation of crude extracts

5 grams of *E. creticum* powder were used in each of the extraction technique along with 250 mL of ethanol as a solvent. Maceration method was performed for 48 hours with stirring. Moreover, reflux and Soxhlet methods were performed for 4 hours under heat. On the other hand, microwave-assisted extraction was performed for 2 minutes under a power of 750 watt.

Standard curves preparation (gallic acid and rutin)

Stock solutions of gallic acid have been prepared as a standard for the quantification of the total amount of phenols (in mg per gram of dry plants powdered). Gallic acid (5 mg) was added to 50 mL of methanol (10 %) to prepare 0.1 mg mL^{-1} stock solution. Then different dilutions were done to prepare several concentrations (5 to 40 µg mL^{-1}) in order to show the standard curve of gallic acid.

Stock solutions of rutin have been prepared as a standard for the quantification of the total amount of flavonoids (in mg per gram of dry powdered). This stock contains 5mg of rutin + 5 mL of methanol. Then, dilution (by twenty times) was done by taking 1.25 mL from this solution and diluting it in 25 mL methanol. Several concentrations (4 to 32 µg mL^{-1}) were prepared in order to show the standard curve of rutin.

Determination of the total phenolic content (TPC)

The Folin–Ciocalteau reagent method was used for estimating the total quantity of phenolic extracts. Five concentrations of all extracts of the used plant were prepared and then 100 µL were taken from each concentration and mixed with: 0.5 mL of Folin–Ciocalteau reagent (1/10 dilution) and 1.5 mL of Na$_2$CO$_3$ 2% (w/v). The blend was incubated in the dark at the room temperature for 15 min. The absorbance of blue-colored solution of all samples was measured at 765 nm using a Gene Quant 1300 UV-Vis spectrophotometer. The results were expressed according to the Gallic acid standard curve.[8]

Determination of the total flavonoid content (TFC)

The aluminium chloride method was used for determining the total flavonoids content of all extracts of the studied plant. 1 ml of the various concentrations of all crude extracts was mixed with 1 mL of 2 % methanolic aluminium chloride solution. After an incubation period (15 min) at the room temperature in the dark, the absorbance of all samples was determined at 430 nm using a Gene Quant 1300 UV-Vis spectrophotometer. The results were expressed according to Rutin standard curve.[9]

DPPH radical scavenging activity

1 mL of the different concentrations (0.1, 0.2, 0.3, 0.4, and 0.5 mg mL^{-1}) from the diluted extracts of the plant's parts in ethanol was added to 1 mL of DPPH (0.15 mM in ethanol), and at the same time, a control consisting of 1mL DPPH with 1 mL of ethanol was prepared. The reaction mixtures were mixed very well (manually) and then were incubated in the dark at the room temperature for 30 min, and the absorbance was measured at 517 nm by a Gene Quant 1300 UV-Vis spectrophotometer. The ascorbic acid was used as a positive control and the ethanol was used as the blank. The DPPH scavenging ability (φ, in %) of the plant extracts was calculated using the following equation:

$$\varphi = \frac{A_c - A_s}{A_c} \, 100$$

where

A_c is the absorbance of DPPH + ethanol;
A_s is the absorbance of DPPH + sample.[10]

Extraction and esterification of the fatty acids

The extraction and esterification of the fatty acids was done according to the method of Abdul Hayee-memon *et al.* [11] with some modifications. To 20 g of the powdered plant materials, 100 mL of petroleum ether has been added and was set in a water bath for 15 min at the room temperature (the extraction was repeated in triplicate). Then petroleum ether has been evaporated using a rotary evaporator at 40°C, under a low pressure. In a beaker, 250 mL of methanol were added to 29 g of NaOH and were dissolved by agitation at room temperature. For 0.5 mL of the extracts obtained from the powdered plant material, 20 mL of hexane and 100 mL of NaOH were added and dissolved in methanol. After the separation of the mixture, the hexane layer was taken and washed two times with distilled water. Finally, the obtained extracts were filtered and sent to GC-MS (Gas Chromatography-Mass Spectrometry) for the analysis of the esterified fatty acids.[11]

GC-MS analysis

GC-MS analysis was carried out on "Clarus 500 Perkin Elmer" system comprising the AOC-20i auto-sampler and the gas chromatograph that is interfaced to the mass spectrometer (GC-MS) instrument, employing the following conditions: an Elite-5MS (5 % diphenyl/95 % dimethyl poly siloxane) fused a capillary column (30 × 0.25 µm ID × 0.25 µmdf). For GC-MS detection, an electron ionization system was operated in a fast atomic bombardment mode using an ionization energy of 70 eV. Helium gas (99.999%) was used as a carrier gas at a constant flow rate of 1.4 mL min^{-1} through an injection of 50 mL min^{-1} (a split less mode). The injector temperature was maintained at 220 °C, and the oven temperature was programmed at 45 °C for 5 min with an increase of 3 °C per min to reach a temperature of 220 °C, in which this temperature was maintained for 15 min. Mass spectra was taken at 70 eV; a scan interval of 0.3 s for all fragments mass. The solvent delay was 0 to 2 min and the total GC/MS running time was 80 min.

Determination of the Total Alkaloids amount

The quantification method for alkaloids determination has been used according to Harborne method[12] with some modifications. 100 mL of 10 % acetic acid in ethanol was added to 1 g of dry powdered plant. The extracts were then covered and allowed to stand for 4 hours. After that, the extracts were filtrated and concentrated in a water bath to 25 mL of its original volume. Droplets of concentrated ammonium hydroxide were added to the extract until the whole solution has precipitated. The precipitate was then washed by dilute ammonium hydroxide and filtered using whatman filter paper. The residues were dried in the oven at 40 °C and were weighed. The alkaloid content (C_A, in %) was determined using the following formula

$$C_A = 100 \frac{m_f}{m_i}$$

where

m_f is the final weight of the sample
m_i is initial weight of the extract

The samples were done in triplicates.

Determination of the humidity content

1 gram of fresh plant material was taken and placed in an oven at 105 °C for 1 hour. Then, it was placed in a desiccator for half an hour and the mass was recorded after that. The following step was to place the plant again in the oven for another 1 hour. After heating, it was placed in the desiccators for half an hour. These steps led to obtaining a dry plant material in which the mass was recorded in order to calculate the percentage of humidity.[13] The sample was done in triplicates.

Determination of the ash content

1 gram of dried plant powder was placed (until being burnt) in a burning furnace (muffle furnace) at 550 °C for 5 hours until obtaining a powder with an ovary gray color. The residues were weighed and the percentage of ash was estimated according to the essential dry weight of plant powder.[14] The sample was done in triplicates.

RESULTS AND DISCUSSION

Total phenolic content (TPC) and total flavonoid content (TFC)

After the preparation of the gallic acid standard curve (Fig.1 in Supplement, R^2=0.9907) and rutin standard curve (Fig.2 in Supplement, R^2=0.9952), the TPC and TFC of each technique have been demonstrated in Table 1. The results show that the highest amount of phenolic compounds (34.46 µg mL^{-1}) was obtained by microwave-assisted extraction (MAE) while the lowest amount of phenolic compounds (8.57 µg mL^{-1}) was obtained by maceration. On the other

hand, the TPC was found to be 12.22 µg mL^{-1} and 17.68 µg mL^{-1} by using the reflux and Soxhlet methods respectively. Thus, the microwave-assisted extraction is the best method used for the extraction of phenolic compounds from dried plant material.

Concerning the TFC, the obtained results showed that most extraction techniques produced approximately the same values with slight variations between one extraction technique and the other, although the microwave-assisted extraction produced, as for the TPC, the highest yield of TFC 21.05 µg mL^{-1} as shown in Table 1.

Table 1. TPC and TFC expressed as a mean (±SD)

Extraction technique	TPC, µg mL^{-1}	TFC, µg mL^{-1}
Maceration	8.57 ± 0.006	18.61 ± 0.023
Reflux	12.22 ± 0.02	20.19 ± 0.041
Soxhlet	17.68 ± 0.0043	17.73 ± 0.012
Microwave-assisted extraction	± 0.0046	± 0.015

Antioxidants activity

Several reports regarding flavonoids, terpenoids, and polyphenols have proven that these biological compounds possess an antioxidant and free radical scavenging activity.[15] These phyto-constituents may exert multiple biological effects against tumors, heart disease, AIDS, and many other different pathologies due to its free radical scavenging activity. Taking these facts into consideration, our study was conducted to evaluate the antioxidant power of the Lebanese plant, *E. creticum* using different extraction techniques. The easiest, most rapid and sensitive method for screening antioxidants in plant extracts is the free radical scavenging assay using the "DPPH assay". In the presence of an antioxidant, DPPH radical gains one or more electrons and thus the absorbance decreases.[8]
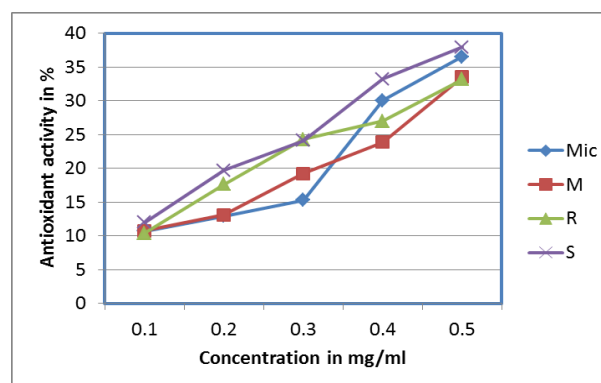

Figure 3. Antioxidant activity obtained by different extraction techniques. Mic = microwave, M=maceration, R=reflux and S= Soxhlet

Figure 1 shows the antioxidant activity obtained from different extraction techniques. The results indicate that there was a slight variation between one extraction technique and the other. In addition, the highest antioxidant

activity in all the extraction techniques was obtained at a concentration of 0.5 mg mL^{-1} and reached a maximum of 30 to 40 % in all of the extraction techniques. Therefore, the antioxidant activity of this plant was increasing with an increase in the concentrations.

Phytocomponents identified in *E. creticum* extracts after GC-MS

The GC-MS analysis (Fig.3 in Supplement) of *E. creticum* extracts revealed the presence of 9 fatty acid derivatives (Table 2), some of which have therapeutic uses (Table 3).

Table 2. Phytocomponents of *E. creticum* extracts based on GC-MS probability (in %)

No.	Name	MW, g mol^{-1}	Content, %	Origin
1	Methyl tetradecanoate	242	32.56	Myristic acid
2	Methyl hexadecanoate	270	49.34	Palmitic acid
3	Methyl 9,12-octadecanoate	294	8.59	Linoleic acid
4	Methyl octadecanoate	298	13.89	Stearic acid
5	Cyclohexyl nonyl oxalate	298	28.94	Oxalic acid
6	1-Methylhexyl hexanoate	214	10.89	Hexanoic acid
7	Allyl nonyl oxalate	256	4.23	Oxalic acid
8	2-propyl tridecylsulphinate	306	2.93	Sulfurous acid
9	Methyl 4-hydroxy octadecanoate	314	5.84	Stearic acid

Table 3. Therapeutic uses of some phytocomponents obtained from *E. creticum*

No.	Name	Therapeutic effect
1	Tetradecanoic acid	Nematicidal, hypocholesterolemic, antioxidant, cancer preventive, lubricant [16]
2	Hexadecanoic acid	Inhibition of growth and apoptosis of gastric cancer cells, antiandrogenic, antioxidant, hypocholestrolemiant [16,17]
3	9,12-octadecadi-enoic acid	Inhibitory effect in passive cutaneous anaphylaxis, inhibitory eicosanoid formation via cyclooxygenase and lipooxygenase inhibition [18]
4	Octadecanoic acid	Antibacterial, analgesic, sedative, anti-inflammatory, and antifungal [16,17]
6	1-Methylhexyl hexanoic acid	Useful in the inhibition of inducible isoform of nitric oxide synthesis [19]

They can be useful as an antimicrobial agent, an anti-inflammatory agent, a diuretic, a lubricant, an analgesic, an antifungal agent, an antioxidant, and also as a cancer preventive agent for the treatment of patients having cancer.

Active content of *E. creticum*

Table 4 shows the percentage of total alkaloids obtained in *E. creticum* as well as the humidity content and the total ash percentage. *E. creticum* has a low amount of alkaloids (0.57 %), with a high humidity content (79.16 %) and ash content (18.10 %).

Table 4. Percentage of active content obtained from *E. creticum* expressed as a mean (±SD)

Component	Content, in wt. %
Total alkaloids	0.57 ± 0.0058 ± 0.0057
Humidity	79.16 ± 0.0078 ± 0.0078
Total ash	18.10 ± 0.0015 ± 0.0015

Conclusion

Eryngium creticum, besides having a high phenolic and flavonoid content, has an important antioxidant activity. The difference in the obtained results indicated that microwave assisted technique produced the highest amount of TPC and TFC and thus can be used for the extraction of flavonoids and phenolic compounds in high amounts. Also, the GC-MS analysis of *E. creticum* extracts revealed the presence of a variety of bioactive compounds which explains the possibility of using this plant in folk medicine for the treatment of several illnesses. Future studies need to be done on the use of these bioactive compounds as a source of multi resistant medicaments.

References

[1]Kris-Ethreton, P. M., Hecker, K. D., Bonanome, A., Coval, S. M., Binkoski, A. E., Holpert, K. F., Griel-Ethreton, T. D., *Am. J. Med*., **2002**, 71s-81s. P: 11-17.

[3]Farhan, H., Malli, F., Rammal, H., Hijazi, A., Bassal, A., Ajouz, N., Badran, B., *Asian Pacific J. Trop. Biomed.,* **2012,** 1-4.

[4]Abu-Rabia, A., A*sian Pacific J. Cancer Prevent.,* **2005**, *6*, 404-7.

[5]Alkofahi, A., Sallal, A. J., Disi, A. M., *Phytotherapy Res.,* **1997**, *11*, 540-2.

[6]Rammal, H., Farhan, H., Mohsen, M., Hijazi, A., Kobeissy, A., Daher, A., Badran, B., *Int. Res. J. Pharm.,* **2013,** *4*, 132-136.

[7]Dirani, Z., Makki, R., Rammal, H**,** Naserddine, S., Hijazi, A., Kazan, H. F., Nasser, M., Daher, A. and Badran, B., *Int. J. Biol. Pharm. Allied Sci.,* **2014**, *3*(10), 2199-2222.

[8]Lister, E., Wilson, P., *Measurement of Total Phenolics and ABTS Assay for Antioxidant Activity.* Crop Research Institute Lincoln, New Zealand, **2001**.

[9]Quettier-Deleu, C., Gressier, B., Vasseur, J., Dine, T., Brunet, C., Luyckx, M., Cazin, M., Cazin, J. C., Baileul, F., Trotin, F., *J. Ethnopharm.,* **2000,** *72*, 35-42.

[10]Chew, Y. L, Goh, J. K., Lim, Y. Y, *Food Chem.,* **2009**, *119*, 373-378.

[11]Hayee-Memon, A., Shameel, M., Usmanghani, K., Ahmad, M., Ahmad, V. U., *Pakistan J. Pharm. Sci.,* **1991**, *4,* 137-144.

[12]Harborne, J. B., Phytochemical methods. A guide to modern techniques of plant analysis. 3rd ed. New Delhi: Spinger Pvt. Ltd.**, 2005.**

[13]American Association of Cereal Chemists (AACC)**.** Method 08-01. The Association St. Paul MN. *Approved Methods of the AACC*, 8th Edition, **1984.**

[14]Association of Official Analytical chemists (AOAC). *Official Methods of Analysis,* 13th ed. Washington D.C., **1980**.

[15]Frankel, E., Nutritional benefits of flavonoids. *Int. Conf. Food Factors: Chem. Cancer Prevent*., Hamamatsu, Japan abstracts, C6-2, **1995.**

[16]Kalaivani, C. S., Sathish, S. S., Janakiraman, N., Johnson, M., *Int. J. Med. Aromatic Plants.* **2012,** *2*, 69-74.

[17]Ponnamma, S. U., Manjunath, K., *Int. J. Pharma Biosci.,* **2012,** *3(3),* 570-576.

[18]Stasi, L. C., Gomes, J. C., Vilegas, W., *Chem. Pharm. Bull.,* **1999,** *47*, 890-893.

[19]Donald, W., Hansen, J. R., Skokie, I. L., **(2002)**. Homoiminopiperidinyl Hexanoic Acid Inhibitor of Induced Nitric Oxide Synthase, *US 6495544.*

OLIGOMERIZATION OF THE ETHYLENE IN THE PRESENCE OF NEW HETEROGENIZED Zr-CONTAINING COMPLEX CATALYTIC SYSTEMS

A. H. Azizov,[a],[b]* M. J. Khamiyev,[a] A. A. Khanmetov,[a] R. V. Alieva,[a] B. M. Aliyev [a] and S. F. Ahmedbekova[a]

The new heterogenized zirconium phenolate complexes containing different bulky ionic liquid type amine hydrochloride substituents in ortho-position have been synthesized and characterized. The oligomerization of the ethylene was carried out with use of these complexes activated by aluminium organic compounds in heptane, toluene and chlorobenzene. In the presence of diethyl aluminium chloride these complexes show higher activity than in the presence of ethylaluminium dichloride. The distributions and composition of the obtained oligomer products depend on the nature of aluminium organic compound used. The oligomerization products consist of C4 - C18 oligomers when diethyl aluminium chloride is used as a cocatalyst. In the presence of ethylaluminium dichloride the higher branched structured oligomers (oil fraction with boiling point > 350 °C) is obtained with >75 % yield. The products are easily separated from the catalysts by simple decantation and zirconium complexes may be repeatedly reused in successive ethylene oligomerization.

* Corresponding Authors
    Fax: (+99418) 642-04-00
    E-mail: akazizov@ymail.com
[a]   Institute of Petrochemical Processes, Azerbaijan National Academy of Sciences, 30, Khojaly Ave., AZ1025, Baku, Azerbaijan
[b]   Institute of Polymer Materials, Azerbaijan National Academy of Sciences, 124, S.Vurgun str., Az5004, Sumgait, Azerbaijan

Introduction

Oligomerization of ethylene is a process in which higher olefins and end vinyl caped macromonomers are produced. These olefins are used for the production of fuels, detergents, plasticizers, comonomers for linear low density and long-chain branched polyethylenes, blend compatibilizers, synthetic oils, corrosion inhibitor etc.[1-4]

Oligomerization of ethylene in the presence of the homogeneous catalyst systems based on transition metal complexes has been widely studied.[5,6] In spite of high catalytic activity and selectivity of these catalysts in oligomerization of ethylene, they have essential disadvantages such as difficulties assosiated with separation of the catalyst from olgomerization products and impossibility of their recycling.

To avoid these disadvantages in recent years the intensive researches aimed at development of olefins oligomerization processes with participation of ionic liquids are being conducted.[7-9] In particular, the use of ionic liquids for "heterogenizing" homogenous catalysts has received increasing attention.

Three main methodologies have been developed for applications of ionic liquids in catalytic oligomerization reactions of olefins. In the first method, the ionic liquids were used both as the solvents and the catalysts for oligomerization reactions.[10-12] The chloroaluminate type ionic liquid systems have been studied most under this category.[13-15] The main advantages of using ionic liquids as the solvents include carrying out the process in a biphasic system, which eases separation of reaction products from reaction medium and reuse of the catalyst in a cyclic process.[16-19]

In the second approach, the catalyst (in general a transition metal complex) is immobilized in the ionic liquid phase and the reaction products are formed in the upper organic phase.[20] For implementing such an approach in the continuous process, the key point is the stable immobilization of the catalyst (or catalytic system) in the ionic liquid phase. This approach was used successfully in the oligomerization and polymerization processes of olefins.[21-24] A distinctive feature of immobilization of metal-complexes in such a manner is that they are compatible with many ionic liquids, which opens up many possibilities for their applications in biphasic processes. Besides, increased effectiveness of metal-complex catalysts in the oligomerization and polymerization of ethylene, propylene and other α-olefins in the presence of ionic liquids was observed, which causes additional interest for development of recyclable ionic-liquid based highly active metal-complex catalytic systems for these processes. Studies devoted to oligomerization of ethylene in the presence of complex catalytic systems immobilized in ionic liquids taken as the solvents have demonstrated the possibility of conducting the process in a more efficiently and environmentally friendly manner.

The third approach, suggested by us, is based on the use of transition metal (Ti, Zr) precursor complexes containing ionic liquid type ligands in their coordination sphere. These complexes, combined with aluminium-organic activators, act as a recyclable heterogenous oligomerization catalysts both in the molecular organic and ionic liquid solvents.[25-28]

In this article, some results of investigation of oligomerization of ethylene in hydrocarbon solvents in the presence of complex catalytic systems consisting of zirconium precursor compounds, containing different ionic-liquid type amine hydrochloride substituents, and aluminium

alkyl chlorides have been overviewed. Influence of corresponding ligands of the substituted phenolate type precursor compounds of zirconium, the nature and molar ratio of the catalyst components, a modifier compound and process temperature on the activity of the catalyst, distribution and structure of the oligomerization products have been studied.

Experimental

General Procedures

All solvents were purified and dried by standard procedures and distilled under inert atmosphere. All aluminium organic compounds and $ZrCl_4$ were purchased from Aldrich Chemical Co. and used without additional purification. The corresponding phenol derivatives were synthesized according to the reported procedures.[29,30] The catalysts precursors were synthesized by an interaction of $ZrCl_4$ with phenol derivatives in THF solution at 50-55 °C.[31]

Oligomerization

Oligomerization of ethylene was carried out in the jacketed autoclave equipped with a magnetic stirrer, thermometer and heated with thermostated water or glycerine. Before charging with reaction mixture and catalyst components, the autoclave was washed with dry toluene and acetone, checked for leak tightness under nitrogen pressure, dried in vacuum under heating by connecting the reactor connected to the vacuum line and heating for 1-1.5 h at 90 °C. The catalyst and solvent were placed into reactor under an inert gas atmosphere. The reactor was heated to reaction temperature and then ethylene was pressurized into it with intensively mixing the reaction mixture by magnetic stirrer. The pressure of ethylene in the reactor was controlled by a manometer. The oligomerization product solution was removed from the reactor by simple decantation. The Zr-component of catalyst, remaining in the reactor, was repeatedly used in the oligomerization prosess by addition of new portions of solvent and aluminium organic compound. The obtained oligomerization products were washed with aqueous solution of sodium hydroxide for removing aluminium organic compound residues, dried over aluminium oxide and fractionated.

Analytical procedures

Oligomerization products and metal complexes (MC) were analyzed by gas-liquid and exclusion chromatography, DSC, IR- and ^{1}H NMR-spectroscopy, element analysis and scanning electron microscope (SEM).

Oligomers of ethylene, boiling up to 350 °C were analyzed by gas-liquid chromatography on "Focus GS", with a 100 m long column and 100 % dimethyl silicone as the liquid phase. The analyses were performed in the following programming mode: temperature from 50 °C to 320 °C rising at a rate of 6 °C min⁻¹. The rate of flow of carrier gas (helium) was 30 ml min⁻¹. The temperature of evaporator was 320-350 °C.

^{1}H NMR spectra were recorded on a Bruker pulsing Fourier spectrometer (Germany) operating at the frequency of 300 MHz. Deuterated benzene and dimethyl sulfoxide were used as a solvent.

IR-spectra were recorded on the "BRUKER" Fourier spectrometer in the range of 50-4000 cm⁻¹.

DSC analysis was carried out on a Thermoelectron Q-20 Differential Scanning Calorimeter at a heating rate of 10 °C min⁻¹ in an air or nitrogen atmosphere.

Element analysis of the catalyst precursor components was performed on TruSpec Micro analyzer of Horiba company.

Molecular-weight distribution (MWD) of the obtained products was studied by size exclusion chromatography method using high performance "Kovo" (Czech Republic) liquid chromatograph with a refractive index detector. Two 3.3 mm-150 mm columns packed with the "Separon-SGX" stationary phase with a particle size of 7 mm and a porosity of 100 Å were used. DMF was used as an eluent (flow rate 0.3 ml min⁻¹, temperature 20-25 °C). A calibration plot of log M versus V_R in the range M = 2-100 x 10² was obtained using polyethylene glycol standards and transformed to the common dependence of fraction (%) of chains from their molecular weights. Calculations of the average molecular weights and MWD characteristics were made using the data of size exclusion chromatographic analysis in accordance with the described procedure.[32] Average molecular weights (M_w and M_n) were calculated using the following formulas:

$$M_w = \sum M_i \omega_i, \quad M_n = 1/\sum \omega_i / M_i \qquad (1)$$

where M_i is the molecular weight, corresponding to the ith slice of the chromatogram; ω_i is the area fraction of the ith slice.

The degree of branching in the oligomer chains of oil fractions were determined by the method presented in the literature[33] and the ratios of CH_3 group to 1000 CH_2 and of vinyl group ($CH_2=CH-$) to 1000 CH_3 were calculated according to the following formulas

$$\frac{CH_3}{1000CH_2} = 188\frac{D_{1380}}{D_{720}} \quad \text{and} \quad \frac{CH_2=CH-}{1000CH_2} = 98\frac{D_{910}}{D_{1380}}, \text{ respectively}$$

Average structural parameters of oligomers were calculated from NMR spectra according to the method reported in the literature,[34] adapted to hydrocarbons. For calculations the following initial data were used.

1. Quantity of C and H atoms, determined on the basis of data obtained from elemental analysis and values of average molecular weights (*M*).

2. Distribution of protons in the structural groups (H_β and H_γ) according to ^{1}H NMR data.

3. Proton-deficiency of an average molecule (Z), determined according to equation $Z = 2C - H$ on the basis of above-mentioned input data the following average structural parameters of the synthesized oligomers were calculated.

a) quantity of saturated cycles in the molecule: $K_n = 0.5Z+1$;

b) quantity of C atoms in naphthenic cycles: $C_n = 3.85K_n+2$;

c) quantity of C atoms in paraffinic structures: $C_p = C – CH$;

d) quantity of terminal methyl groups: $C_\gamma = 1/3H_\gamma$;

e) total quantity of secondary, tertiary and quaternary C atoms in paraffinic chains: $C_{\beta p} = C_p – C_\gamma$;

(f) number of carbon atoms in the alkyl and naphthenic fragments in the amount: $C_\beta = C – C_\gamma$.

Synthesis and characterization of phenol derivatives and precursor metal complexes

The phenol derivatives, required for the syntheses of corresponding precursor Zr-complexes, were prepared, by Ch. Rasulov and collaborators of the Institute of Petrochemical Processes of Azerbaijan National Academy of Sciences, according to the reported methods.[29,30] The precursor Zr-phenolate complexes were synthesized by us according to the literature method[31] by interaction of $ZrCl_4$ with four phenol derivatives viz., 2–piperidinylmethyl-4-methylphenol (**L1**), 2-morfolylmethyl-4-methylphenol(**L2**), 2-diethylaminomethyl-4-methylphenol(**L3**) and 2-[(2,6-di(isopropyl)phenyl)imino]phenol(**L4**). The syntheses were carried out by heating the reactants to 50-55 °C for 2 h, in a three-necked flask under an inert atmosphere in THF solution with different $ZrCl_4$ / phenol molar ratios. The complexes were obtained as their hydrochloride salts. The obtained complexes were separated from the solvent by simple decantation, washed with dry solvent and dried under vacuum for 2 h. These complexes are not soluble in hydrocarbon solvents (aromatic, aliphatic, haloid aromatics) but dissolve in DMSO and ionic liquids. They are unstable in air Scheme 1 illustrates the general synthesis schemes taking an example of MC1 ($ZrCl_4$: Ligand = 1 : 2 molar ratio).
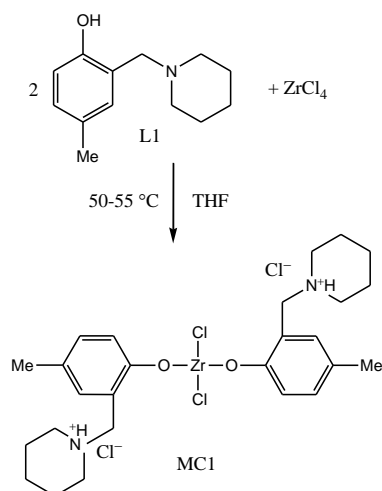
Scheme 1. Synthesis of zirconium complexes.

Synthesis of MC1 and MC2

MC1 and MC2 were synthesized by interaction of $ZrCl_4$ with ligand **L1** at molar ratio of 1:2 and 1:3 respectively in THF at 50-55 °C for 2 h with mechanically stirring. The precipitated products were separated from THF and dried for 2 h in vacuum. The products obtained as white powders were characterized by spectral and elemental analysis data. MC1: ^{1}H NMR (300 MHz, DMSO-d_6), δ (ppm): 2.19 (6H, s, Ph-CH$_3$), 6.90-7.29 (6H, m, Ph-H), 4.10 (4H, s, CNH), 3.46 (8H, t, NCH$_2$ of piperidinyl), 2.84-3.72 (8H, m, -CH$_2$- of piperidinyl), 1.36-1.62 (4H, m, >CH$_2$ of piperidinyl), 1.74 (4H, m, CH$_2$ of THF) 3.46 (4H, t, OCH$_2$ of THF), 10.0 (2H, s, N$^+$H). ^{13}C NMR (300 MHz, DMSO-d_6): 154.9, 134.0, 131.7, 128.1, 116.1, 115.8, 67.5, 54.1, 52.0, 25.6, 22.6, 21.7, 20.5. Calc. $C_{26}H_{38}N_2O_2ZrCl_4$ ·THF C 50.31, H 6.43, N 3.91%; found C 49.78, H 6.70, N 4.01 %. MC2: ^{1}H NMR (300 MHz, DMSO-d_6), δ (ppm): 2.23 (9H, s, Ph-CH$_3$), 6.65-7.28 (9H, m, Ph-H), 4.04 (6 H, s, CNH), 3.44 (12H, s, N(CH$_2$)$_2$ of piperidinyl), 2.99 (12 H, m, -CH$_2$- of piperidinyl), 1.71 (6H, m, >CH$_2$ of piperidinyl), 10.0 (3H, s, N$^+$H). Calc. for $C_{39}H_{57}N_3O_3ZrCl_4$ C 55.18, H 6.72, N 4.95 %; found C 54.81, H 6.90, N 4.65 %.

Synthesis of MC3

MC3 was synthesized by interaction of $ZrCl_4$ with phenolic derivative **L2** at molar ratio 1:2 in THF. The reaction was carried on for 2 h with mechanically stirring. The product, obtained as a white powder, was characterized by ^{1}H NMR (300 MHz, DMSO-d_6), δ (ppm): 2.23 (6H, s, Ph-CH$_3$), 6.69-7.33 (6H, m, Ph-H), 3.52 (4H, s, CNH), 3.12 (8H, s, N(CH$_2$)$_2$ of morpholyl), 3.84 (8H, s, (CH$_2$)$_2$O of morpholyl), 1.74 (4H, m, CH$_2$ of THF) 3.59 (4H, t, OCH$_2$ of THF), 10.0 (2H, s, N$^+$H). Calc. for $C_{24}H_{34}N_2O_4ZrCl_4$·THF C 44.51, H 5.25, N 4.32 %; found: C 44.49, H 5.18, N 4.20 %.

This complex is also unstable in air, rapidly soluble in water and hardly soluble in DMSO and ionic liquids.

Synthesis of MC4

MC4 was synthesized by interaction of $ZrCl_4$ dissolved in THF with phenol derivative **L3** at molar ratio 1:2 in the similar manner. The product was obtained as white powder. Calc. for $C_{39}H_{57}N_3O_3ZrCl_4$ C 44.51, H 5.87, N 4.32 %; found C 45.28, H 5.18, N 2.99 %.

Synthesis of MC5

MC5 was synthesized by interaction of $ZrCl_4$ dissolved in THF with phenolic compound **L4** at molar ratio 1:2 in a similar manner. The product, obtained as a yellow powder, was characterized by ^{1}H NMR (300 MHz, DMSO-d_6), δ (ppm): 2.23 (6H, s, Ph-CH$_3$), 6.93-7.66 (614H, m, Ph-H), 8.57 (2H, s, CNH), 1.10-1.23 (24H, d, CH$_3$), 2.87 (4H, m, CH(CH$_3$)$_2$), 10.25 (2H, s, N$^+$H), 3.25 (4H, t, of OCH$_2$ of THF) 1.74 (4H, m, CH$_2$ of THF). ^{13}C NMR (300 MHz, DMSO-d_6): 23.7, 24.0, 27.8, 28.2, 117.1, 119.7, 123.6, 124.1, 125.8, 132.3, 134.1, 138.4, 160.6, 168.2. Calc. for $C_{38}H_{46}N_2O_2ZrCl_4$·THF C 57.35, H 5.78, N 3.52 %; found C 57.29, H 7.69, N 3.49 %.

In the IR spectrum of the synthesized complexes, absorption bands are observed at 2547 cm⁻¹, 2573 cm⁻¹ and 2633 cm⁻¹ corresponding to N^+R_3H ammonium group, 1614 cm⁻¹ corresponding to the stretching deformation vibrations of the N-H bonds in ammonium salts. Bands in the absorption area of 530-600 cm⁻¹, characteristic for stretching vibrations of Zr-O bond and 280 cm⁻¹ absorption band characteristic for stretching vibrations of Zr – Cl bond were also observed (Fig..1).
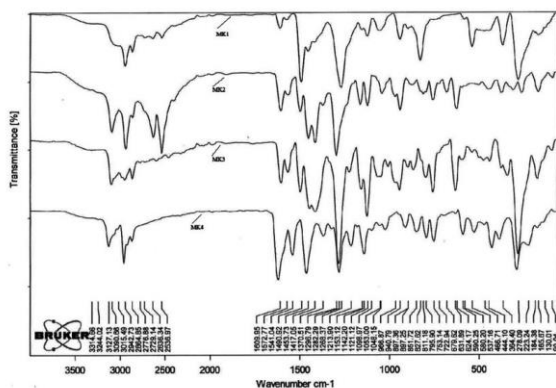

Figure 1. IR spectra of MC1, MC2, MC3 and MC5.

The surface structures of the MC1 and of the complex catalyst system obtained by its interaction with ethyl aluminium dichloride were investigated by the scanning electron microscope. The images are presented in Figure 2a and 2b, respectively.
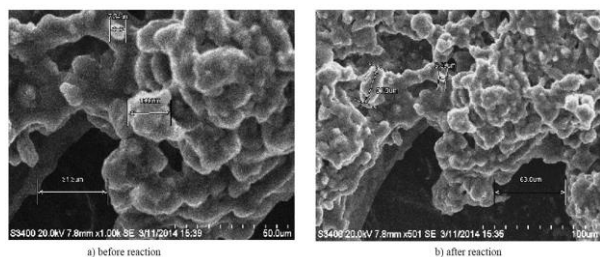

Figure 2. Scanning electron microscope images of MC1 and complex catalyst system (x 500F).

As is seen, the freshly prepared complex MC1 (prior to reaction with aluminium organic compound) has a well-developed structure. After the reaction, the surface remains sufficiently well developed. But the separate fragments of the complex are closely interconnected forming a single mass. The system is very porous and it has lots of pores and channels where the reacting components can be placed, which favours its reuse as heterogeneous catalyst in the oligomerization process of ethylene in heptane.

Results and Discussion

Dependence of ethylene oligomerization products distribution and catalyst activity on the reaction conditions

The results obtained during the reaction of ethylene oligomerization in the presence of complex catalytic systems consisting of different synthesized zirconium precursors and aluminium organic compounds are given in the Table 1. The reaction products are oligomers of ethylene with a carbon atom number from C_4 to C_{20+} and higher. The distribution of the oligomerization products depends on the composition of zirconium compound containing ammonium hydrochloride substituents (Table 1). In the presence of MC1 and ethylaluminium dichloride the yields of C_4 - C_6, C_8 - C_{18} and C_{20+} oligomer fractions are 13.3 %, 26.7 % and 60 %, respectively. Use of more polar solvent chlorobenzene increases the reactivity of the catalyst system and the yields of low oligomer products C_4-C_6 increase to 31.5 %. The yields of higher molecular weight oligomer fractions C_8 - C_{18} and C_{20+} decrease and reach 18.5 % and 50 % respectively. When ethylaluminium sesquichloride is used as an aluminium organic compound the yield of dimer product increases and amounts to 41.3 %. In this case the yields of C_8 - C_{18} and C_{20+} fractions are 10.6 % and 7.1 % of the converted ethylene. Using diethylaluminium chloride as the co-catalyst in toluene increases the catalyst activity nearly threefold. In this case, the reaction product consists mainly of the dimers (2.7 %), trimers (63.2 %) and C_8-C_{18} oligomers (34.1 %).

While using ethyl aluminium dichloride as an activator, replacement of MC1 by MC3 and MC5 increases the yields of dimers, trimers and C_8 - C_{18}, and decreases the yield of C_{20+} fraction. In the presence of MC5 as zirconium compound the oligomerization product consists mainly of C_6-C_8 fraction. In this case the yields of C_4 and C_6 fractions are 5.6 %, 62.9%, while the yields of the C_8 – C_{18} and oil fractions are 25.5 % and 6 %, respectively. In the presence of MC3 and ethylaluminium dichloride the yields of dimer and trimer fractions are 15.2 %, 40% and of the oil fraction is 46 % respectively.

As is seen from Table 1, the catalytic activity also depends on the compositions of the different zirconium precursors and aluminium organic compounds as well as on the solvents used. In particular, when ethylaluminium dichloride is used as an aluminium organic compound and MC1 as Zr-precursor the activity of the system in heptane is 156 g oligomer/g Zr h⁻¹. Replacement of ethylaluminium dichloride by diethylaluminium chloride and heptane by toluene leads to the increase of catalytic activity up to 1210 g oligomer/g Zr h⁻¹. In heptane MC3 + ethylaluminium dichloride and MC5 + ethylaluminium dichloride systems show the highest activity (1100 -1150 g oligomer/g Zr h⁻¹).

The nature of solvent and modifier influences also on the properties and the yield of the oil fraction of oligomerization products. The results obtained in the presence of MC1, MC4, ethylaluminium dichloride and different modifiers in the medium of chlorobenzene and heptane are given in the Table 2. In heptane medium without modifier the yield of the obtained oil fraction is 61.8 %, kinematic viscosity 83 .6 cSt at 40 °C, 8.70 cSt at 100 °C and index viscosity is 68. Addition of modifier (durene, mesitylene, etc) to the catalytic system increases the yield of oil fraction up to 5 – 10 % and index viscosity 12-18 units.

The molecular mass distribution of oligomer molecules in the oil fractions are given in the Table 3. The oligomerization products obtained in the presence of MC1, MC2 and MC4 have the molecular masses within the limits, M_w = 323-384, M_n = 217-296 and the degree of polydispersity (M_w/M_n) changes within 1.28-1.52.

Table 1. Influence of the catalyst composition and solvents nature on the ethylene oligomerization product distribution and catalyst activity.

No.	Aluminium organic compound	Al:Zr, molar ratio,	Solvent	Activity of the catalyst g oligomer/g Zr ·h⁻¹	Product distribution (%)			
					C_4	C_6	C_8-	C_{20+}
MC1	$C_2H_5AlCl_2$	25 : 1	Heptane	156	3.5	9.8	26.7	60.0
	$C_2H_5AlCl_2$	25 : 1	chloro-benzene	273	5.0	26.5	18.5	50.0
	$(C_2H_5)_3Al_2Cl_3$	25 : 1	Toluene	420	41.3	15.8	10.6	7.1
	$(C_2H_5)_2AlCl$	30 : 1	Toluene	1210	2.7	63.2	34.1	traces
MC2	$C_2H_5AlCl_2$	30 : 1	Heptane	428	4.2	10.9	32.3	52.6
MC3	$C_2H_5AlCl_2$	25 : 1	Heptane	1150	15.2	40.0	30.8	14.0
MC4	$C_2H_5AlCl_2$	25 : 1	Heptane	185	18.2	15.3	20.5	46
MC5	$C_2H_5AlCl_2$	28 : 1	Heptane	1100	5.6	62.9	25.5	6.0

Reaction Conditions: Temperature 90 °C, solvent 50 mL, time 5 h, pressure 2.5 MPa.

Table 2. Influence of modifier and solvent on the properties and the yield of oil fraction.

MC	Solvent	Modifier (M)	Molar ratio of Al:Zr:M	Activity of catalyst g oligomer/g Zr ·h⁻¹	Composition of product %		Kinematic viscosity, mm s⁻¹		IV	F.P. °C	Flash point °C
					T_{qay} <350 °C	T_{qay} >350°C	40°C	100 °C			
	Heptane	-	25:1	156	38.2	61.8	83.36	8.70	68	-20	205
	PhCl	-	25:1	250	50.0	50.0	91.93	8.20	57		
	Heptane	Durene	25 :1:3	159	33.0	67.0	278.1	19.8	80	-12	
	Heptane	Mesitylene	25:1:5	125	32.0	68.0	214.2	16.7	79	-20	
	Heptane	Durene	25:1:5	140	24.4	75.6	754.2	38.5	86	-10	
MC1	PhCl	Ph_2O	25:1:1.5	130	40.3	59.7	315.2	20.3	70	-12	210
	Toluene	-	25:1	220	62.0	38.0	122.0	10.0	51		
MC4	Heptane	-	1:30:0	168	63.0	57.0	116.3	10.23	58		
	Heptane	Durene	1:30:5	132	27.7	72.3	168.8	13.2	62		

Reaction condition: temperature 90 °C, time 5 h, pressure of ethylene 2.5 MPa.
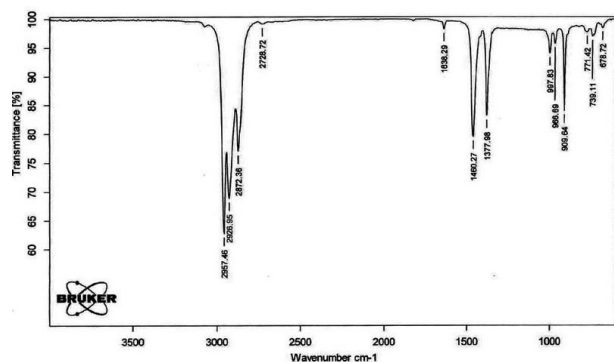
Figure 3. The IR spectrum of C8 - C18 olefin fraction.

Structures and properties of oligomerization products

The structures of the obtained oligomers were examined by IR and ¹H NMR-spectroscopic methods and thermal properties by DSC method. The IR-spectrum of C_8 - C_{18} olefin fraction is given in the Figure 3. As can be seen the intensive absorption bands are observed at 909 cm⁻¹, 997 cm⁻¹ and 1638 cm⁻¹ which is referred to the deformation and valence vibrations of olefin double bonds respectively.

Furthermore, there is deformation vibration at 966 cm⁻¹ with low intensity, which is characteristic of olefins with internal double bonds.

Table 3. The molecular-mass characteristics and physical-chemical properties of the oil fractions.

MC	M_w	M_n	M_w/M_n	Density g cm⁻³	Refractive index, n_D^{20}
MC1	330	217	1.52	0.8395	1.4637
MC1ᵃ	379	296	1.28	0.8340	1.4628
MC2	345	280	1.32	0.8369	1.4643
MC4	323	236	1.37	0.8389	1.4651
MC4ᵃ	384	272	1.4	0.8529	1.4615

a = modified catalysts

The IR-spectrum of the oil fraction obtained in the presence of catalytic system based on MC1 and ethylaluminium dichloride is shown in the Figure 4. In the IR-spectrum (Figure 4) the absorption bands of pendulum oscillation (734 cm⁻¹) of C-H bonds of the CH_2 groups, deformation vibrations (909 cm⁻¹) of the vinyl groups – $CH=CH_2$ are present.

Table 4. IR spectroscopic data of the oil fractions obtained by oligomerization of ethylene.

MC	Zr:Al:M	D_{735}	D_{909}	D_{990}	D_{1380}	D_{1460}	CH$_3$/ 1000CH$_2$	CH$_2$=CH/ 1000CH$_3$
MC1	1 : 30 : 0	0.016	0.014	-	0.082	0.115	963	21
	1 : 30 : 5	0.017	0.021	0.015	0.082	0.004	906	25
MC2	1 : 30 : 0	0.013	0.017	-	0.077	0.114	1113	21
MC4	1 : 30 : 0	0.017	0.020	0.014	0.080	0.004	884	24
	1 : 30 : 5	0.018	0.023	-	0.082	0.004	856	27

Table 5. Average structural parameters of the oil fractions of ethylene oligomerization products.

MC	Average mol. wt.	Empirical formula	No. of carbon atoms		No. of cycles, K_n	Share of carbon atoms,%		No. of carbon atoms in the fragments		
			C_n	C_p		C_n	C_p	C_γ	C_β	$C_{\beta p}$
MC1	217	$C_{15,6}H_{31,2}$	5.9	9.7	1.0	37.8	62.2	4.8	10.8	4.9
MC1[a]	296	$C_{21,0}H_{42,7}$	4.5	16.5	0.65	21.4	78.6	6.3	14.7	10.2
MC2	280	$C_{19,9}H_{40,3}$	4.9	15.0	0.75	24.6	75.4	6.1	13.8	8.9
MC4	236	$C_{16,8}H_{34,2}$	4.7	12.1	0.70	28.0	72.0	4.9	11.9	7.2
MC4[a]	272	$C_{19,3}H_{39,4}$	4.3	15.0	0.60	22.3	77.7	6.0	13.3	9.0

C_n, C_p – carbon atoms in naphthenic and paraffinic fragments, respectively; K_n– quantity of naphthenic cycles in an average molecule; C_γ – number of terminal methyl groups; C_β– an average number of secondary, tertiary and quaternary carbon atoms in a paraffinic chain; number of carbon atoms in the alkyl and naphthenic fragments amount $C_\beta = C - C_\gamma$.

The absorption bands at 1375 cm^{-1} and 1460 cm^{-1} refer to the symmetrical deformation vibrations of the CH$_3$ and deformation vibrations of the CH$_2$ groups respectively. Presence of the intensive bands at 2924 cm^{-1} and 2956 cm^{-1} refers to valence vibrations of C–H bond of the methylene groups in (CH$_2$)$_n$ chain. The absorption bands at 1000 cm^{-1} and 964 cm^{-1} may be considered as an evidence for the deformation vibrations of C - H bond of CH$_2$ groups in the naphthenic ring.

IR spectroscopic analysis data are given also in Table 4. As is seen, the degree of branching of the oligomer chain of oil fractions obtained by oligomerization of ethylene in the presence of the unmodified catalytic systems MC1, and MC4 are characterized by the values of the ratio CH$_3$ / 1000 CH$_2$, equalled 963 and 884, respectively (the degree of branching of the oligomer chain was calculated from IR data). The branching degrees of oligomer molecules obtained in the presence of catalyst systems with π - electron donor modifier compound (MC1[a] MC4[a] in Table 3) are 906 and 856, respectively. Hence, adding π-electron donor modifier to the catalyst system reduces the branching degree of the oligomer chain, increases the yield and improves the viscosity - temperature properties of the oil fraction. The main physical - chemical characteristics of these oil fractions are given in Table 3

^{1}H NMR-spectrum of the oil fractions obtained at using unmodified and modified catalyst systems are given in the Figure 5(a-e). As can be seen, in the all spectra it is identified four analytical areas corresponding to resonance absorptions of ^{1}H atoms bound to carbon atoms of different structural elements. The most intense peaks are observed in the strong field with chemical shifts 0.7 - 1.0 ppm and 1.0 - 1.5 ppm. The first resonance band refers to the hydrogen atoms in the terminal methyl groups (Hγ), and the second to a CH$_2$ - groups of the alkyl chain. The resonance signals in the region 1.5 - 1.8 ppm refer to naphthenic protons. The resonance signals in the region of 2.05 ppm is related to the

first -CH$_2$- group which directly attached double bonds. However, the intensity of this band is very weak that indicates to the low content of these groups in the structure of the oligomer molecule. A weak resonance signal in the 5.5 - 6.0 ppm also indicates to the small amounts of double bonds - CH = CH - or >C=CH$_2$.

In Table 5 the average structural parameters of ethylene oligomerization products obtained in the presence of the investigated catalytic systems with ethyl aluminium dichloride as an activator are presented. The calculations were performed according to the method[34] on the basis of average molecular weights values, 1 H NMR and element analysis data. The molecules of the oil fractions contain naphthenic fragments with average 4.3-5.9 carbon atoms in the ring.

The average number of carbon atoms in paraffinic chains changes within 9.7-16.5. The percentage of naphthenic and paraffinic carbon atoms in the molecules of the oil fractions amounts to 22.3 - 37.8 % and 62.2 - 78.6 %, respectively. The content of terminal methyl groups changes within 4.8 - 6.3 depending on the composition of the catalyst systems.
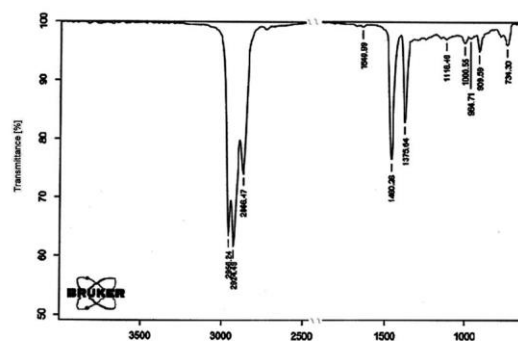
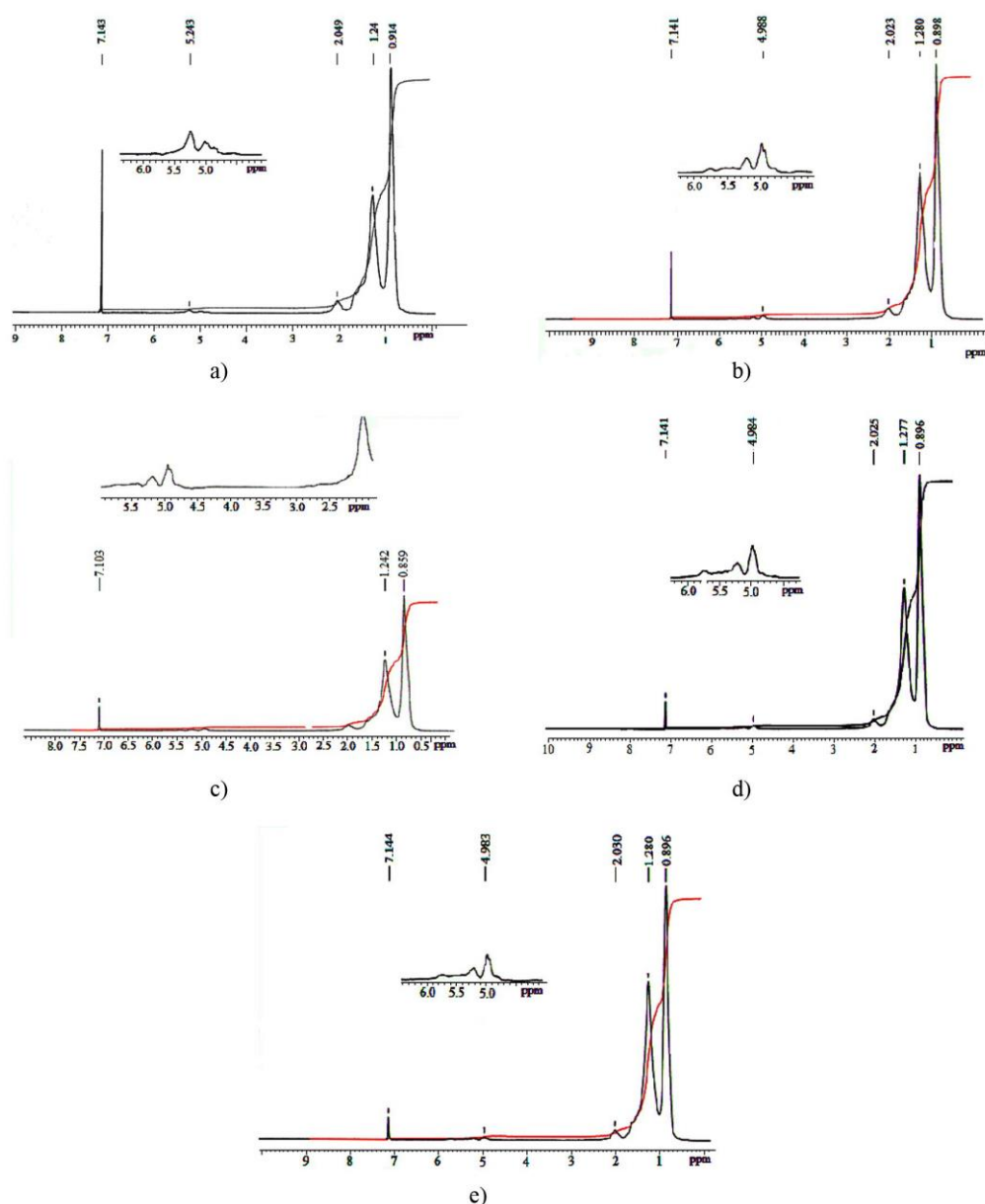**Figure 4.** IR-spectrum of the oil fraction of ethylene oligomerization product.

Figure 5. ^{1}H NMR spectrum of the oil fractions obtained in the presence of MC1 (a) MC1a (b), MC2 (c), MC4 (d) and MC4a (e).

The group distribution of hydrogen atoms in the oil fractions structures are given in the Table 6. As can be seen, the content of hydrogen atoms in the oligomer molecules terminal methyl groups is 43.1 - 46.6 % that indicates to a highly branched structure of the molecule. The percent content of hydrogen atoms in the alkyl - CH_2 - groups and naphthenic CH and CH_2 fragments (H_β) is 42.3 - 46.3 % and 6.5 - 11.0 %, respectively.

The thermal properties of the oil fractions obtained in the presence of unmodified (MC1) and modified (MC1[a]) complex catalytic systems and ethyl aluminium dichloride were determined by DSC analysis and are given in the Figure 6.

Table 6. Distribution of hydrogen atoms in the oil fractions structures

MC	Distribution of H-atoms in fragments, %				
	H_γ	H_β*	H_α	$H_{ol.}$	$H_s.$
MC1	46.6	37.6 (11.0)	3.9	0.9	99.1
MC1[a]	44.6	42.3 (8.7)	3.3	1.1	98.9
MC2	46.5	40.4 (7.9)	3.9	1.3	98.7
MC4	45.5	43.0 (7.4)	3.0	1.1	98.9
MC4[a]	43.1	46.3 (6.5)	3.0	1.1	98.9

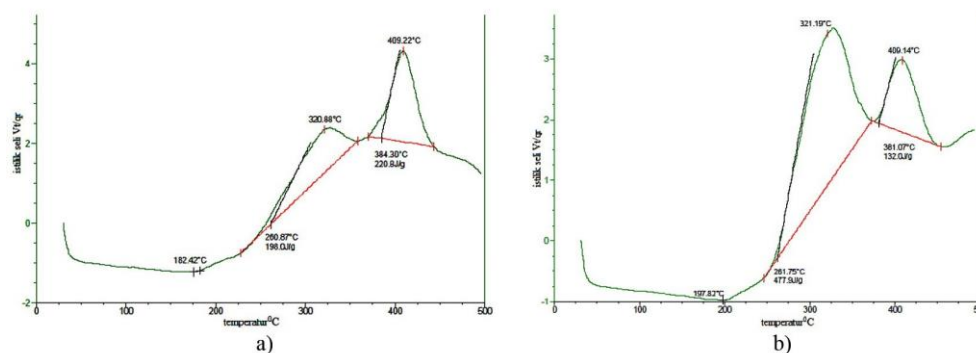[a]The modified catalysts. *The values for naphthenic structures are indicated in brackets

Figure 6. DSC curves of oil fraction obtained in the presence of MC1 and MC1a

As can be seen from the pictures, prior to starting oxidation temperatures 182.42 °C and 200.19 °C, the oils fractions do not expose to any thermal process. Addition of electron donor type modifier as durene to the catalytic system increases starting oxidation temperature of the oil fraction, presumably due to increased linearity of the oligomer molecules chains.

Conclusions

The ethylene oligomerization process was studied using the synthesized zirconium precursor complexes containing ionic liquids type amino and imino hydrochloride ligands and ethylaluminium chlorides as the activators. The structures of the synthesized complexes and oligomer products obtained have been examined by means of IR, ^{1}H NMR spectroscopy, element analysis, SEM, size exclusion chromatography and the DSC. It was shown that the compositions of the ethylene oligomerization products change depending on the aluminium organic and Zr-precursor compounds. The oil fractions obtained in the presence of zirconium complexes and ethyl aluminium dichloride have highly branched molecules, contain naphthenic rings in the molecule structures and are oligoalkylnaphtenic oil character with low viscosity indexes. Adding π-electron donor modifiers to the catalysts systems decreases the branching degree of oligomer chain, improves the viscosity - thermal properties of oil fractions by increasing their viscosity index values.

References

[1]Plaksupov, T. K., Belov, G. P., Potanov, S. S., *Vysshiye lineynye α-olefiny i sopolimery etilena na ikh osnove. Proizvodstvo i primeneniya*, **2008**.

[2]Azizov, A. H., Asadov, Z. G., Akhmedov, G. A., *Makromonomery, Baku, Elm*, **2009**.

[3]Khanmetov A. A., *Processy neftekhimii i neftepererabotki*, **2007**, *4(31)*, 40.

[4]Kotov, S. V., Moiseev, I. K., Shabanova, A. V., *Neftekhimiya*, **2003**, *43*, 5, 323.

[5]Forestière, H., Olivier-Bourbigou and Saussine, L., *Oil Gas Sci. Technol. – Rev. IFP*, **2009**, *64(6)*, 649.

[6]Belov, G. P., *Neftekhimiya*, **2012**, *52, 3*, 163.

[7]Lecocq, V., Olivier-Bourbigon, H., *Oil Gas Sci. Technol.*, **2007**, *62*, 761.

[8]Thiele, D., de Souza, R. F., *Catal. Lett.*, **2010**, 138, 50.

[9]Fehér, Cs., Kriván, E., Eller, Z., Hancsók, J. and Skoda-Földes, R., *The Use of Ionic Liquids in the Oligomerization of Alkenes in: Oligomerization of chemical and biological compounds,* Ed. by Lesieur, C., ISBN 978-953-51-1617-2, INTECH, 2014; DOI: 10.5772/57478

[10]Olivier-Bourbigou, H., Magna L., Morvan D., *Appl. Catal.*, **2010**, **A: General**, *373, 1–2*, 1.

[11]Welton, T., *Coord. Chem. Rev.*, **2004**, *248*, 2459.

[12]Wasserscheid, P., Welton, T., *Ionic liquids in synthesis, 2nd Edition*, Wiley-VCH, **2008**.

[13]Stenzel, O., Brüll, R., Wahner, U. M., Sanderson, R. D. and Raubenheimer, H. R., *J. Mol. Catal.*, **2002A**, *3770*, 1.

[14]Azizov, A. H., Aliyeva R. V., *Am. J. Chem. Appl.*, **2015**, *2(3)*, 21.

[15]Matthias, D. and Helmut G., *Chem. Cat. Chem.*, **2011**, *11(3)*, 1799.

[16]Earle, Martyn J. and Seddon Kenneth R., *Pure Appl. Chem.*, **2000**, *72(7)*, 1391.

[17]Wasserscheid, P., Gordon, C. M., Hilgers, C., Muldoon, M. J., Dunkin, I. R., Chem. Comm., 2001, 13, 1186.

[18]Einloft, S., Dietrich, F. K., de Souza R. F., Dupont, J., *Polyhedron*, **1996**, *19*, 3257.

[19]Khanmetov, A. A., Askerova, Kh. G., Aliyeva, R. V., Azizov, A. H., *Process. Neftekhim. Neftepererab.*, **2010**, *II. 4(44)*, 309.

[20]Thiele, Daniel, de Souza, Roberto Fernando, *J. Mol. Catal., A. Chem.,* **2011**, *340(1)*, 83.

[21]Pei, L- X., Liu, X. M., Gao, H. Y, Wu, Q., *Appl. Organomet. Chem.*, **2009**, *23*, 455.

[22]Ke, M. S., Hai, Y. Q., Feng, S. L., Jin, P. Li, H. G., Shao, B. Z., Qing, W,, *J. Catal. Lett.,* **2009**, *131(3-4)*, 566.

[23]Ochędzan-Siodłak, W., Dziubek, K., Czaja, K., *Polym. Bull.*, **2013**, *70(1)*, 1.

[24]Christian, P., Mehnert, D., *Chem. – Eur. J.*, **2005**, 50.

[25]Azizov, A. G., Alieva, R. V., Martynova, G. S., Bagirova, Sh. R., Kalbalieva, E. S., *Polym. Sci.*, **2009**, *B51(11-12)*, 444.

[26]Azizov, A. G., Aliyeva, R. V., Kalbalieva, E. S., Ibragimova, M. C., *Appl. Catal., A: General,* **2010** *375*, 70.

[27]Azizov, A. H., *Izbrannye trudy, Baku, ELM*, **2010**.

[28]Azizov, A. H., Aliyeva, R. V., Asgerova, K. H., *Green Sustain. Chem.*, **2013**, *3*, 18.

[29]Rasulov, Ch. K., Nabiyev, F. A., Babayeva, R. K., *Process. Neftekhim. Neftepererab.,* **2001**, *2*, 37.

[30]Rustəmov, S. T., Nabiyev, F. A., Azizov, A. H., Rasulov, Ç. Q., *Azərbaycan Kim. J. (in Azeri)*, **2014**, *2*, 36.

[31]Azizov, A. H., Aliyeva, R. V., Bagirova, Sh. R., Mamedova, R. Z., Kalbaliyeva, E. S., Azizbeili, G. R., Khanmetov, A. A., Guliyev, B. V., *Azerbaijan Pat. I 2008 0048* (**2008**).

[32]Bektashi, N. R., Jafarov, V. A., *Polym. Chem.*, **2004**, **A**, *46, 10,* 1769.

[33]Gryunevedzh, M. P., Shuyer, Dzh., Schmidt, Dzh., Gyudman, K. A. F., *Absorbcionnye i relaksacionnye spektry poliolefinov. V sb. Kristallicheskie poliolefiny, M. Khimiya,* **1970**, *2*, 279.

[34]Kamyanov, V.F., Bolshakov, G. F., *Pet. Chem.*, **1984**, *24(4)*, 450.

THORIUM(IV) SORPTION ONTO SODIUM BENTONITE AND MAGNETIC BENTONITE

Abdelkader Miraoui[a] and Mohamed Amine Didi[a]*

Keywords: Bentonite; nanoparticle; isotherm; thorium; magnetic process.

In this paper, the liquid-solid extraction of thorium(IV) by sodium bentonite and magnetic bentonite is reported. Magnetic adsorbent can be quickly separated from a medium by a simple magnetic process. Various parameters have been studied to assess the performance of maghemite nanocomposite clay for the removal of Th(IV). The operating variables studied are initial Th(IV) concentration, pH, ionic strength, temperature and contact time. The time needed for magnetic bentonite to adsorb the maximum of Th(IV) is 45 min and 60 min for sodium bentonite. For magnetic bentonite, optimal extraction yield was achieved at an initial pH equal at 6.2 and for sodium bentonite, the variation of initial pH has no influence on the extraction yield. The sorption capacities of sodium bentonite and magnetic bentonite are 41.24 and 31.34 mg.g^{-1} respectively. Adsorption equilibrium data were calculated for Langmuir and Freundlich isotherms. It was found that the sorption of Th(IV) on sodium and magnetic bentonite was better suited to the Langmuir adsorption model. Thermodynamics data leads to endothermic and spontaneous process for magnetic bentonite and exothermal for sodium bentonite. The quantitative elution study of thorium can be realized with acetic acid for sodium bentonite and sulfuric acid for magnetic bentonite.

* Corresponding Authors
    Fax: +21343213198
E-Mail: madidi13@yahoo.fr
Laboratory of Separation and Purification Technologies,
Department of Chemistry- Faculty of Sciences, Box119.
Tlemcen University -13000, Algeria.

Introduction

Industrial activities generate a wide diversity of wastewaters, often containing agents that cause pollution, which can cause dangerous consequences for human beings by affecting the ecosystems.[1] Due to the high toxicity of radioactive metals, exposure to these pollutants is a problem for human health and contamination of the environment, hence removal of these heavy metals from eco-system is necessary.[2,3] Significant research efforts are currently directed towards removing radioactive ions such as thorium, uranium and other actinides from residual waters.[4] Thorium is abundantly available in earth's crust in association with rare earths and uranium,[5] it is about three times more abundant than uranium.[6] Thorium is only stable at its four valence state in solution.[7] The main sources of thorium are monazite, rutile and thorianite. It occurs in the tetravalent form in its compounds in nature,[8] the major sources of it in nature are plants, sand, soil, rocks and water. Normally, very little amounts of thorium from rivers, oceans, and lakes are accumulated into fish or seafood.[9-11] Since the last century, thorium has been extensively used in a variety of applications in various fields like geology, metallurgy, chemical industry, nuclear industry and medicine.[5,12,13] Thorium oxide finds application as catalyst, high temperature ceramic and high quality lenses.[11]

In view of the extensive use of radioactive elements in various industries, their leakage, even at trace levels, has been a public health problem for many years and causes serious environmental hazards,[1,11,14,15] for example, these elements affect the human health by changes in genetic material of body cell and causing diseases like the lung and liver cancers.[9,15,16]

To safeguard human life, cost-effective removal of thorium from eco-system has received much attention.[17] The most widely used techniques for separation of thorium include liquid-liquid extraction, ion exchange, chemical precipitation, extraction chromatography, membrane dialysis, flotation, electrodeposition and adsorption.[5,10,14] Sorption and ion exchange are the most popular methods for the removal of toxic or radioactive metal ions from aqueous solution. High efficiency, simple operation and environmental compatibility are some of the advantages of sorption process.[14,16] Various types of materials have been used for thorium sorption, for example activated carbon,[18] modified clays,[19] XAD-4 resin,[20] hematite,[21] PAN/Zeolite.[22] However, because of its relatively high cost, there have been attempts to utilize low cost and efficient, locally available materials for the removal of thorium.[23] In recent years, the preparation of organic–inorganic superabsorbent composites has attracted great attention because of their relatively low production cost, high water absorbency and their considerable range of applications in agriculture and horticulture.[24] Recently, clays and clay minerals were found to be very important for preparation of this superabsorbent nanocomposite.[25] In this regard, montmorillonite-rich materials like bentonites exhibit highly interesting properties, e.g. high specific surface area, cation exchange capacity (CEC), porosity, and tendency to retain water or other polar and non-polar compounds.[26] The clay used in this work is bentonite because of its natural abundance and low cost,[24] it is found in many places of the world. Any clay of volcanic origin that contains montmorillonites is referred to as bentonite. Bentonite belongs to the 2:1 clay family, the basic structural unit of which is composed of two tetrahedrally coordinated sheets of silicon ions surrounding a octahedrally coordinated sheet of aluminium ions. Compared with other clay types, bentonite has excellent adsorption properties and possesses adsorption sites available within its interlayer space as well as on the outer surface and edges. Therefore, bentonite has recently been employed in many separation applications with or without modification.[27] Removal by clay is a simple and low cost technology. However, some problems

still exist with regard to the application of clay technique like, unacceptable low adsorption capacity and difficulty in the separation of the resulting solid waste. Magnetic adsorbent can be quickly separated from a medium by a simple magnetic process, in view of this property, we have studied a new strategy toward multifunctional magnetic bentonite material.[28] The objectives of this study are to assess the performance of maghemite nanocomposite clay for the removal of thorium ions. Effects of pH and temperature on the adsorption process are also investigated. used to determine the best isotherm equation which represents the experimental Further studies can explore the possible regeneration of nanocomposite clay for reuse.[31]

Experimental

Reagents

Thorium solution at 10^{-2} M was prepared by dissolving of $Th(NO_3)_4$. 4 H_2O (from FLUKA) (0.552 g) in 100 mL of distilled water. The initial pH of the sample solutions were adjusted by using dilutes HNO_3 or NaOH (from Sigma-Aldrich). $NaNO_3$, sodium acetate and NaS_2O_3 (from Merck) were used in the salt effect. Arsenazo III 10^{-3} M (from Fluka) was prepared by dissolving 0.0820 g in absolute ethanol. Hydrochloric acid (from Organics), sulfuric acid (from Fluka), nitric acid (from Cheminova), and acetic acid (from Riedel Dehaen) were used from elution study.

The natural bentonite used in this study was obtained from deposits in the area of Maghnia, Algeria.

For synthesis of magnetic nanoparticles, $FeCl_2.4H_2O$ (from Sigma-Aldrich), $FeCl_3.6H_2O$ (from Panreac), NH_4OH (from Sigma-Aldrich), HNO_3 and $Fe(NO_3)_2$ (from Sigma-Aldrich) were used.

Apparatus

The extraction of Th(IV) was studied by the batch process using a stirring vibrator (Haier model). pH measurements were performed with a pH meter using a combined electrode mark (Adwa). Thermogravimetric analyses of samples (TGA) were performed using a SDT Q600 thermogravimetric analyzer at a heating rate of 20 °C/min under nitrogen atmosphere, Tlemcen–Algeria. The BET-N_2 method was used to determine the specific surface area of the bleaching earths, using a Volumetric Analyzer (Nova-1000). A magnet and centrifugation for the recovery of the magnetic particles and sodium bentonite, respectively, in the aqueous phase were used. Samples containing Th(IV) were analyzed by spectrophotometer (Analytik Jena Specord 210 Plus, at Tlemcen-Algeria) with Arsenazo III as ligand.

Preparation of sodium bentonite

For the purification of bentonite, 120 g of natural bentonite was dispersed in 1.5 L of distilled water, and after agitation during 15 min, a buffer solution of sodium citrate (pH 7.3) was added. The mixture was heated under agitation at 75° C for 20 min and then, 15 g of sodium thiosulfate ($Na_2S_2O_4$) was slowly added.

After 15 min under agitation, the mixture was cooled and centrifuged at a rotational speed of 6000 rpm for 15 min. The solid recovered was washed two times with HCl 0.05 M (1.5 L) during 3 h.

To convert the purified bentonite into sodium form an amount of bentonite was dispersed in NaCl solution (1 M) with a 1/5 mass ratio and after agitation for 2 h, the solid was separated by centrifugation at a rotational speed of 6000 rpm for 15 min, this operation was repeated three times. The solid was washed three times with distilled water, and it was dried at 40° C for 3 days.
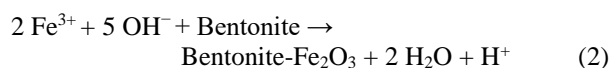
The chemical composition of purified bentonite was found to be 64.7 % SiO_2, 18.1 % Al_2O_3, 0.95 % Fe_2O_3, 2.66 % MgO, 0.8 % K_2O, 0.61 % CaO, 0.2 % TiO_2, 1.43 % Na_2O, 0.05% As, 10.0% loss on ignition. The cation-exchange capacity (CEC) of bentonite was determined according to the ammonium acetate saturation method and was found to be 70 mEq per 100 g of dry natural-Bt and 98 mEq per 100 g of dry Na–Bt. The BET specific surface area increase from 50 m^2 g^{-1} in natural-Bt to 95 m^2 g^{-1} in Na–Bt .[23]

Preparation of magnetic particles

The ferrofluid magnetic used was the maghemite (γ-Fe_2O_3) nanoparticles dispersed in an aqueous solution. Particles were synthesized by co-precipitation of a stoichiometric mixture of ferrous and ferric chloride in an ammonium hydroxide solution. The precipitate magnetite (Fe_3O_4) obtained was acidified by nitric acid (2 M) and oxidized into maghemite (γ -Fe_2O_3) at 90 °C with iron (III) nitrate. The maghemite particles obtained were precipitated by acetone, then dispersed into water leading to an ionic ferrofluid acid (pH=2.0). After these step, nanoparticles were positively charged, with nitrate as counter ions.[29,30]

Preparation of magnetic bentonite

The composites were prepared by dissolving $FeCl_3$ (7.8 g, 28 mmol) and $FeSO_4$ (3.9 g, 14 mmol) in 400 mL of water at 70 °C. 3.3, 6.6 or 9.9 g of clay bentonite was added in order to obtain the following adsorbent: iron oxide weight ratios 1.0:1.0, 1.5:1.0 and 2.0:1.0, respectively. To these suspensions was added a solution of NaOH (100 mL, 5 mol L^{-1}) drop wise to precipitate the iron oxides. The obtained solid materials was washed with distilled water and dried in an oven at 100 °C for 2 h. A simple test with a magnet (0.3 T) of the product showed that the whole material is completely attracted to the magnet.[32] Positive ferrous and ferric ions are co-precipitated on Bentonite due to the reactions between ferrous and ferric ions and silanol groups and aluminol groups of Bentonite.

$$Fe^{2+} + 2\ Fe^{3+} + 8\ OH^- + Bentonite \rightarrow$$
$$Bentonite\text{-}Fe_3O_4 + 4H_2O \quad (1)$$

$$2\ Fe^{3+} + 5\ OH^- + Bentonite \rightarrow$$
$$Bentonite\text{-}Fe_2O_3 + 2\ H_2O + H^+ \quad (2)$$

The BET specific surface area increases from 50 m^2 g^{-1} in sodium-Bt to 72 m^2 g^{-1} in magnetic–Bt.

Extraction and analysis procedure

The method of extraction used for this study, was carried out by a mixture of 4 mL of Th(IV) solution of known concentration, and 0.01 g of ther solid adsorbent (sodium bentonite and magnetic bentonite) in an Erlenmeyer with stopper, under vigorous stirring. Both liquid and solid phases were separated by centrifugation for sodium bentonite and magnet for magnetic bentonite, the solid phase was regenerated for other applications and the liquid phase was measured by the UV-visible spectrometer. The sample of Th(IV) was analyzed by a mixture of 100 µL ArsenazoIII and 100 µL of Th(IV) in a medium of 9 M HCl (2 mL). The product of interaction of Arsenazo III with Th(IV) was determined at λ_{max}= 660 nm.[33]

The percentage of thorium ions that was extracted by solids extractant was determined as by Eqn. 3.

$$E\ (\%) = 100 \frac{C_i - C_e}{C_i} \qquad (3)$$

The amount of thorium uptakes at time t, q_t (mg g^{-1}), was calculated by Eqn. 4.

$$q_t (mg\ g^{-1}) = V * M * \frac{c_i - c_t}{w} \qquad (4)$$

where

C_i, C_t and C_e are the initial, time t and equilibrium Th(IV) concentration (mol L^{-1}), respectively,
V (4 mL) is the volume of the solution,
M molecular weight, and
w is the mass of the solids adsorbents (0.01 g).

Desorption procedure

After saturation of sodium bentonite and magnetic bentonite by the thorium ions, it can be regenerated for another extraction, using the following acids: HCl, HNO$_3$, H$_2$SO$_4$ and CH$_3$COOH. We can determine the best eluting with help of Eqn.5.

$$\text{Elution yield}\ (\%) = 100 \frac{C_{elution}}{C_i - C_e} \qquad (5)$$

where

$C_{elution}$, concentration of Th(IV) (mol L^{-1}) after acid treatment.

Results and Discussion

Effect of contact time

To study this effect we obtained the extraction yields at different time (Fig. 1). It is seen that the extraction efficiency increases rapidly with increasing time. The time needed for magnetic bentonite to adsorb the maximum of Th(IV) is 45 min (58 %, 8.26 mg.g^{-1}) and 60 min for sodium bentonite (89 %, 8.65 mg.g^{-1}). Thus extraction with

magnetic bentonite is more efficient than with sodium bentonite. The thorium does not occupy only the non-occupied spaces by the maghemite.
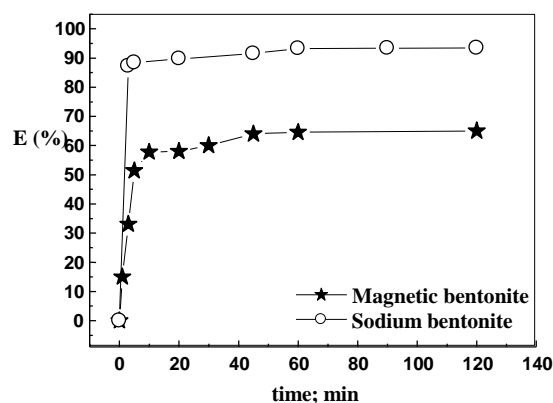

Figure 1. Removal of thorium by magnetic and sodium bentonites as a function of time. [Th(IV)]$_0$ = 1 x 10^{-4} mol L^{-1}, w = 0.01 g, V = 4 mL, Ø = 250 rpm, T= room temperature.

Adsorption kinetics

Kinetics of sorption describing the solute uptake rate, which, in turn, governs the residence time of the sorption reaction, is one of the important characteristics defining the efficiency of sorption.[34] The linear form of the pseudo-first-order rate equation by Lagergren is expressed as Eqn. 5

$$ln(q_e - q_t) = lnq_e - k_1 t \qquad (6)$$

The linear form of the pseudo-second order rate equation is given as,[35]

$$\frac{t}{q_t} = \frac{1}{k_2 q_e^2} + \frac{t}{q_e} \qquad (7)$$

where

q_e and q_t are the amounts of sorbed Th(IV) on magnetic bentonite and sodium bentonite at equilibrium and at time t, respectively (mg g^{-1}),
k_1 is the first-order adsorption rate constant (min^{-1}),
k_2 is the pseudo-second-order adsorption rate constant (g mg^{-1} min^{-1}).

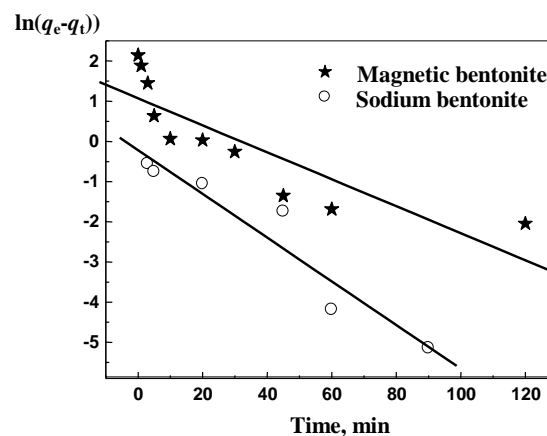**Figure 2.** Pseudo-first order plot of Th(IV) adsorption kinetics onto the magnetic and sodium bentonites as a function. w = 0.01 g, V = 4 mL, Ø = 250 rpm. T= room temperature.
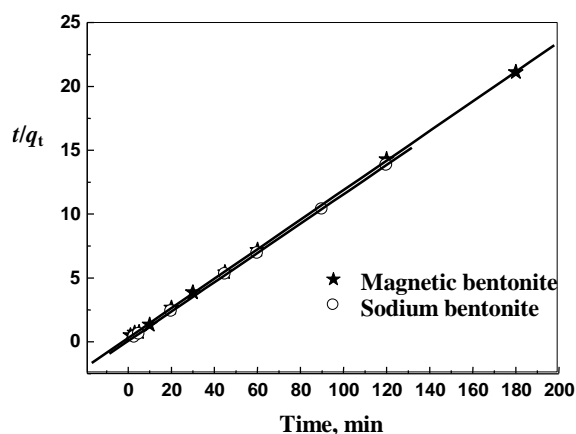
Figure 3. Pseudo-second-order plot of Th(IV) adsorption kinetics onto the magnetic and sodium bentonites as a function. $w = 0.01$ g, $V = 4$ mL, Ø = 250 rpm, T= room temperature.

The correlation coefficients (*r*) for the pseudo-first-order equation and the theoretical q_e values calculated from the pseudo-first-order equation are not in agreement with the experimental data (Table 1), suggesting that this adsorption system is not a pseudo-first-order reaction. High correlation coefficients are obtained when employing the pseudo-second-order model and the calculated equilibrium sorption capacity is similar to the experimental data (Table 1). This indicates that the pseudo-second order model can be applied to predict the adsorption kinetic. Boyd et al. relationship represents an intra-particle diffusion model as follows:[36]

$$\frac{q_t}{q_e} = 1 - \frac{6}{\pi^2} \sum_{n=1}^{ex=1+\frac{x}{1!}+\frac{x^2}{2!}+\frac{x^3}{3!}+\dots,-\infty<x<\infty} \frac{1}{n^2}\exp\left(-\frac{Dn^2\pi^2}{r^2}t\right) \quad (8)$$

where

D is the intra-particle diffusion coefficient and

r is the particle radius.

For short times (when q_t/q_e is less than 0.3), Eqn. 8 can be reduced to Eqn. 9.

$$q_t = k_{ID}\sqrt{t} \quad (9)$$

where

k_{ID} is the intra-particle diffusion constant.

The significant property of this equation is that, if the intra-particle diffusion is the only rate-limiting step, then the linear plot of q_t versus $t^{1/2}$ should pass through the origin. On the other hand, if the intercept of plots do not equal zero, then it indicates that the intra-particle diffusion is not the sole rate determining step.[37] Then Eqn. 9 is modified to,[38]

$$q_t = k_{ID}\sqrt{t} + S \quad (10)$$

where S is a constant and reflects the boundary layer effect.

Investigation of various reports about the sorption rate shows that the intra-particle diffusion model is the most popular one for the diffusion rate-controlling step that has been used in conjunction with the surface reaction models to recognize the adsorption kinetics.

The plot of the Boyd relationship for the sorption of thorium, at initial concentration equal to 0.1 mmol L⁻¹, by sodium bentonite and magnetic bentonite is shown in Figure 4. Therefore, from Figure 4 it follows that the intra-particle diffusion (at the later portion) proceeds faster than the film diffusion (at the beginning portion). Moreover, the second stage of the lines does not pass through the origin. This means that the intra-particle diffusion, although important over longer contact time periods, is not the rate-limiting step in the adsorption process. The intra-particle diffusion constants and regression coefficients for these two stages (k and R^2) are given in Table 2.
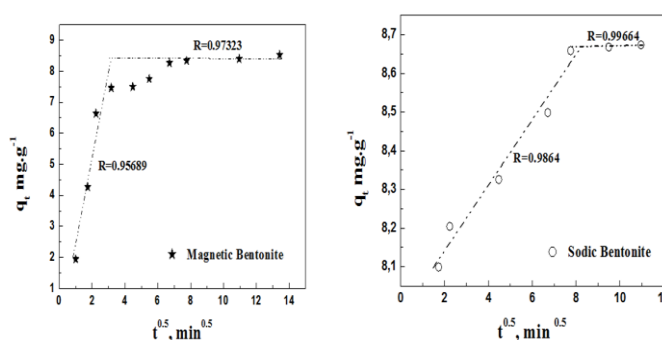

Figure 4: Intra-particle diffusion Kinetic models for the adsorption of Th⁴⁺, [Th(IV)]₀=10⁻⁴ mol L⁻¹, $w = 0.01$ g, $V = 4$ mL, Ø = 250 rpm, T= room temperature.

Table 1. Comparison of the pseudo-first order and pseudo-second order models for the adsorption of thorium.

Adsor-bent	q_e (exp.) mg g⁻¹	Pseudo-first order	Pseudo-second order
Sodium bentonite	8.65	$r = 0.95904$ q_e(calc.)= 0.805 mg g⁻¹ K_1=0.05442	$r = 0.99997$ q_e(calc.)=8.71 mg g⁻¹ K_2=0.2109
Magnetic bentonite	8.26	$r = 0.86008$ q_e(calc.) = 1.076 mg g⁻¹ K_1=0,03356	$r = 0.99991$ q_e(calc.)=8.63 mg g⁻¹ K_2=0.0451

Table 2. Intra-particle diffusion model parameters for thorium adsorption onto sodium bentonite and magnetic bentonite

Adsorbent	Intra-particle diffusion model parameters	
	Stage 1	Stage 2
Sodium bentonite	r =0.9864 K= 0.0835 mg g¹ min⁰·⁵	r =0.99664 K=0.0047 mg.g⁻.min⁰·⁵
Magnetic bentonite	r = 0.95689 K= 2.626 mg g⁻¹ min⁰·⁵	r = 0.97323 K= 0.0346 mg g⁻¹ min⁰·⁵

Diffusion study

The thorium(IV) ions transport from the solution phase to the surface of the sodium bentonite and magnetic bentonite particles occurs in several steps viz., the diffusion of ions from the solution to the sodium bentonite and magnetic bentonite surface, the diffusion of ions within the solid extractant, chemical reactions between ions and functional groups of the bentonites.

If the liquid film diffusion controls the rate of exchange, the Eqn. 11 can be used.

$$-ln(1-F) = kt \qquad (11)$$

where

F is the fractional attainment of equilibrium, which is expressed as $F = q_t/q_e$.

If the case of diffusion of ions in the sodium bentonite and magnetic bentonite phase controlling process, the relation used is Eqn.12.

$$-ln(1-F^2) = kt \qquad (12)$$

In both Eqns. 11 and 12, k is the kinetic coefficient or rate constant. k is defined by Eqn. 13.

$$k = \frac{D_r \pi^2}{r_0^2} \qquad (13)$$

where

D_r is the diffusion coefficient in the sodium bentonite and magnetic bentonite phase and

r is the average radius of sodium and magnetic bentonite.

When the adsorption of metal ion involves mass transfer accompanied by chemical reaction the process can be explained by the moving boundary model. This model assumes a sharp boundary that separates a completely reacted shell from an unreacted core and that advances from the surface toward the center of the solid with the progression of adsorption. In this case, the rate equation is given by Eqn. 14.[34, 35]

$$3 - 3(1-F)^{2/3} - 2F = kt \qquad (14)$$

Testing both mathematical models proposed above (Figure 5), indicates that film diffusion model is adequate for magnetic bentonite, however, adsorption can be explained by both the diffusion models for sodium bentonite.

Table 3. Kinetic and diffusion parameters of thorium onto magnetic bentonite and sodium bentonite.

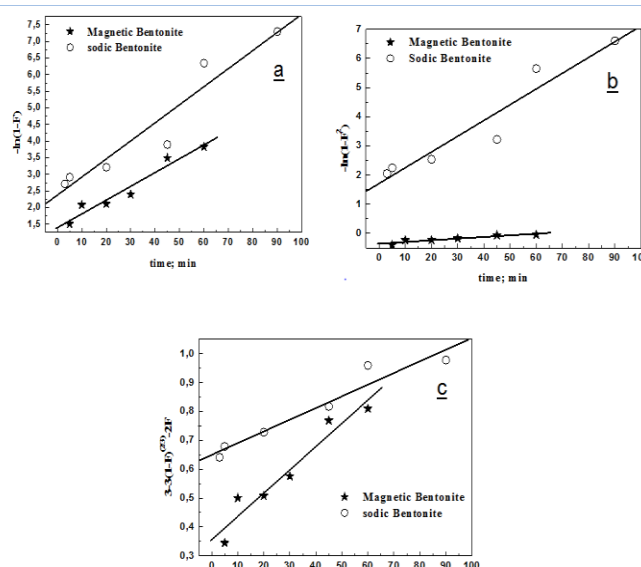| Adsorbent	Film diffusion Eqn. 6	Particle diffusion, Eqn. 7	Chemical reaction, Eqn. 8
Sodium bentonite	$K = 0.0544$ min^{-1} $R = 0.95904$	$K = 0.0540$ min^{-1} $R = 0.95852$	$K = 0.0041$ min^{-1} $R = 0.96773$
Magnetic bentonite	$K = 0.0415$ min^{-1} $R = 0.97369$	$K = 0.0057$ min^{-1} $R = 0.93072$	$K = 0.00805$ min^{-1} $R = 0.96492$

Figure 5. Plots of diffusion study for Th(IV) sorption on Magnetic bentonite and sodium bentonite at different time. [Th(IV)]$_0$=10^{-4} mol L^{-1}, w = 0.01 g, V = 4 mL, Ø = 250 rpm, T= room temperature: Film diffusion (a), internal diffusion (b), chemical reaction (c).

Effect of pH

Sorption of thorium by magnetic bentonite and sodium bentonite were studied at different pH ranging from 1.43 to 9.35 and the results are show in Figure 6. The extraction yield, with magnetic bentonite is very low acidic region and the removal of thorium begins to increase with increase in pH and reaches a maximum value in the pH 6.20, decreasing at higher pH. In pH in the range of 1.4-5.1, hydrogen ions compete strongly with Th(IV) ions for the active sites, which results in less metal sorption. As the hydrogen ion concentration dcreases, thorium(IV) ions sorption increases. At pH is 6.2, a large number of active adsorption sites are released, so there are the maximum Th(IV) sorption efficiency at the pH values 6.2. Beyond pH 6.2, insoluble thorium hydroxide started precipitating, which leads to low Th(IV) ions sorption efficiency.[10] The variation initial pH has no influence on the extraction yield for sodium bentonite, which is between 80 % and 85 %.
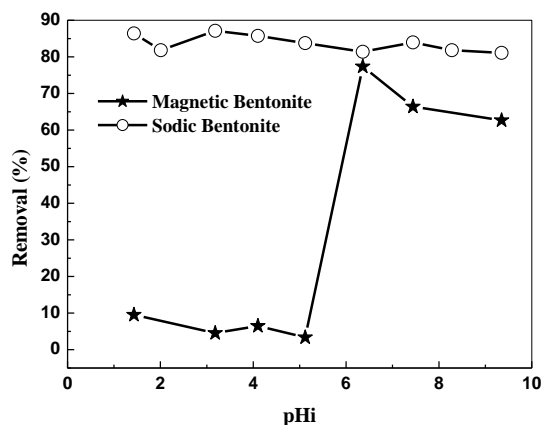
Figure 6. Removal of thorium by magnetic and sodium bentonites as a function of initial pH.

Effect of initial metal concentration

Several experiments were also undertaken to study the effect of varying the initial thorium concentration on uptake (q) from the solution by 0.01 g of the adsorbent. The amount of Th(IV) sorbed per unit mass of the particles magnetic increased with the initial metal concentration.
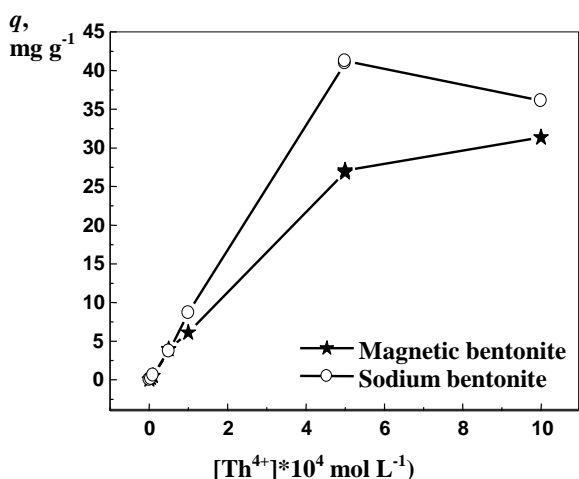

Figure 7. Removal of thorium by magnetic and sodium bentonites as a function of [Th(IV)]. $w = 0.01$ g, $V = 4$ mL, $\emptyset = 250$ rpm, $T=$ room temperature.

Figure 7 show that the maximum sorption capacities for the metal ions were 41.24 mg.g^{-1} (0.177 mmol g^{-1}) for sodium bentonite and 31.34 mg.g^{-1} (0.135 mmol g^{-1}) for magnetic bentonite, this values indicate that sodium bentonite and magnetic bentonite were effectives sorbents in treatment of diluted thorium solutions. This sorption capacity is comparatively higher than those of some other sorbent materials reported in the literature (Table 4).

Isotherm adsorption

The sorption data, commonly known as adsorption isotherms, are basic requirements for the design of adsorption systems. Classical adsorption models, Langmuir (Eqn.15) and Freundlich (Eqn. 16), were used to describe

the equilibrium between adsorbed Th(IV) ions on the sodium and magnetic bentonite site.[35] For the interpretation of both models, we have used the following equations.[47]

$$\frac{C_e}{q_e} = \frac{C_e}{q_m} + \frac{1}{q_m K_L} \qquad (15)$$

$$\ln q_e = \ln K_F + n \ln C_e \qquad (16)$$

where

C_e is the equilibrium concentration of thorium (mg L^{-1}),

q_e is the amount of thorium sorbed on the sodium and magnetic bentonite (mg g^{-1}),

k_L is the Langmuir adsorption constant (L mg),

q_{max} is the maximum amount of thorium that can be sorbed,

k_F is the Freundlich adsorption constant and

n is a constant that indicates the capacity and intensity of the adsorption, respectively.

Table 4. The comparison of adsorption capacity of sodium and magnetic bentonite for thorium with those of various other sorbents reported in the literature.

Adsorbent	Sorption capacity (mmol g^{-1})	Reference
Activated carbon	0.087	[18]
PAN/zeolite	0.04	[22]
Resin (MCM)	0.984	[39]
Amberlite XAD-4	0.25	[20]
SiO$_2$	0.001	[40]
MX-80	0.275	[42]
Amberlite XAD	0.113	[43]
Perlite	0.025	[44]
Modified clay MTTZ	0.116	[19]
Attapulgite	0.067	[45]
Raw diatomite	0.03	[46]
Calcined diatomite	0.06	[7]
Flux calcined diatomite	0.05	[7]
Sodium bentonite	0.177	This work
Magnetic bentonite	0.135	This work

Under the given reaction conditions, experimental data correlate better with Langmuir isotherm (Fig. 8) than with Freundlich isotherm (Fig. 9). From adsorption equilibrium of thorium ions by magnetic bentonite and sodium bentonite, a monolayer adsorption is suggested. The maximum adsorption values were in accordance with the values obtained experimentally (Table 5).

Effect of ionic strength

The effect of NaNO$_3$, CH$_3$COONa, Na$_2$S$_2$O$_3$ on the performance of extraction was studied. Figures 10 and 11 show that the influence of the ionic strength on sorption of thorium is important.
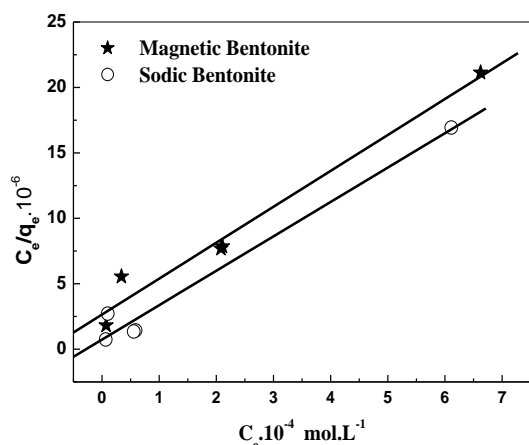
Figure 8. Langmuir isotherm plot for the sorption of Th(IV) onto sodium and magnetic bentonite.
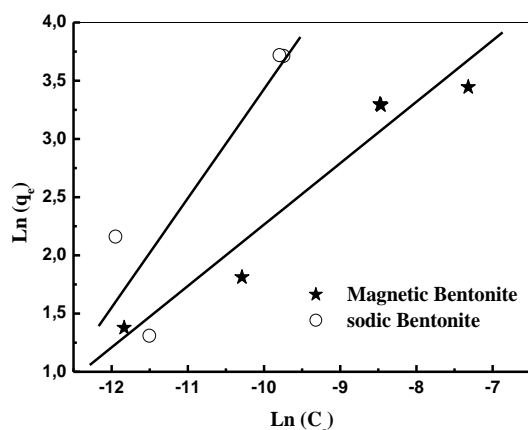

Figure 9. Freundlich isotherm plot for the sorption of Th(IV) onto sodium and magnetic bentonite.

Table 5. Isotherm models parameters for the adsorption of Th(IV) on magnetic bentonite and sodium bentonite

Adsorbent	q_m(exp.)	Langmuir isotherm	Freundlich isotherm
Sodium bentonite	41.24 mg g^{-1}	$r = 0.9883$ q_m(calc.) = 38.03 mg g^{-1} $K_L = 9927.7$	$r = 0.8983$ $K_F = 362217.44$ $n = 0.9380$
Magnetic bentonite	31.34 mg g^{-1}	$r = 0.9863$ q_m(calc.) =36.44 mg g^{-1} $K_L=10362.69$	$r = 0.9663$ $K_F = 1881.83$ $n=0.527$

Changing the ionic strength by the addition of an electrolyte influences adsorption in at least two ways,[48,49] one by affecting interfacial potential and therefore the activity of electrolyte ions and adsorption and secondly by affecting the competition of the electrolyte ions and adsorbing anions for sorption sites.

It is evident in Figure 10 , that there is a positive impact on increasing $Na_2S_2O_3$ concentration from 0.077 M to 0.123 M (100% of removal), the addition of $NaNO_3$ in a concentration less than 0.7 M decreased extraction yield of

Th(IV), this can be explained by a competitiveness in the extraction between Th^{4+} and Na^+,[50] but at concentrations $[NaNO_3] \geq 0.7$ M extraction efficiency increased to 100 % at 0.8 M, , it may due to the common ion effect that lowers the solubility of Th(IV) salt.[51] From 0.1M to 1M, the effect of CH_3COONa is negligible.

Figure 11 show that the extraction yield of Th(IV) increases with the increasing of the $Na_2S_2O_3$ concentration from 0.042 M until it reaches its maximum value of 100% at 0.077 M. The addition of CH_3COOH decreased extraction yield of Th(IV), this effect is attributed to the competition between Na^+ provided by the addition of salt and Th(IV) in the formation of bonds with the active sites of sodium bentonite. The addition of $NaNO_3$ has no influence on the extraction of Th(IV).
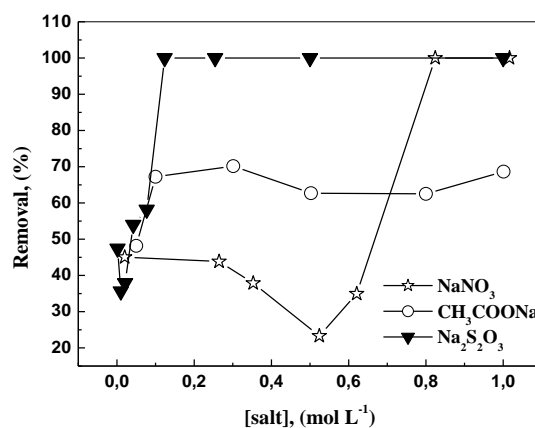

Figure 10. Removal of thorium by magnetic bentonites as a function of electrolytes under standard conditions.
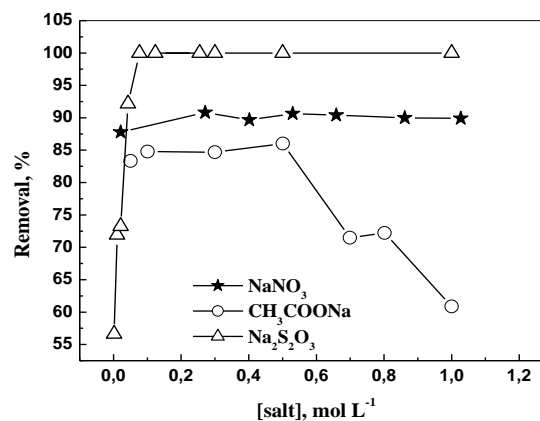

Figure 11. Removal of thorium by sodium bentonite as a function of electrolytes under standard conditions.

TG Analysis and DSC of the modified bentonite

The amount of intercalated product deduced from the TGA experiment for magnetic bentonite was shown in Figure 12.

Concerning the dried sodium bentonite pattern, 1.128 % weight-loss was checked at the temperature range of 59.61-123.15 °C, 1.982 % weight-loss appeared at 472.48–591.97 °C and 1.708 % weight-increase appeared at 873.61-880.48 °C due to the absorption of the nitrogen.

Concerning the dried bentonite magnetic pattern, 6.362 % weight-loss was checked at the temperature range of 39.00-121.43 °C, 1.187 % weight-loss appeared at 171.24-231.34 °C, 1.077 % weight-loss appeared at 301.82-396.74 °C and 1.50 % weight-loss appeared at 567.71-664.01 °C. The low values of weight-loss show a good thermal stability for sodium bentonite and magnetic bentonite.

The difference between the weight-loss of the sodium bentonite and the magnetic bentonite can be explained by the quantity of magnetic particles grafted into the sodium bentonite which corresponds to 8.4 %.

The TGA curve of bentonite shows two marked departures of water, one at low temperature (less than 110°C) corresponding to the hygroscopic water, the second at 470-540 °C corresponding to the loss of structural water. According to literature data,[52] we can attribute the different mass losses for different types of interactions between the water and bentonite. Below 80 °C, adsorbed water is lost. Between 80 and 110 °C, chemisorbed water in the porous structure of bentonite is lost. Water formed from the recombination of the OH groups of the structure is lost between 470 and 540 °C.
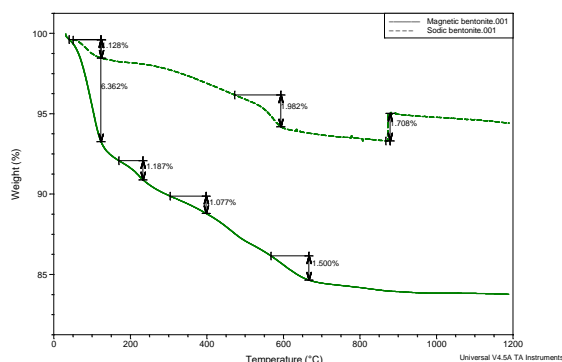

Figure 12. TGA patterns of sodium bentonite and magnetic bentonite.

The comparison between the DSC of the sodium bentonite and the magnetic bentonite (Figure 13) shows that the transition of phases were not any more the same. This is due to the presence of the maghemite in the structure of the bentonite.

Thermodynamic Parameters

The effect of temperature on the sorption of thorium from nitrate solution by sodium bentonite and magnetic benonite at pH 6.2, V=4 mL, w=0.010 g, Ø=250 rpm and concentration Th(IV) 10^{-4} mol L^{-1} was studied for the determination of thermodynamic data such as, the Gibbs free energy change (ΔG), enthalpy change (ΔH) and entropy change (ΔS). ΔG was calculated using the following equations :[53]

$$\Delta G = \Delta H - T\Delta S \qquad (17)$$

$$\Delta G = -RT \ln D \qquad (18)$$

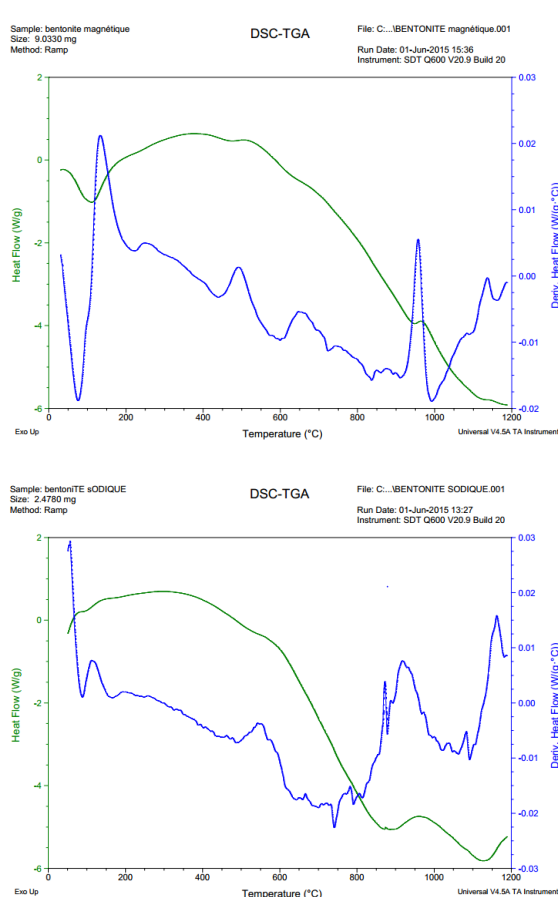**Figure 13.** Differential scanning calorimetry of magnetic bentonite and sodium bentonite

where

R is the gas constant (8.314 J mol^{-1}K^{-1}), and

T the temperature (K).

The relation between D, ΔH and ΔS can be described by Van't Hoff correlation in Eq.19.[54]

$$\ln D = \frac{\Delta S}{R} - \frac{\Delta H}{RT} \qquad (19)$$

Figure 14 shows removal percent (%) of thorium ion onto sodium bentonite and magnetic bentonite as a function of the temperature. It can be seen that the yield extraction of Th(IV) increases with increasing temperature for magnetic bentonite, this behaviour indicates that thorium sorption onto magnetic bentonite is an endothermic and spontaneous process, as supported by the positive values of ΔH and ΔS (Fig. 15 and Table 6); decrease in ΔG values with increase in temperature showed that the sorption was most favourable at higher temperature.

In contrast, increasing temperature from 25 °C to 50 °C was found to have a detrimental effect on the extraction process for sodium bentonite, the negative value of ΔH indicate that the extraction process is exothermal.[50, 35]
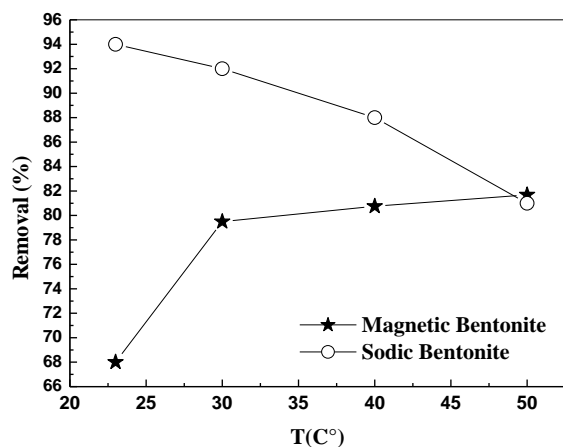
Figure 14. Removal of thorium by magnetic and sodium bentonites as a function of temperature. $[Th(IV)]_0 = 10^{-4}$ mol L^{-1}, $w = 0.01$ g, $V = 4$ mL, $\varnothing = 250$ rpm.
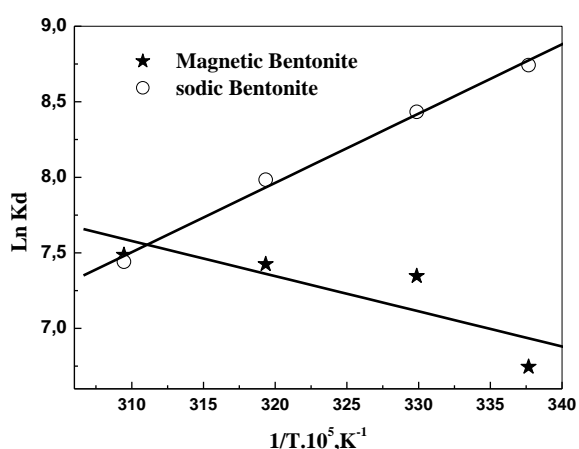

Figure 15. Plot of Eq.6 for the thorium sorption on by magnetic and sodium bentonites.

Table 6. Thermodynamic parameters for the sorption of Th(IV) on sodium and magnetic bentonite.

Material	ΔH (kJ mol^{-1})	ΔS (J mol^{-1} K^{-1})	ΔG (kJ mol^{-1}) at 303 K
Sodium bentonite	-38.1	-55. 8	-21.2
Magnetic bentonite	5.7	79.9	-18.52

Desorption Study

In order to investigate the elution behavior of Th(IV) from the sodium bentonite and magnetic bentonite, elution experiments were conducted with using various eluting agents viz, CH₃COOH, H₂SO₄, HNO₃, and HCl of a concentration of 0.5 mol L^{-1}. Firstly, sodium bentonite and magnetic bentonite are saturated with the solution of thorium and elution yield is calculated by Eqn. 5. To a saturated sample the appropriate bentonite (0.01 g), 4 mL of the selected acid was added and kept for 3 h. Though all the acids gave significant elution yield for sodium bentonite, for magnetic bentonite better yields was obtained with CH₃COOH (78 %) and H₂SO₄ (100 %).
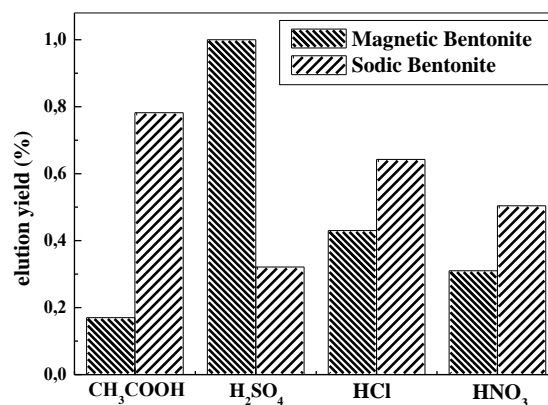

Figure 16. Optimum eluants for quantitative recovery of thorium.

Conclusion

In this investigation, liquid-solid extraction of Th(IV) is made with sodium bentonite and magnetic bentonite. The extraction efficiency was determined as a function of various parameters such as time, initial pH, Thorium concentration, temperature and ionic strength. The experimental capacity obtained was 31.34 mg g^{-1} for magnetic bentonite and 41.24 mg g^{-1} for sodium bentonite. The sorption of Th(IV) achieves equilibration at 45 minutes and 60 minutes for magnetic bentonite and sodium bentonite, respectively. Optimal extraction yield was achieved in a initial pH equal at 6.2 for magnetic bentonite, By against, the variation of initial pH has no influence on the extraction yield. Desorption study of thorium can be effected with acetic acid 0.5 mol L^{-1} and sulfuric acid 0.5 mol L^{-1} for sodium bentonite and magnetic bentonite, respectively after 3 h of shaking.

There is not much difference between the bentonites, but magnetic bentonite have a unique superiority in separation, it can be quickly separated from a medium by a simple magnetic process. In view of the results obtained in this study, magnetic bentonite can be a promising material for sorption, immobilization and pre-concentration of rare earth elements, radioactive metal and heavy metal ions from large volume of solutions.

References

[1]Guerraa, D., Vianab, R., Airoldi, C., *J. Hazard. Mater.,* **2009**, *168*, 1504-1511.

[2]Rahmani-Sani, A., Hosseini-Bandegharaeia, A., Hosseinib, S., Kharghani, K., Zarei, H., Rastegar, A., *J. Hazard. Mater.*, **2015**, *286*, 152-163.

[3]Phillips, D. H., Watson, D. B., *J. Hazard. Mater.,* **2015**, *285*, 474-482.

[4]Hritcua, D., Humelnicub, D., Dodia, G., Popa, M., *Carbohyd. Polym.*, **2012**, *87*, 1185-1191.

[5]Anirudhan, T. S., Sreekumari, S. S., Jalajamony, S., *J. Environ. Radioactiv.,* **2013**, *116*, 141-147.

[6]Huang, H., Ding, S., Su, D., Liu, N., Wang, J., Tan, M., Fei, J., *Sep. Purif. Technol*., **2014**, *138,* 65-70.

[7]Yusan, S., Gok, C., Erenturk, S., Aytas, S., *Appl. Clay Sci.,* **2012**, *67–68*, 106-116.

[8]Anirudhan,T. S., Jalajamony, S., *J. Environ. Sci*., **2013**, *25(4)*, 717-725.

[9]Khajeha, M., Pedersen-Bjergaard, S., Barkhordar, A., Bohlooli, M., *Spectrochim. Acta A*, **2015**, *137*, 328-332.

[10]Yang, S. K., Tan, N., Yan, X, M., Chen, F., Long, W., Lin, Y, C., *Mar. Pollut. Bull*., **2013**, *74*, 213-219.

[11]Nilchi, A., Shariati Dehaghan, T., Rasouli Garmarodi, S., *Desalination*, **2013**, *321*, 67-71.

[12]Chandramouleeswaran, S., Ramkumar, J., *J. Hazard. Mater.*, **2014**, *280*, 514-523.

[13]Metaxasa, M., Kasselouri-Rigopoulou,V., Galiatsatou, P., Konstantopoulou, C., Oikonomou, D., *J. Hazard. Mater. B97*, **2003**, 71-82.

[14]Akkaya, R., *J. Environ. Radioactiv.,* **2013**, *120*, 58-63.

[15]Anirudhan, T., Rijith, S., Tharun, A., *Colloid. Surface A*, **2010**, *368*, 13-22.

[16]Abbasizadeh, S., Reza Keshtkar, A., Mousavian, M., *Chem. Eng. J.*, **2013**, *220*, 161-171.

[17] Bradbury, M. H., Baeyens, B., *Geochim. Cosmochim. Ac.*, **2005**, *69 (4)*, 875-892.

[18]Kütahyalı, C., Eral, M., *J. Nucl. Mater.*, **2010**, *396*, 251-256.

[19]Guerraa, D., Viana, R., Airoldi, C., *J. Hazard. Mater.*, **2009**, *168*, 1504-1511.

[20]Dev, K., Pathak, R., Rao, G., *Talanta*, **1999**, *48*, 579-584.

[21]Murphy, R., Lenhart, J., Honeyman, B., *Colloid. Surface A*, **1999**, *157*, 47-62.

[22]Kilincarslan Kaygun, A., Akyil, S., *J. Hazard. Mater.*, **2007**, *147*, 357-362.

[23]Makhoukhi, B., Djab, M., Didi, M. A., *J. Environ. Chem. Eng.*, **2015**, 3, 1384-1389.

[24]Bulut, Y., Akçay, G., Elma, D., Ersin Serhatli, I., *J. Hazard. Mater.*, 2009, *171*, 717-723.

[25]Wu, L., Ye, Y., Liu, F., Tan, C., Liu, H., Wang, S., Wang, J., Yi, W., Wu, W., *Appl. Clay Sci.*, **2013**, *83–84*, 405-414.

[26]Makhoukhi, B., Didi, M. A., Moulessehoul, H., Azzouz, A., Villemin, D., *Appl. Clay Sci.*, **2010**, *50*, 354-361.

[27]Chen, Y., Zhu, B., Wuc, D., Wangc, Q., Yang, Y., Ye, W., Guo, J*., Chem. Eng. J.,* **2012**, *181–182*, 387-396.

[28]Lian, L., Cao, X., Wua, Y., Sun, D., Lou, D., *Appl. Surf. Sci.,* **2014**, *289*, 245-251.

[29]Idris. A.. Ismail, N., Hassan, N., Misran, E., Ngomsik,A., *J. Ind. Eng. Chem.,* **2012**, *18*, 1582-1589.

[30]Miraoui, A., Didi, M. A., Villemin. D., *J. Radioanal. Nucl. Chem*., **2015**, doi : 10.1007/s10967-015-4267-2. In press.

[31]Panneerselvam, P., Morad, N., Lim, Y., *Sep. Sci. Technol.,* **2013**, *48*, 2670-2680.

[32]Sapag, K., Rios, R. V. R. A., Fabris, J. D., Oliveira, L. C. A., Lago, R. M., *J. Chem. Edu.,* **2004**, *81*, 248-250.

[33]Bayyaria, M. A., Nazal, M .K., Khalili, F, A., *J. Saudi Chem. Society*, **2010**, *14*, 311-315.

[34]Benaissa , E., Abderrahim, O., Didi , M. A., *J. Radioanal. Nucl. Chem.* **2014**, *299*, 439-446.

[35]Ferrah, N., Abderrahim, O., Didi, M. A., Villemin, D., *J. Radioanal. Nucl. Chem*., 2011, *289*, 721-730.

[36]Boyd, G. E., Adamson, A.W., Jr Myers, L, S., *J. Am. Chem. Soc.,* **1947**, *69*, 2836-2848.

[37]Haerifar, M., Azizian, S., *J. Phys. Chem. C*., **2013**, *117*, 8310-8317.

[38]Barkakati, P., Begum, A., Das, M, L., *Chem. Eng. J.*, **2010**, *161*, 34-45.

[39]Ferrah, N., Abderrahim, O., Didi, M. A., Villemin, D., *Desalination*, **2011**, *269*, 17-24.

[40]Raju, Ch. S. K., Subramanian, M. S., *J. Hazard. Mater.*, **2007**, *145*, 315-322.

[41]Chen, C., Wang, X., *Appl. Radiat. Isotopes,* **2007**, *65*, 155-163.

[42]Zhao, D. L., Feng, S. J., Chen, C. L., Chen, S. H., Xu, D., Wang, X. K., *Appl. Clay Sci.*, **2008**, *41*, 17-23.

[43]Seyhan, S., Merdivan, M., Demirel, N., *J. Hazard. Mater.*, **2008**, *152*, 79-84.

[44]Talip, Z., Eral, M., Hicsonmez, U., *J. Environ. Radioactivity,* **2009**, *100*, 139-143.

[45]Chen, L., Gao, X., *Appl. Radiat. Isotopes*, **2009**, *67*, 1-6.

[46]Sheng, G., Hu, J., Wang, X., *Appl. Radiat. Isotopes*, **2008**, *66*, 1313-1320.

[47]Kul, A. R., Koyuncu, H., *J. Hazard. Mater.*, **2010**, *179*, 332-339.

[48]Abderrahim, O., Didi, M. A., Villemin, D., *J. Radioanal. Nucl. Chem*., **2009**, *279 (1)*, 237-244.

[49]Vilar, V. J. P., Botelho C. M. S, Boaventura, R.A.R., *Process Biochem*., **2005**, *40*, 3267-3275.

[50]Didi, M. A., Villemin, D., Abderrahim, O., Azzouz, A., *J. Radioanal. Nucl. Chem.*, **2014**, *299*, 1191-1198.

[51]Abderrahim, O., Didi, M. A., Villemin, D., *Anal. Lett.*, **2009**, *42***,** 1233-1244.

[52]Keller L., Thesis of chemistry. **2004**, Haute Alsace University, p.198.

[53]Kadous, A., Didi, M. A., Villemin, D., *J. Radioanal. Nucl. Chem.*, **2010**, *284*, 431-438.

[54]Zhao, Y., Liu, C., Feng, M., Chen, Z., Li, S., Tian, G., Wang, L., Huang, J., Li, S., *J. Hazard. Mater.,* **2010**, *176(1–3)*, 119-124.

CRYSTAL STRUCTURE OF 2,7-DIMETHOXY-1,8-BIS(1-NAPH-THOYL)NAPHTHALENE: COOPERATIVE HYDROGEN BONDS AND THEIRS ROLE IN THE MOLECULAR PACKING

Akiko Okamoto[a], Takehiro Tsumuki[a], and Noriyuki Yonezawa[a]

The aromatic rings in 2,7-dimethoxy-1,8-bis(1-naphthoyl)naphthalene in crystal accumulate non-coplanarly to each other, with the dihedral angle between the terminal naphthalene and the 2,7-dimethoxynaphthalene rings of closer to 90° than the homologous compounds, 1,8-dibenzoyl-2,7-dimethoxynaphthalene and 2,7-dimethoxy-1,8-bis(2-naphthoyl)naphthalene. Molecular packing structures of the title compound and the homologous two compounds are classified by screw-sense and orientation of molecular assembly with a two-fold screw axis. In the title compound, right(left)-handed 2^1 helical assemblies are oriented in a *downward* (an upward) direction forming a plane. The plane is alternately stacked with the counter handed version. In the homologous compounds, right (left)-handed 2^1 helical assemblies are oriented in an *upward* (a downward) direction to form a plane. In other words, the 2^1 helical assemblies in the molecular packing of the title compound correspond to the 180° rotated one of the homologous compounds as space geometry. In the right(left)-handed 2^1 helical assembly of the title compound, *two types* of effective C–H…O=C hydrogen bonds are observed, i.e., (sp^3)C–H…O=C hydrogen bond and (sp^2)C–H…O=C hydrogen bond. On the other hand, either of two types of C–H…O=C hydrogen bonds is found in a right(left)-handed 2^1 helical assembly of the homologous two compounds. Besides, the title compound has (sp^3)C–H…O=C hydrogen bonds between the right-handed 2^1 helical assembly and the left-handed one, and the homologous two compounds have effective π…π stacking interactions and (sp^2)C–H…O=C hydrogen bonds. Cooperative two types of C–H…O=C hydrogen bonds in right(left)-handed helical assembly induce a *downward* (an upward) orientation of the 2^1 helical assemblies, showing P2₁/c space group. Sole function of either (sp^3)C–H…O=C hydrogen bond or (sp^2)C–H…O=C one in right(left)-handed helical assembly leads the opposite oriented right(left)-handed 2^1 helical assemblies, showing C2/c space group.

Corresponding Author
    Phone: +81-42-388-7601
    E-Mail: aokamoto@cc.tuat.ac.jp
[a]   Department of Organic and Polymer Materials Chemistry, Tokyo University of Agriculture and Technology, 2-24-16 Naka-machi, Koganei, Tokyo 184–8588, Japan

Introduction

Molecular interactions have gained growing interest for one of the property realizing factors as well as concrete covalent chemical bonding in wide-range of chemistry including pharmaceutical chemistry, organic chemistry and material chemistry, e.g., molecular recognition of supramolecular materials, expression of regio- and chemoselectivity in organic reaction.[1] Organic crystals are composed of organic molecules arranged spatially by the molecular interactions such as hydrogen bonds and van der Waals interactions,[2] which are far weaker than covalent bonds. In other words, organic crystals can be regarded as *flexible* solid structure. From this point of view, to employ organic crystal as model or probe for molecular interaction analysis is rational. Organic crystals sometimes show interesting phenomena of polymorphs[3] and phase transition by heat and pressure,[4] and characteristic properties on the basis of the molecular accumulation structures such as light emission and electric properties.[5,6] Understanding the role of non-bonding interactions in/among molecules is one of important aspects of organic crystal chemistry for design of organic crystal showing desirable properties.[7] Miyata and the colleagues have demonstrated an elegant concepts to reveal expression of chirality in organic crystals, a so-called supramolecular-tilt-chirality method, i.e., for the molecules

in front of a two-fold screw axis inclined to the right or left, the assemblies can be defined to be right- or left-handed, respectively.[8,9] They have focused on a series of compounds forming molecular assembly with 2^1 screw axis in the CSD (the Cambridge Structure Database), and analyzed the correlation of the handedness of 2^1 helical assembly and molecular interactions.[10]

Several years ago, the authors have found that electrophilic aromatic substitution reaction of 2,7-dialkoxynaphthalene with benzoyl chloride derivative affords *peri*(1,8)-diaroylated naphthalene compounds with high regioselectivity and conversion.[11] By changing the substituent on the benzoyl chloride, various *peri*-aroylnaphthalene compounds were obtained in reasonable yields, e.g., symmetrically and unsymmetrically substituted *peri*-aroylnaphthalene compounds. Fortunately, *peri*-aroylnaphthalene compounds tend to afford single crystals suitable for X-ray crystallography. The single molecular structure and the structural features of the molecular packing for roughly eighty *peri*-aroylnaphthalene compounds and the homologues have been reported by the authors' group.[12] There are two common features in single molecular structure of *peri*-aroylnaphthalene compounds: 1) two aroyl groups are attached in a nearly perpendicular fashion against the naphthalene rings and 2) two aroyl groups are oriented in opposite direction each other form almost all homologous and analogous aroylnaphthalene compounds. In the crystal packing, non-bonding interactions arising from the chemically modified moieties are distinguishable from those by the original aromatic rings-accumulated framework. Under these circumstances, the authors have attempted to clarify effect of substituents of the benzoyl groups in *peri*-aroylnaphthalene compounds on molecular packing

structure through the systematic comparison of non-bonding interactions.[13-21] Herein, the crystal structure of novel *peri*-aroylnaphthalene compound, 2,7-dimethoxy-1,8-bis(1-naphthoyl)naphthalene (**1**)[22] is reported and the difference in both single crystal structure and crystal packing structure is discussed by comparing with those of the substituent-*free* type homologues, 1,8-dibenzoyl-2,7-dimethoxynaphthalene (**2**)[23] and the regioisomer of 2,7-dimethoxy-1,8-(2-naphthoyl)naphthalene (**3**)[24] to clarify the influence of the modification of the aromatic rings-accumulated framework and the role of molecular interactions in the molecular packing (**Figure 1**).
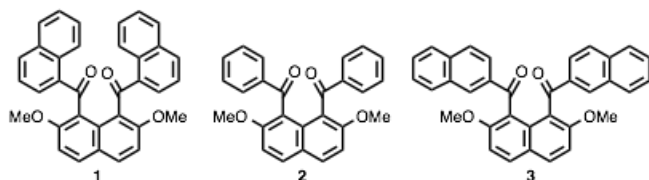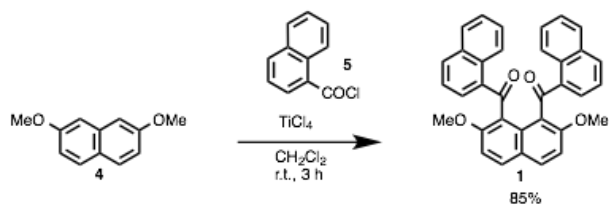

Figure 1 2,7-dimethoxy-1,8-bis(1-naphthoyl)naphthalene (**1**) and the homologues **2** and **3**.

Results and discussion

The title compound (**1**) was synthesized *via* electrophilic aromatic substitution mediated by TiCl₄ of 2,7-dimethoxynaphthalene (**4**) with 1-naphthoyl chloride (**5**) (**Scheme 1**). This reaction proceeded with high efficiency (85% yield). Single crystals suitable for X-ray analysis were obtained by recrystallization from chloroform and methanol.

Scheme 1. Synthesis of 2,7-dimethoxy-1,8-bis(1-naphthoyl)naphthalene (**1**).

Figure 2 gives *ORTEP* representation of the molecular structure of the title compound (**1**), as determined by the structured X-ray analysis.[22] **Table 1** shows the crystallographic data of the title compound (**1**). **Table 2** shows selected bond lengths and angles. **Table 3** gives selected torsion angles. The nonbonding distances are listed in **Table 4**.

In molecular structure of title compound **1**, the two naphthoyl groups are twisted away from the 2,7-dimethoxynaphthalene moiety, and oriented in an opposite direction. Dihedral angles between the naphthalene rings of 1-naphthoyl groups and the 2,7-dimethoxynaphthalene moiety are 89.84° and 85.06° [torsion angles = -77.8(4)° (O1–C11–C1–C9) and -70.64° (O2–C22–C8–C9)]. Furthermore, the terminal naphthalene rings of the 1-naphthoyl moieties make large dihedral angle of 49.12°.
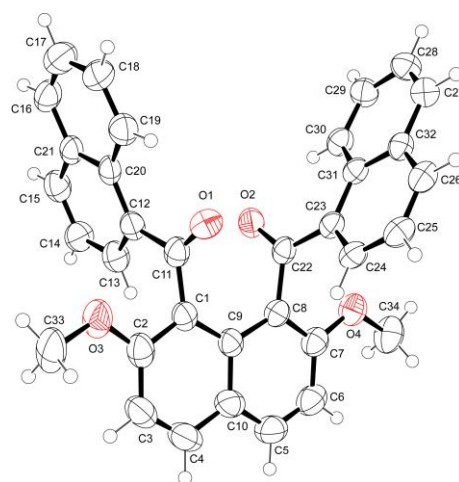

Figure 2 Molecular structure of 2,7-dimethoxy-1,8-bis(1-naphthoyl)naphthalene (**1**), with the atom-labeling scheme and displacement ellipsoids drawn at the 50% probability level.

Table 1. Crystallographic data and structure refinement parameters of title compound

Empirical formula	C₃₄H₂₄O₄
Formula weight	496.53 g mol⁻¹
Crystal shape, colour	Needle, colourless
Temperature	173 K
Wavelength	1.54187 Å
Crystal system	Monoclinic
Space group	*P*21/*c*
Unit cell dimensions	*a* = 19.551 (6) Å
	b = 8.229 (2) Å
	c = 16.529 (5) Å
	α = 90.00°
	β = 111.547(4)°
	γ = 90.00°
Volume	2473.5 (12) Å³
Z	4
Calculated density	1.333 Mg m⁻³
Absorption coefficient	0.09 mm⁻¹
F(000)	1040
Crystal size	0.40 × 0.30 × 0.20 mm
θ range for data collection	2.2 to 26.5°
Limiting indices	-19≤ *h* ≤ 24
	-10≤ *k* ≤10
	-20≤ *l* ≤20
Reflections collected/unique	18194/5120 [*R*ₗₙₜ=0.030]
Completeness to θ=26.5°	99.7%
Max. and min. transmission	0.9829 and 0.9662
Refinement method	Full-matrix least-squares on *F*²
Data/restraints/parameters	5120/0/345
Goodness-of-fit on F^2	1.123
Final *R* indices	R(*F*²) = 0.085,
[*F*² >2☐(*F*²)]	wR(*F*²) = 0.2164
R indices (all data)	R(*F*²)= 0.1016,
	wR (*F*²) = 0.2293
Largest diff. peak and hole	0.63 e Å⁻³ and −0.22 e Å⁻³

Table 2. Selected bond lengths (Å) and angles (°) of molecule **1**.

Bond lengths		Bond angles	
O1–C11	1.2164 (4)	O1–C11–C12	124.1 (3)
C11–C12	1.507 (4)	O1–C11–C1	119.2 (3)
C1–C9	1.5158 (19)	C1–C9–C8	125.1 (3)
C1–C2	1.389 (4)	C2–C1–C11	115.0 (3)
C11–C12	1.507 (4)	C13–C12–C11	118.1 (3)
C12–C13	1.363 (4)	C20–C12–C11	123.7 (3)
C12–C20	1.409 (4)	O2–C22–C23	123.3 (3)
O2–C22	1.223 (3)	O2–C22–C8	118.5 (3)
C22–C24	1.490 (4)	C7–C8–C22	116.1 (3)
C8–C9	1.432 (4)	C24–C23–C22	118.2 (3)
C7–C8	1.380 (4)	C31–C23–C22	122.4 (3)
C22–C23	1.490 (4)		
C23–C24	1.391 (4)		
C23–C31	1.429 (4)		

Table 3. Selected torsion angles (°) of molecule **1**.

| Linkage	Angle
O1–C11–C1–C2	102.8 (3)
O1–C11–C1–C9	−77.8 (4)
O1–C11–C12–C13	163.6 (3)
O1–C11–C12–C20	−14.7 (5)
C1–C11–C12–C13	−17.9 (4)
C1–C11–C12–C20	163.9 (3)
O2–C22–C8–C7	105.6 (3)
O2–C22–C8–C9	−70.6 (4)
O2–C22–C23–C24	152.6 (3)
O2–C22–C23–C31	−24.3 (4)
C8–C22–C23–C24	−27.0 (4)
C8–C22–C23–C31	156.0 (3)
C8–C9–C1–C11	4.1 (5)
C1–C9–C8–C22	−0.1 (4)

Table 4. Nonbonding distances and related geometrical parameters in 2,7-dimethoxy-1,8-bis(1-naphthoyl)naphthalene (**1**).

D–H···A	D–H (Å)	H···A (Å)	D···A (Å)	D–H···A (deg.)
C33–H33A···O2[i]	0.98	2.49	3.390 (5)	152
C34–H34B···O1[ii]	0.98	2.44	3.377 (4)	161
C29–H29···O1[i]	0.95	2.582	3.512 (4)	166
C3–H3···O2[i]	0.95	2.678	3.196	140

Symmetry codes: (i) *x*, *y*-1, *z*; (ii) *x*, −*y*+1/2, *z*-1/2.

Figure 3 and **Figure 4** exhibit X-ray crystal structures of the homologous *peri*-aroylnaphthalene compounds, 1,8-dibenzoyl-2,7-dimethoxynaphthalene (**2**) and 1,8-bis(2-naphthoyl)-2,7-dimethoxynaphthalene (**3**) (For crystallographic data, see Table S-1).[23,24] The molecule of 1,8-dibenzoyl-2,7-dimethoxynaphthalene (**2**) possesses crystallographically imposed twofold C_2 symmetry. Therefore, the asymmetric unit contains one-half of the molecule. Thus, the two benzoyl groups are oriented in an opposite direction. The two benzene rings of the benzoyl groups are situated to the naphthalene ring with dihedral angle of 80.25(6)°, and placed in an almost parallel fashion to each other with dihedral angle of 12.18°. Compound **3**, 1,8-(2-naphthoyl)-2,7-dimethoxynaphthalene, has deep similarities to the benzoyl group-bearing homologue **2** in single molecular structure. The molecule of 1,8-(2-naphthoyl)-2,7-

dimethoxynaphthalene (**3**) lies across a crystallographic two-fold axis. Dihedral angle between the terminal naphthalene ring and 2,7-dimethoxynaphthalene and that between terminal naphthalene rings are 75.13(4)° and 5.21(5)°, respectively.
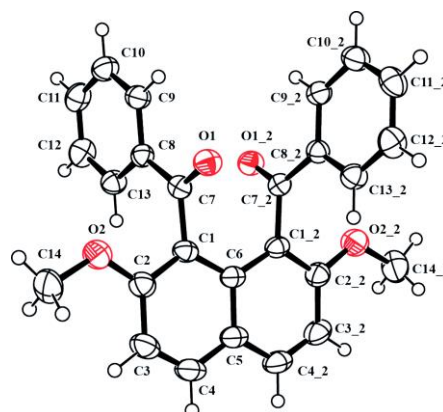
Figure 3. Molecular structure of 1,8-dibenzoyl-2,7-dimethoxynaphthalene (**2**), with the atom-labeling scheme and displacement ellipsoids drawn at the 50% probability level. The symbol "_2" refers to symmetry code: −x, y, −z + 1/2.
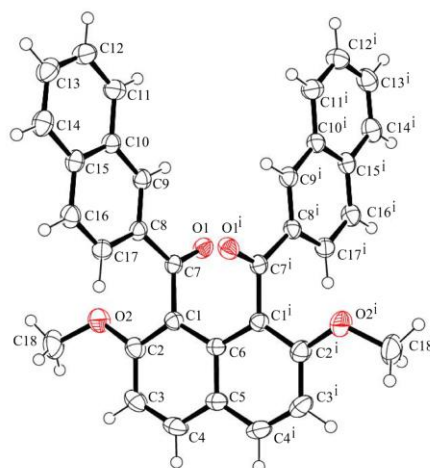
Figure 4 Molecular structure of 2,7-dimethoxy-1,8-bis(2-naphthoyl)naphthalene (**3**), with the atom-labeling scheme and displacement ellipsoids drawn at the 50% probability level. The symbol "i" refers to symmetry code: -x+1, y, -z+1/2.

In title compound **1**, dihedral angle between the terminal naphthalene ring and 2,7-dimethoxynaphthalene moiety is closer to 90° than other two homologues. Furthermore, the dihedral angle between the terminal naphthalene rings is larger than the two homologues, i.e., 49.12° > 12.18° (molecule **2**) > 5.21° (molecule **3**). These results indicate that title compound **1** has large internal steric repulsion.

Figure 5, **Figure 6**, and **Figure 7** show the crystal structure of title compound **1** and the homologues **2** and **3** with symmetry elements. In molecular packing of title compound **1**, the molecules related to two-fold screw axis form two types of helical structures, i.e., right-handed 2^1 helical assembly and left-handed one. Right-handed 2^1 helical assemblies are oriented in a *same* direction, and aligned along *a* axis forming a plane (**Figure 5**, bottom). Left-handed 2^1 helical assemblies are oriented in an opposite direction to the right-handed ones, and aligned along *a* axis.

The plane composed of right-handed 2^1 helical assemblies and that composed of left-handed 2^1 helical assemblies are alternately stacked into stripe structure along *c* axis.
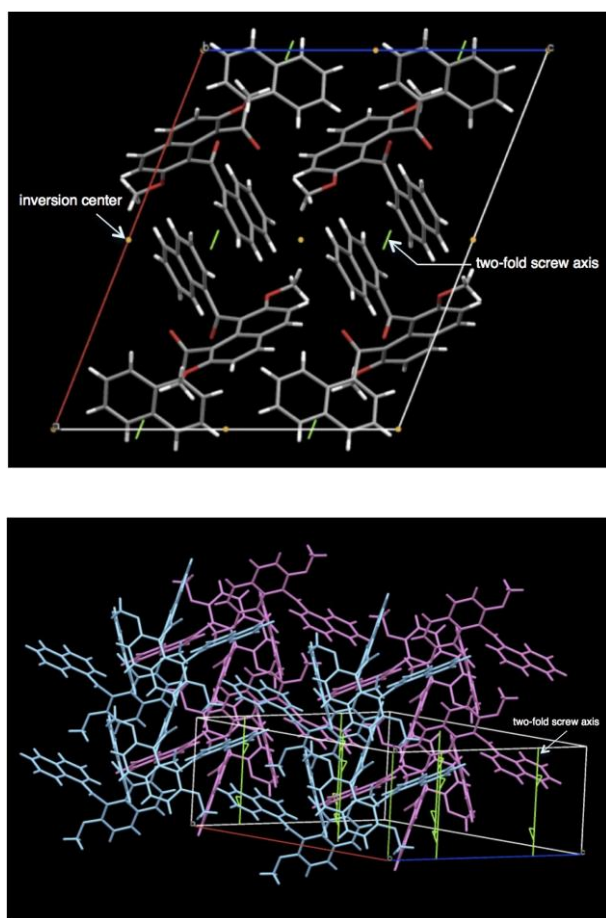

Figure 5. Molecular packing structure of 2,7-dimethoxy-1,8-bis(1-naphthoyl)naphthalene (**1**) with symmetry elements: Molecular packing viewed down *b* axis (top). Colour-coded molecular packing according to screw-sense of 2^1 helical assembly (bottom). Right-handed 2^1 helical assembly and left-handed one are expressed as blue molecules and pink molecules, respectively.
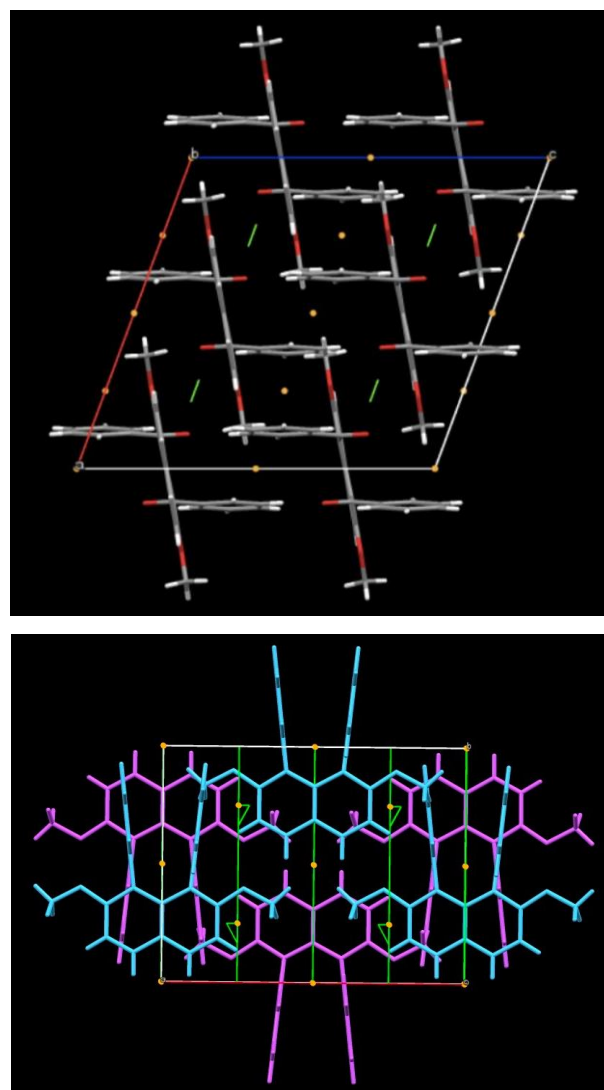

Figure 6. Molecular packing structure of 1,8-dibenzoyl-2,7-dimethoxynaphthalene (**2**) with symmetry elements: Molecular packing viewed down *b* axis (top). Colour-coded molecular packing according to screw-sense of 2^1 helical assembly (bottom).

In the cases of the homologues **2** and **3**, half of the molecules make 2^1 helical assembly. In a similar manner as title compound **1**, there are two types of 2^1 helical assemblies generated by two-fold screw axes.

Right(left)-handed 2^1 helical assemblies are aligned along *a* axis, however they are oriented in an *upward* (a downward) direction (**Figure 6** and **Figure 7**, bottom). The right(left)-handed 2^1 helical assemblies are alternately overlapped with the counter-handed version 2^1 helical assemblies along *c* axis. These features of molecular packing structure in each compound are illustrated as **Figure 8**. The 2^1 helical assemblies in the molecular packing of the title compound **1** correspond to the 180° rotated one of the homologous compounds **2** and **3** as space geometry.

Molecular interactions elucidated on the basis of shorter distance of two atoms less than the sum of the van der Waals radii are observed in right(left)-handed 2^1 helical assembly and between right-handed 2^1 helical assembly and left-handed one (**Figures 9–11**).
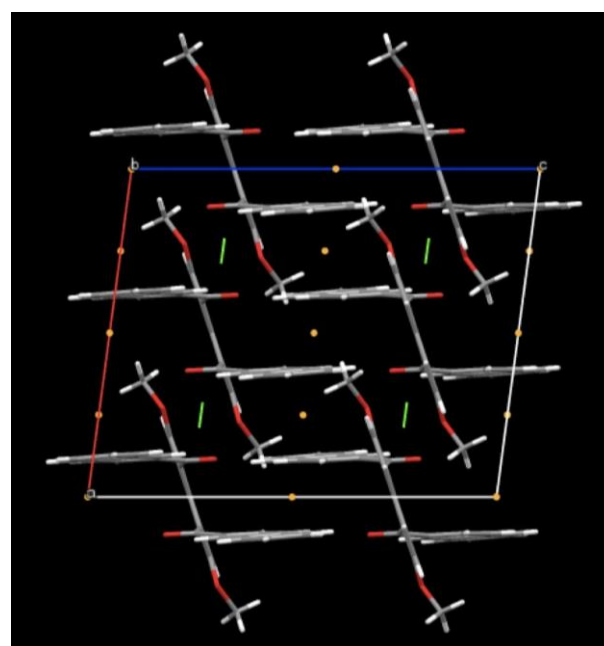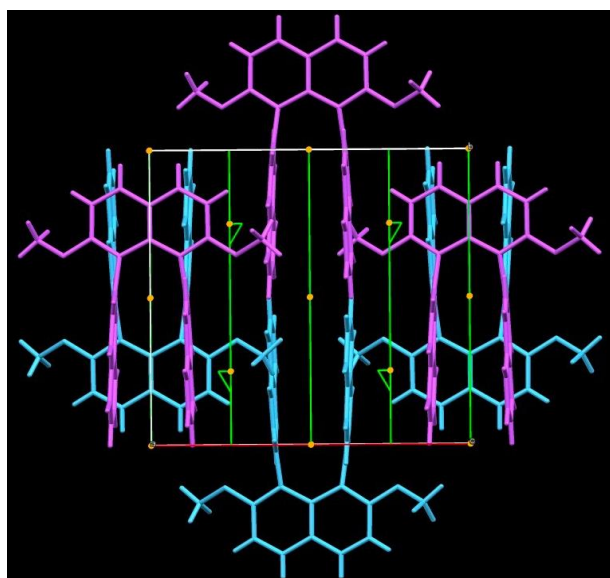
Figure 7. Molecular packing structure of 2,7-dimethoxy-1,8-bis(2-naphthoyl)naphthalene (**3**) with symmetry elements: Molecular packing viewed down *b* axis (top). Colour-coded molecular packing according to screw-sense of 2^1 helical assembly (bottom).
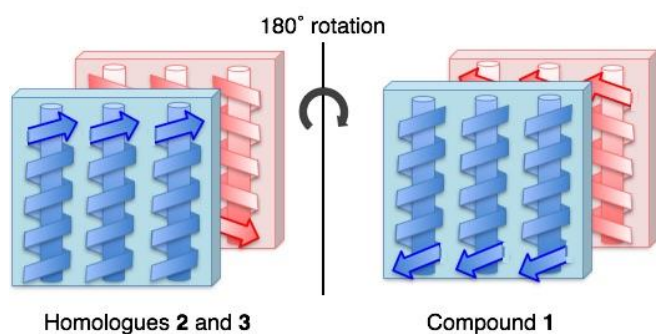

Figure 8 Molecular packing structures of compounds **1**, and homologues **2** and **3** illustrated with 2_1 helical assemblies.

In title compound **1**, two types of C–H…O=C hydrogen bonds, (sp³)C–H…O=C hydrogen bonds [C33–H33A…O2ⁱ = 2.492 Å, symmetry code: (i) *x*, -*y*+1, *z*] and relatively weak two (sp²)C–H…O=C ones [C29–H29…O1ⁱ = 2.582 Å, C3–H3…O2ⁱ = 2.678 Å, symmetry code: (i) x, -1+y, z] are observed in a right(left)-handed 2^1 helical assembly (**Figure 9**, top). In addition, (sp³)C–H…O=C hydrogen bonds [C34—H34B···O1ⁱⁱ = 2.44 Å, symmetry code: (ii) *x*, −*y*+1/2, *z*-1/2] are observed between the right-handed 2^1 helical assembly and the left-handed one (**Figure 9**, bottom). In molecular packing of 1,8-dibenzoyl-2,7-dimethoxynaphthalene (**2**), (sp³)C–H…O=C hydrogen bonds (2.391 Å) are observed in a right(left)-handed 2^1 helical assembly (**Figure10**, top). On the other hand, the right-handed 2^1 helical assembly and the left-handed one are connected through (sp²)C–H…O=C hydrogen bonds (2.597 Å) in opposite direction (**Figure 10**, bottom). In addition, π...π stacking interactions between benzene rings [centroid–centroid and interplanar distances of 3.6383(10) Å and 3.294 Å, respectively] are observed in parallel to the (sp²)C–H…O=C hydrogen bonds (2.597 Å). Molecules of 2,7-dimethoxy-1,8-bis(2-naphthoyl)naphthalene (**3**) form

essentially similar intermolecular interactions to the benzoyl group-bearing homologue (**2**). Hydrogen bonds of (sp²)C–H…O=C (2.590 Å) are observed in a right(left)-handed 2^1 helical assembly (**Figure 11**, top). Hydrogen bonds of (sp²)C–H…O=C (2.491 Å) and π...π stacking interactions between naphthalene rings in 2-naphthoyl groups [centroid–centroid and interplanar distances of 3.6486(8) Å and 3.3734(5) Å, respectively] link the right(left)-handed 2^1 helical assembly and the left(right)-handed one in opposite direction (**Figure 11**, bottom). The above intermolecular interactions are summarized in **Table 5**. In molecular packing of title compound **1**, strong (sp³)C–H…O=C hydrogen bond and weak (sp²)C–H…O=C hydrogen bonds cooperatively stabilize the right(left)-handed 2^1 helical assembly. Hydrogen bond (sp³)C–H…O=C also contributes to connect the right-handed 2^1 helical assembly and the left-handed one. On the other hand, molecular packing of homologues **2** and **3** has either of (sp³)C–H…O=C hydrogen bond or (sp²)C–H…O=C hydrogen bond as the predominant interaction in the right(left)-handed 2^1 helical assembly. Additionally, π...π stacking interaction and (sp²)C–H…O=C hydrogen bond connect with the right-handed 2^1 helical assembly and the left-handed one.
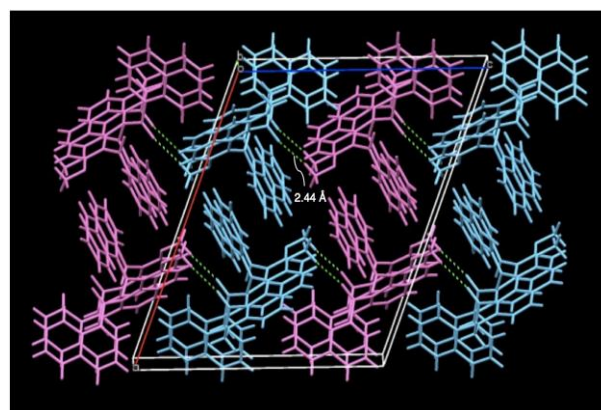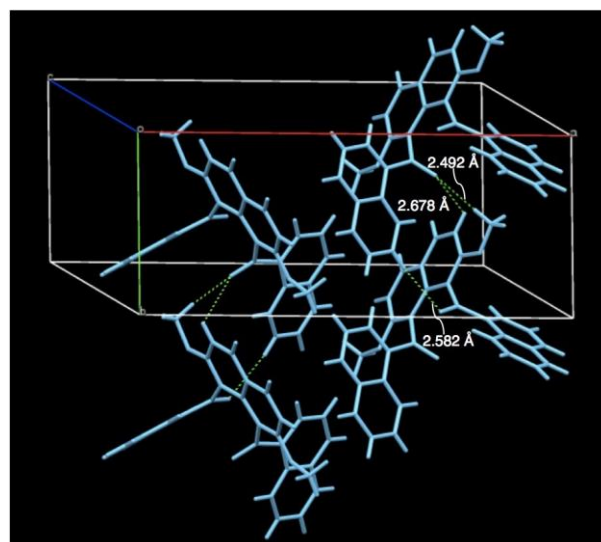

Figure 9. Intermolecular hydrogen bonds in molecular packing structures of 2,7-dimethoxy-1,8-bis(1-naphthoyl)naphthalene (**1**): Molecules are colour-coded according to sense of 2^1 helical assembly. Intermolecular hydrogen bonds in a right-handed 2^1 helical assembly (top) and intermolecular hydrogen bonds between right-handed 2^1 helical assembly and left-handed one (bottom).
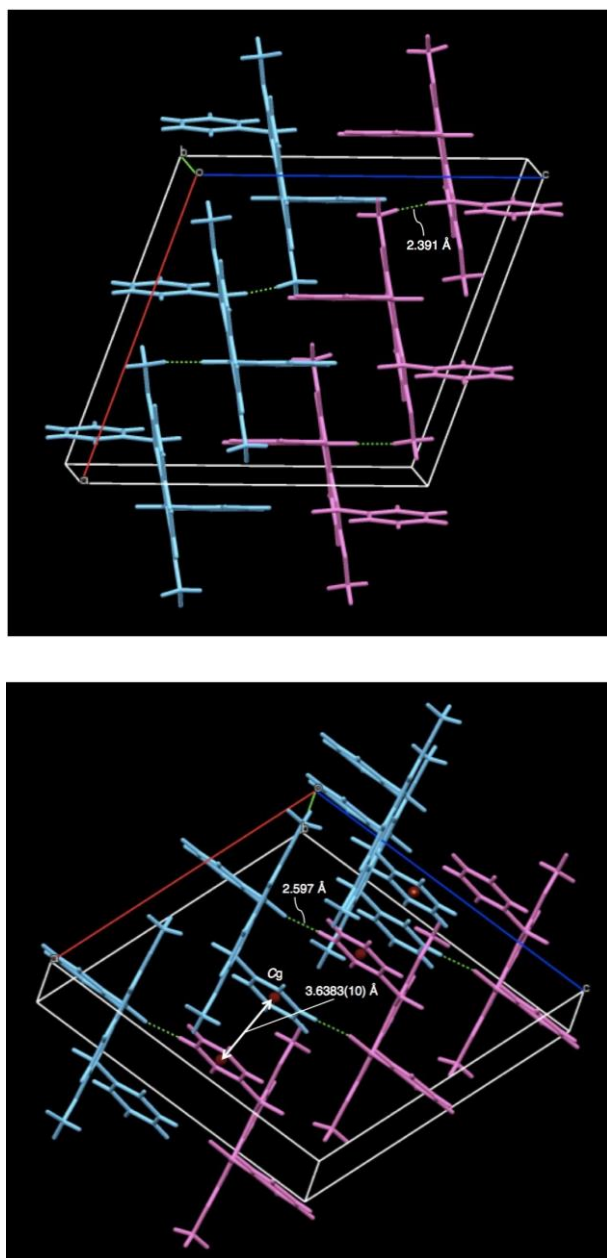
Figure 10. Intermolecular hydrogen bonds in molecular packing structures of 1,8-dibenzoyl-2,7-dimethoxynaphthalene (**2**): Intermolecular hydrogen bonds in a right(left)-handed 2^1 helical assembly (top) and intermolecular hydrogen bonds between right-handed 2^1 helical assembly and left-handed one (bottom). *Cg* is the centroid of the C8–C13 ring.

Either (sp^3)C–H…O=C hydrogen bond or (sp^2)C–H…O=C one in a right(left)-handed 2^1 helical assembly has no contribution to form the planar accumulation of the downward (upward) oriented right(left)-handed 2^1 helical assemblies for homologues **2** and **3**. When two types of C–H…O=C hydrogen bonds cooperatively stabilize a right(left)-handed 2^1 helical assembly, the right(left)-handed 2^1 helical assemblies are oriented in a downward (an upward) direction as 2,7-dimethoxy-1,8-bis(1-naphthoyl)naphthalene (**1**). Formation of (sp^3)C–H…O=C hydrogen bond between the right-handed 2^1 helical assembly and the left-handed one scarcely influence into the "cooperative" C–H…O=C hydrogen bonds in the right(left)-handed 2^1 helical assembly. However, π...π stacking interactions between the right-handed 2^1 helical assembly and the left-handed one apparently mask the C–H…O=C

hydrogen bonds in the right(left)-handed 2^1 helical assembly. In other words, formation of cooperative C–H…O=C hydrogen bonds in the right(left)-handed 2^1 helical assembly determines space group of P2$_1$/c. Sole function of either two types of C–H…O hydrogen bonds in the right(left)-handed 2^1 helical assembly induce space group of C2/c to the molecular packing. In the case of title compound **1**, the internal steric repulsion of the molecule seems to disturb overlapping of 1-naphthoyl rings with the adjacent molecules in the molecular packing. In consequence of this, two types of C–H…O=C hydrogen bonds stabilize the crystal structure of compound **1** in place of π...π stacking interactions.
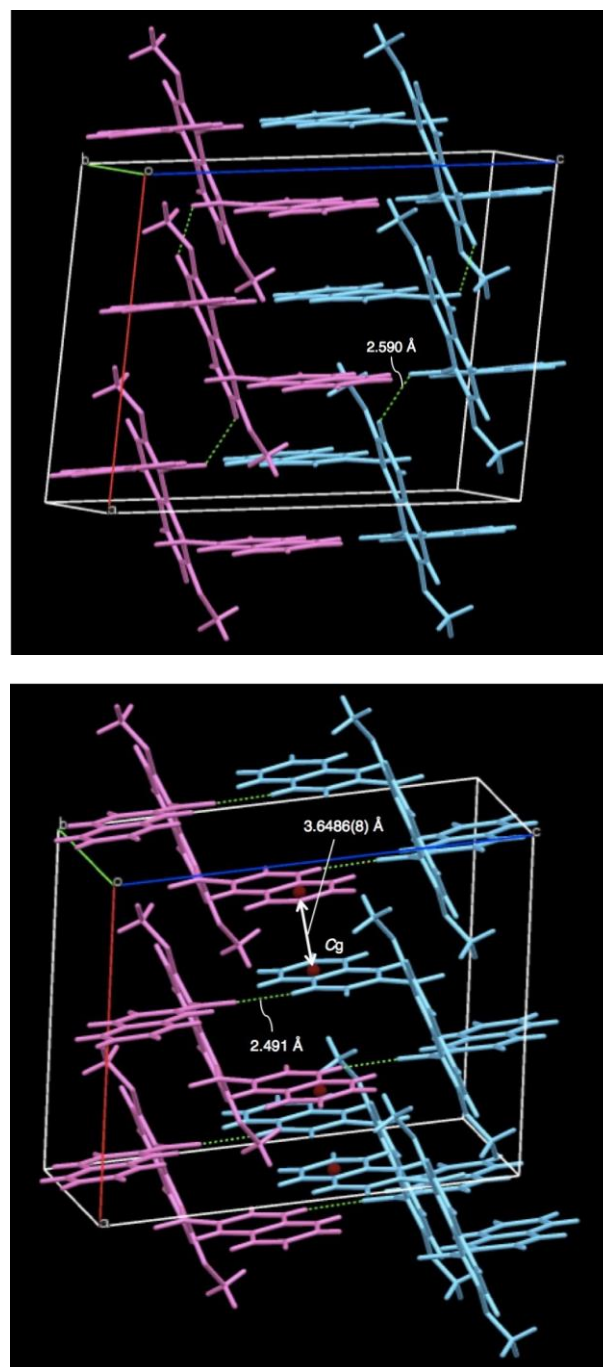

Figure 11 Intermolecular hydrogen bonds in molecular packing structures of 2,7-dimethoxy-1,8-bis(2-naphthoyl)naphthalene (**3**): Intermolecular hydrogen bonds in a right(left)-handed 2^1 helical assembly (top) and intermolecular hydrogen bonds between right-handed 2^1 helical assembly and left-handed one (bottom). *Cg* is the centroid of the C10–C15 ring.

Table 5. Nonbonding distances of 2,7-dimethoxy-1,8-bis(1-naphthoyl)naphthalene (**1**), and the homologues **2** and **3** (Å).

	Compound 1	Compound 2	Compound 3
In right(left)-handed 2^1 helical assembly			
(sp^3)C–H…O=C	2.492	2.391	-
(sp^2)C–H…O=C	2.582, 2.678	-	2.590
Between right-handed 2^1 helical assembly and left-handed 2^1 one			
(sp^3)C–H…O=C	2.44	-	-
(sp^2)C–H…O=C	-	2.597	2.491
π…π *stacking interaction*			
Cg…Cg distance [interplanar distance]	-	3.6383(10) [3.294]	3.6486(8) [3.3734(5)]
Space group	P2$_1$/c	C2/c	C2/c

Experimental

All reagents were of commercial quality and were used as received.[25] Solvents were dried and purified using standard techniques. 2,7-dimethoxynaphthalene (**4**) was prepared according to literatures.[26]

Measurements

^{1}H NMR spectra were recorded on a JEOL JNM-AL300 spectrometer (300 MHz) and a JEOL ECX400 spectrometer (400 MHz). Chemical shifts are expressed in ppm relative to internal standard of Me$_4$Si (δ 0.00). ^{13}C NMR spectra were recorded on a JEOL JNM-AL300 spectrometer (75 MHz). Chemical shifts are expressed in ppm relative to internal standard of CDCl$_3$ (δ 77.0). IR spectra were recorded on a JASCO FT/IR-4100 spectrometer. High-resolution FAB mass spectra were recorded on a JEOL MStation (MS700) ion trap mass spectrometer in positive ion mode.

X-ray crystallography

For the crystal structure determination, the single-crystals of title compound and the homologues were used for data collection on a four-circle Rigaku RAXIS RAPID diffractometer (equipped with a two-dimensional area IP detector). The graphite-mono-chromated Cu Kα radiation (λ = 1.54187 Å) was used for data collection. The lattice parameters were determined by the least-squares methods on the basis of all reflections with $F^2 > 2\sigma(F^2)$. The data collection and cell refinement were performed using *PROCESS-AUTO* software. The data reduction was performed using *CrystalStructure*. The structures were solved by direct methods using *SIR2004* and refined by a full-matrix least-squares procedure using the program *SHELXL97*. All H atoms were found in a difference map and were subsequently refined as riding atoms, with the aromatic C–H = 0.95 Å and methyl C–H = 0.98 Å, and with $U_{iso}(H) = 1.2U_{eq}(C)$.

Synthesis of 2,7-dimethoxy-1,8-bis(1-naphthoyl)naphthalene(1)

To a solution of 2-naphthoyl chloride (**5**, 629.1 mg, 3.3 mmol) and TiCl$_4$ (1802.0 mg, 9.5 mmol) in CH$_2$Cl$_2$ (2.5 mL), 2,7-dimethoxynaphthalene (**4**, 188.2 mg, 1.0 mmol) was

added. The reaction mixture was stirred at rt for 3 h, then poured into ice-cold water (40 mL) and the aqueous layer was extracted with CHCl$_3$ (40 mL × 3). The combined organic extracts were washed with 2 M aqueous NaOH (20 mL × 3) followed by washing with brine (20 mL × 3). The organic layer was dried over anhydrous MgSO$_4$. The solvent was removed under reduced pressure to give a cake. The crude product was washed with chloroform (85 % yield). Furthermore, the isolated product was crystallized from methanol/chloroform (1:1, v/v) solution to give single crystals suitable for X-ray analysis.

2,7-dimethoxy-1,8-bis(1-naphthoyl)naphthalene (1)

Colourless needle (methanol/chloroform); m.p. = 604.0-606.0 K; IR (KBr) : 1665(C=O), 1607(Ar), 1511(Ar), 1264(OMe) cm^{-1}; ^{1}H NMR (300 MHz, CDCl$_3$, 40°C): 3.54 (6H, s), 7.17-7.28 (6H, m), 7.22 (2H, d, *J* = 9.0 Hz), 7.58-8.00 (6H, m), 7.98 (2H, d, *J* = 9.0 Hz), 8.68 (2H, broad) ppm; HRMS (m/z) : [M+H]$^+$ calcd. for C$_{34}$H$_{25}$O$_4$, 497.1753, found, 497.1751.

Synthesis of 1,8-dibenzoyl-2,7-dimethoxynaphthalene (2)

To a mixture of 2,7-dimethoxynaphthalene (0.200 mmol, 37.6 mg) and benzoic acid (0.440 mmol, 174 mg), P$_2$O$_5$–MsOH (0.88 mL) was added by portions at rt. After the reaction mixture was stirred at 60 °C for 3 h, it was poured into iced water (20 mL) and the mixture was extracted with CHCl$_3$ (15 mL × 3). The combined extracts were washed with 2 M aqueous NaOH and followed by sat. NaCl aq. The organic layers thus obtained were dried over anhydrous Na$_2$SO$_4$. The solvent was removed under reduced pressure to give powdery product. Isolation of the title compound was carried out by column chromatography [hexane : AcOEt = 2 : 1 v/v] (1,8-diaroylnaphthalene 63%; 3-aroylated naphthalene 19%; 1-aroylated naphthalene 3%). Colourless single crystals suitable for X-ray diffraction were obtained by recrystallization from ethanol.

1,8-benzoyl-2,7-dimethoxynaphthalene (2)

Colourless needle (EtOH); m.p. = 530 K; IR (KBr): 1665, 1626 cm^{-1}; ^{1}H NMR (400 MHz, CDCl$_3$): 3.68 (6H, s), 7.21 (2H, d, *J* = 9.2 Hz), 7.34 (4H, dd, *J* = 7.6, 7.6 Hz), 7.49 (2H,

t, J = 7.4 Hz), 7.70 (4H, d, J = 7.4 Hz), 7.95 (2H, d, J = 9.2 Hz) ppm; ^{13}C NMR (75 MHz, CDCl$_3$): 56.40, 111.24, 121.47, 125.55, 127.95, 129.09, 129.84, 132.03, 132.64, 138.61, 156.28, 196.875 ppm. The above melting point and spectral data are compatible with the literature.[27]

Synthesis of 2,7-dimethoxy-1,8-bis(2-naphthoyl)naphthalene (3)

To a solution of 2-naphthoyl chloride (629.1 mg, 3.3 mmol) and TiCl$_4$ (1802.0 mg, 9.5 mmol) in CH$_2$Cl$_2$ (2.5 mL), 2,7-dimethoxynaphthalene (188.2 mg, 1.0 mmol) was added. The reaction mixture was stirred at rt for 3 h, then poured into ice-cold water (40 mL) and the aqueous layer was extracted with CHCl$_3$ (30 mL × 3). The combined organic extracts were washed with 2 M aqueous NaOH (20 mL × 3) followed by washing with brine (20 mL × 3). The organic layer was dried over anhydrous MgSO$_4$. The solvent was removed under reduced pressure to give a cake (72% yield). The crude product was purified by recrystallization from acetone (22% isolated yield). Furthermore, the isolated product was crystallized from acetone to give single crystals suitable for X-ray analysis.

2,7-dimethoxy-1,8-bis(2-naphthoyl)naphthalene (3)

Colourless block (acetone); m.p. = 505.0–506.0 K; IR (KBr): 1660(C=O), 1624(Ar), 1510(Ar), 1258(OMe) cm^{-1}; ^{1}H NMR (300 MHz, CDCl$_3$) δ 3.67 (6H, s), 7.26 (2H, d, J = 9.0 Hz), 7.37 (2H, t, J = 7.5 Hz), 7.45 (2H, t, J = 7.5 Hz), 7.68–7.77 (8H, m), 8.03 (2H, d, J = 9.0 Hz), 8.09 (2H, broad) ppm; ^{13}C NMR (75 MHz, CDCl$_3$) δ 56.47, 111.38, 121.73, 124.75, 125.64, 125.92, 127.54, 127.60, 127.83, 129.62, 130.16, 131.11, 132.17, 132.40, 135.50, 136.05, 156.52, 196.66 ppm; HRMS (m/z): [M + H]$^+$ calcd for C$_{34}$H$_{25}$O$_4$, 497.1753; found, 497.1751.

Acknowledgement

References

[1](a) Giese, M., Albrecht, M., Rissanen, K., *Chem. Rev.*, **2015**, *115* (16), 8867–8895. (b) Ueno, A., *Fluorescent Chemosensors for Ion and Molecular Recognition*, Umashankara, Ed.: Czarnik, A. W.; American Chemical Society, **1993**, Vol. 538, pp 74-84. (c) Matlahov, I., Iline-Vul, T., Abayev, M., Lee, E. M. Y., Nadav-Tsubery, M., Keinan-Adamsky, K., Gray, J. J., Goobes, G., *Chem. Mater.*, **2015**, *27* (16), 5562–5569. (d) Feng, L., Fawaz, R., Hovde, S., Gilbert, L., Choi, J., Geiger, J. H., *Biochemistry,* **2015** (ASAP). (e) Haddad, S., Boudriga, S., Porzio, F., Soldera, A., Askri, M., Knorr, M., Rousselin, Y., Kubicki, M. M., Golz, C., Strohmann, C., *J. Org. Chem.,* **2015** (ASAP). (f) Diez-Barra, E., Hoz, A., Merino, S., Sánchez-Verdú, P., *Phase-Transfer Catalysis,* Ed.: Halpern, M. E.; American Chemical Society, **1997**, Vol. 659, pp 181–189. (g) Sonar, M. V., Bansode, N. D., Ganeshlfonso, K. N., *J. Org. Chem.,* **2015** (ASAP).

[2] (a) Politzer, P., Lane, P.; Concha, M. C., Ma, Y.; Murray, J. S., *J. Mol. Model.* **2007**, *13*, 305−311. (b) Legon, A. C., *Phys. Chem. Chem. Phys.* **2010**, *12*, 7736−7747. (c) Metrangolo, P., Resnati, G., *Chem. - Eur. J.,* **2001**, *7*, 2511−2519.

[3](a) Tao, J., Jones, K. J., Yu, L., *Crystal Growth & Design*, **2007**, *7* (12), 2410–2414. (b) Altheimer, B. D., Pagola, S., Zeller, M., Mehta, M. A., *Crystal Growth & Design*, **2013**, *13* (8), 3447–3453. (c) Karanam, M., Dev, S., Choudhury, A. R., *Crystal Growth & Design*, **2012**, *12* (1), 240–252. (d) Kitamura, M., *CrystEngComm*, **2009**, *11,* 949–964. (e) Goud, N. R., Nangia, N., *CrystEngComm*, **2013**,*15,* 7456–7461.

[4](a) Jin, J., Jin, L., Su, E-B., *CrystEngComm*, **2014**,*16*, 9284–9290. (b)Yang, X., Li, Q., Liu, R., Liu, B., Jiang, S., Yang, K., Liu, J., Chen, Z., Zou, B., Cui, T., Liu, B.,*CrystEngComm*, **2014**,*16*, 4441–4446. (c) Nishizawa, N., Furukawa, D., Kobatake, S., Matsumoto, A., *Crystal Growth & Design*, **2010**, *10* (7), 3203–3210.

[5](a) Yadav, H., Sinha, N., Tyagi, N., Kumar, B., *Crystal Growth & Design*, **2015**, (ASAP). (b) Wagner, B. D., McManus, G. J., Moulton, B., Zaworotko, M. J., *Chem. Commun.* **2002**, 2176−2177. (c) Lee, E. Y., Jang, S. Y., Suh, M. P., *J. Am. Chem. Soc.*, **2005**, *127*, 6374−6381.

[6](a) Long, X., Ling, J., Li, X., Wang, Z., Ye, Z-G, *Crystal Growth & Design*, **2009**, *9* (2), 657–659. (b) Chambrier, M-H., Bouhmaida, N., Bonhomme, F., Lebègue, S., Gillet, J-M., Jelsch, C., Ghermani, N. E., *Crystal Growth & Design*, **2011**, *11* (6), 2528–2539.

[7](a) Aakeröy, C. B., Wijethunga, T. K., Desper, J., Đaković, M., *Cryst. Growth Des.*, **2015**, *15* (8), 3853–3861. (b) Kupcewicz, B., Małecka, M., *Cryst. Growth Des.*, **2015**, *15* (8), 3893–3904. (c) Tsuzuki, S., Sato, N., *J. Phys. Chem. B*, **2013**, *117* (22), 6849–6855. (d) Tsuzuki, S., Orita, H., Honda, K., Mikami, M., *J. Phys. Chem. B*, **2010**, *114* (49), 16329–16336. (e) Tsuzuki, S., Hayamizu, K., Seki, S., *J. Phys. Chem. B*, **2010**, *114* (49), 16329–16336.

[8](a) Hisaki, I., Sasaki, T., Tohnai, N., Miyata, M., *Chem. Eur. J.,* **2012**, 18(33), 10066–10073. (b) Tanaka, A., Hisaki, I., Tohnai, N., Miyata, M., *Chem. Asian J.*, **2007**, *2*, 230–238. (c) Hisaki, I., Tohnai, N., Miyata, M., *Chirality,* **2008**, *20*, 330–336. (d) Yuge, T., Sakai, T., Kai, N., Hisaki, I., Miyata, M., Tohnai, N., *Chem. Eur. J.,* **2008**, *14*, 2984–2993.

[9]For reviews, see: (a) Miyata, M., Tohnai, N., Hisaki, I., *Acc. Chem. Res.* **2007**, *40*, 694–702. (b) Miyata, M., Sada, K., *In Compre. Supramol. Chem.,* MacNicol, D. D., Toda, F., Bishop, R., Eds.; Pergamon: Oxford, **1996**, Vol. 6, pp 147-176. (c) Miyata, M., Sada, K., Yoswathananont, N., In *Encyclopedia of Supramolecular Chemistry*; Atwood, J. L., Steed, J. W.; Eds.; Marcel Dekker: New York, **2004;** Vol. 1, pp 441-451.

[10](a) Watabe, T., Kobayashi, K., Hisaki, I., Tohnai, N., Miyata, M., *Bull. Chem. Soc. Jpn.* **2007**, *80*, 464–475. (b) Hisaki, I., Shizuki, Sasaki, T., Ito, Y., Tohnai, N., Miyata., M., *Cryst. Growth Des.,* **2010**, *10*(12), 5262–5269.

[11](a) Okamoto, A., Yonezawa, N., *Chem. Lett.,* **2009**, *38*, 914. (b) Okamoto, A, Mitsui, R., Yonezawa, N., *Chem. Lett.,* **2011**, *40*, 1283.

[12]For review, see: Okamoto, A., Yonezawa, N., *J. Synth. Org. Chem.*, **2015**, 73(4), 339–360. Reported compounds can be find in *Acta Cryst. Sect. C and E.* e.g., (a) Mohri, S., Ohisa, S., Isozaki, K., Yonezawa, N., Okamoto, A., *Acta Cryst, Sect. C (Struct. Chem.)*, **2015**, C71, 344–350. (b) Yoshiwaka, S., Sasagawa, K., Noguchi, K., Yonezawa, N., Okamoto, A., *Acta Cryst, Section C (Struct. Chem.)*, **2015**, C71, 1096–1100. (c) Mohri, S., Ohisa, S, Noguchi, K., Yonezawa, N., Okamoto, A., *Acta Cryst, Sect. E (Res. Comm.)*, **2014**, E70, 138–141. (d) Narushima, S., Mohri, S., Yonezawa, N., Okamoto, A., *Acta Cryst, Sect. E (Res. Comm.)*, **2014**, E70, 170–173. (e) Mohri, S., Ohisa, S, Tsumuki, T., Yonezawa, N., Okamoto, A., *Acta Cryst, Section E (Res. Comm.)*, **2014**, E70, 278–270. (f) Hijikata, D., Sakamoto, R., Isozaki, K., Yonezawa, N., Okamoto, A., *Acta Cryst, Sect. E*, **2013**, E69, o554. (g) Sasagawa, K., Sakamoto, R., Kusakabe, T., Okamoto, A., Yonezawa, N., *Acta Cryst. Sect. E*, **2013**, E69, o146. (h) Isogai, A., Tsumuki, T., Murohashi, S., Okamoto, A., Yonezawa, N., *Acta Cryst, Sect. E*, **2013**, E69, o71.

[13]Okamoto, A., Nagasawa, A., Yonezawa, N., *Eur. Chem. Bull.,* **2014**, *3*(1), 13–17.

[14]Okamoto, A., Nagasawa, A., Yonezawa, N., *Eur. Chem. Bull.,* **2014**, *3*(3), 263–268.

[15]Okamoto, A., Yoshiwaka, S., Mohri, S., Hijikata, D., Yonezawa, N., *Eur. Chem. Bull.,* **2014**, *3*(8), 829–834.

[16]Yoshiwaka, S., Ohisa, S., Yonezawa, N., Okamoto, A., *Eur. Chem. Bull.,* **2014**, *3*(12), 1142–1147.

[17]Okamoto, A., Watanabe, S., Nakaema, K., Yonezawa, N., *Cryst. Struct. Theor. Appl.*, **2012**, *1*(3), 121–127.

[18]Okamoto, A., Nagasawa, A., Siqingaowa, Yonezawa, N., *Cryst. Struct. Theor. Appl.*, **2013**, *2*(4), 139–147.

[19]Okamoto, A.,Ohisa, S., Yoshiwaka, S., Yonezawa, N., *Eur. Chem. Bull.,* **2015**, *4(2)*, 67–73.

[20]Yoshiwaka, S., Hijikata, D., Yonezawa, N., Okamoto, A., *Eur. Chem. Bull.,* **2015**, *4*(4), 202–206.

[21]Yoshiwaka, S., Ogata, K., Yonezawa, N., Okamoto, A., *Eur. Chem. Bull.,* **2015**, *4*(4), 195–201.

[22]CCDC-1418894 contains the supplementary crystallographic data for this paper. These data can be obtained free of charge from The Cambridge Crystallographic Data Centre via www.ccdc.cam.ac.uk/data_request/cif.

[23]Nakaema, K., Watanabe, S., Okamoto, A., Noguchi, K., Yonezawa, N., *Acta Cryst, Section E*, **2008**, *E64*, o807.

[24]Tsumuki. T., Hijikata, D., Okamoto, A., Oike, H., Yonezawa, N., *Acta Cryst., Section E*, **2011**, *E67*, o2095.

[25]Armarego, W. L. F., Perrin, D. D., "Purification *of Laboratory Chemicals",* Fourth edition, Reed Educational and Professional Publishing Ltd, Oxford, **1996**.

[26]Kuwano, R., Morioka, R., Kashiwabara, M., Kameyama, N., *Angew. Chem. Int. Ed.*, **2012**, 51, 4136.

[27]Gorelik, A. M., Reznichenko, A. V., Andronova, N. A., Luk'yanets, E. A., *Zh. Org. Khim.,* **1983**, 19(1), 199–206.

ANGIOTENSIN-CONVERTING ENZYME AND ITS GENE POLYMORPHISM (I/D) IN ESSENTIAL ARTERIAL HYPERTENSION

Mohamed A. Taher,[*a] Ahmed M. Boghdady,[b] Eman A. Sabet,[b] Usama A. Arafa[b] and Ahmed I. Abd Elneam[c,d]

The polymorphisms of ACE gene is investigated using polymerase chain reaction for detection of ACE I/D genotype frequency in hypertensive cases in sector of Egyptian population. Serum ACE is significant higher in hypertensive group than normotensive one (27.5 ± 4.4 and 21.3 ± 5.4 ng mL^{-1}, respectively. Mean SBP (systolic blood pressure), DBP (diastolic blood pressure) and urinary protein excretion in DD genotype were 181 ± 17 mmHg, 112 ± 19 mmHg, 3.8 ± 0.48 mg mL^{-1} and 141.5 ± 36.8 mg day^{-1}, respectively but in II genotype these were 142 ± 10 mmHg, 99 ± 13 mmHg, 4.35 ± 0.4 mg mL^{-1} and 116.4 ± 36 mg day^{-1}, respectively. In hypertensive patients, serum ACE levels in DD, ID and II genotypes were 36.2 ± 5.7, 22.1 ± 3.7 and 24.5 ± 4.9 unit ?, respectively. D/D ACE gene polymorphism plays a role in the development of target organ damage in severe essential hypertension and might have a prognostic value. It can be considered as one of the risk factor of hypertension.

*Corresponding Authors
Tel: 002- 01226388153
E-Mail: abdelmoaty5@yahoo.com
[a] Medical Biochemistry department Sohag Faculty of Medicine, Sohag University Egypt.
[b] Internal Medicine Departments, Sohag Faculty of Medicine, Sohag University Egypt.
[c] Molecular Genetics and Enzymology Department, Human Genetic Division, National research Center, Cairo, Egypt.
[d] Medical Biochemistry, Department Faculty of Medicine Al Dawadme Shaqra University.

Introduction

Angiotensin-converting enzyme (*EC 3.4.15.1 or ACE*) is Zinc-Metallopeptidase.[1] ACE is secreted in the lungs and kidneys by cells in the endothelium (inner layer) of blood vessels.[2] It indirectly increases blood pressure by causing blood vessels to constrict by converting angiotensin I to angiotensin II which constricts the vessels and stimulates aldosterone secretion and inactivating bradykinin which is a potent vasodilator.[3] As It is a part of RAAS (renin angiotensin aldosterone system), it also, converts Aβ42 (which aggregates into plaques) to Aβ40 (which is thought to be less toxic) forms of beta amyloid. So, it may have a role in preventing accumulation of Aβ42 and progression of dementia.[4] For these reasons, ACE is also known by the following names: *dipeptidyl carboxypeptidase I, peptidase P, peptidyl dipeptide hydrolase, endothelial peptidyl dipeptidase, kininase II, carboxycathepsin, hypertensin converting enzyme* and *dipeptide hydrolase*.[5-7]

ACE gene is located at Location: 17q23.3 and is 21-kilo bases (kb) long and comprises 26 exons and 25 introns.[8] I/D polymorphism was leading to the presence (I) or absence (D) of 287-bp sequence of DNA in intron 16 of the ACE gene as an alu repeat sequences.[9] I/D polymorphism of ACE gene is not only limited to tissues but it is also detected in tissue ACE levels.[10] No evidence was found to support linkage between the ACE locus and essential hypertension.[11]

Likewise, another study failed to find a significant association between the I/D polymorphism and blood pressure status in subjects with high or low blood pressure and in their offspring.[12] This lack of association was reported in later studies.[13-17] However, several other studies reported a positive association between the D allele and high blood pressure.[18-20]

Therefore, we carried out this study to determine if this ACE I/D polymorphism is associated with an altered risk of hypertension and its relation to serum ACE in our population.

Patients and methods

Study subject

Sixty-eight normotensive subjects and sixty six hypertensive patients with SBP ≥ 140 mmHg or DBP ≥ 90 mmHg (WHO/ISH 2003)[21] were selected without history or sign of any other cardiac diseases. All subjects and patients were recruited from Internal Medicine outpatient clinic of Sohag faculty of Medicine from June 2015 to August 2015. Complete personal history from each subject and echocardiography for each hypertensive patients was studied to know the severity of aortic valve calcification. 10 ml blood samples were collected on Na$_2$EDTA to detect ACE I/D polymorphism. Another blood sample was taken, centrifuged and stored at -20 ℃ until use. Collected serums were used to assay cholesterol, triglyceride, LDL, HDL, urea and creatinine and ACE. Urinary protein excretion (g day^{-1}) and 24-hour creatinine clearance (mL min^{-1}) were investigated.

The Ethics Committee at Sohag University approved this study protocol and written consents were obtained from all patients.

Serum ACE detection

Serum ACE concentrations were measured using Human ACE Quantikine ELISA Kit from R&D Biotechne. This assay used the quantitative sandwich enzyme immunoassay technique. A monoclonal antibody specific for human ACE is pre-coated onto a microplate. Standards and samples are pipetted into the wells and the immobilized antibody binds any ACE present. After washing away any unbound substances, an enzyme-linked polyclonal antibody specific for human ACE is added to the wells. Following a wash to remove any unbound antibody-enzyme reagent, a substrate solution is added to the wells and yellow color develops in proportion to the amount of ACE bound in the initial step. The color development is stopped and the intensity of the color is measured by using microplate reader at 450 nm.

Molecular studies

DNA extraction

Genomic DNA was purified from whole blood with the QIAamp® DNA BloodMini Kit according to the Blood and Body Fluid Spin Protocol in the accompanying handbook. DNA was eluted in 200 µl elution buffer and stored at −20°C.

Detection of ACE I/D polymorphism

To determine the ACE gene I/D polymorphism, a genomic DNA fragment on intron 16 of the ACE gene was amplified by using Polymerase Chain Reaction (PCR) method with a pair of oligonucleotide primers: The upstream of primer sequence was: 5'-CTG GAG ACC ACT CCC ATC CTT TCT -3' and the downstream was: 5'- GAT GTG GCC ATC ACA TTC GTC AGA T-3'. The PCR amplification products were obtained using 25 µL reaction system containing; 50 ng µL^{-1} genomic DNA, double distilled H_2O 15.7 µL, 10xbuffer 2.5 µL, dNTP (10 mmol L^{-1}) 0.5 µL, each of primer sequences (10 µmol L^{-1}) 0.5 µL, MgCl$_2$ (25 mmol L^{-1}) 2 µL and 1U Taq enzyme on a PTC-200 thermal cycler (MJ Research Company).

After an initial denaturation at 94 °C for 5 min, the DNA was amplified by 35 PCR cycles of denaturation at 94 °C for 1 min, annealing at 56 °C for 1 min and elongation at 72 °C for 1 min, followed by a final elongation at 72 °C for 10 min. PCR products were separated and sized by electrophoresis on a 2 % agarose gel containing ethidium bromide.

Statistical analysis

Data was presented by means ± SD (standard deviation) and percentages.The compiled data were computerized and analyzed by SPSS version 12. The following tests of significance were used: Analysis of variance (ANOVA) test between more than two means, t-test between mean we used analyze mean difference, *t*-test between percentage to analyze percent difference and chi–square. A level of significance with $p \leq 0.001$ was considered highly significant and $p > 0.05$ was considered insignificant.

Results

A total of 66 hypertensive patients and 68 control subjects were included in this study. 55 males and 11 females (M/F ratio=5) were included in hypertension group but normotensive subjects consisted of 42 males and 26 females (M/F ratio = 1.6).

General and clinical characteristics of all the subjects enrolled in this study are shown in table (1). High serum triglyceride, LDL and ACE with low HDL in hypertensive patients than control subjects were observed. In addition, there was significant 24 h proteinuria in hypertension than control group.

Table 1. General and clinical characteristics of normtension and hypertension groups.

Variable	Normotensive subjects (mean ± SD)	Hypertensive patients (mean ± SD)
Age (years)	45 ± 17	42±14
Mean BMI (kg m^{-2})	31.9± 6.4	32.4 ± 9.3
Total cholesterol (g L^{-1})	2.1± 0.46	2.1± 0.48
LDL(g L^{-1})	1.2± 0.2	1.4± 0.3*
HDL (g L^{-1})	0.49± 0.06	0.42± 0.04*
Triglyceride (g L^{-1})	1.74± 0.43	2.10± 0.55*
Urinary protein excretion (mg day^{-1})	88.5± 24.4	122.4± 36.6*
Creatinine clearance (mg day^{-1})	145.3± 15.2	146.8± 18.7
Serum ACE (ng mL^{-1})	21.3± 5.4	27.5± 4.2*

*: Significant change ($p< 0.05$) between normotensive subjects and hypertensive patients

Table 2. Blood pressure, serum lipogram, urinary protein excretion and creatinine clearance in different ACE genotypes:-

Parameter	DD (mean ± SD)	ID (mean ± SD)	II (mean ± SD)
SBP (mmHg)	181± 17	132± 11*	142± 10∞
DBP(mmHg)	112± 19	94± 16*	99± 13∞
Total cholesterol (g L^{-1})	2.06± 0.48	2.1± 0.49	2.1± 0.49
LDL(g L^{-1})	1.36± 0.31	1.36± 0.3	1.42± 0.3
HDL (g L^{-1})	0.38± 0.05	0.43± 0.04*	0.44± 0.04∞
Triglyceride (g L^{-1})	2.13± 0.06	2.09± 0.5	2.08± 0.55
Urinary protein excretion (mg day^{-1})	141.5± 36.8	110.3± 36.1*	116.4± 36∞
Creatinine clearance (mg day^{-1})	149.6± 19.2	145.7± 18.5	145.1± 18.4

LDL: Low-density lipoprotein, HDL; High-density lipoprotein; SBP systolic BP; DBP diastolic BP. *: Significant change ($p< 0.05$) between ACE ID and DD. ∞ : Significant change ($p< 0.05$)between ACE II and DD.

The specific segment of ACE gene was amplified into 190 bp amplicon in case of homozygous DD genotype, 490 bp in case of homozygous II genotype and both in case of heterozygous DI genotype (Fig. 1). In the current study, there were significant association between severe hypertension (SBP≥ 180 or DBP≥110 mmHg) and ACE DD

genotype. Furthermore, there were significant association between low serum HDL, microalbuminuria (30- 300mg/d) and ACE DD genotype (Table 2).

Table 3. Relation between serum ACE and its genotypes in normotensive Subjects and hypertensive patients.

GENATYPES	Serum ACE (ng mL^{-1})	
	Normotensive subjects	Hypertensive patients
DD	21.3± 4.1	36.2± 5.7*
ID	20.4± 4.2	22.1± 3.7©
II	22.2± 4.9	24.5 ± 4.9∞

*: Significant change between serum ACE in ACE DD genotype in hypertensive patients and that in normotensive subjects.

©: Significant change between serum ACE in DD genotype and that ID in hypertensive patients.

∞: Significant change between serum ACE in DD genotype and that II in hypertensive patients.

In the present study, significant high serum ACE levels were associated with ACE DD genotype in hypertension that controls. In addition, serum ACE levels increased in ACE DD genotype than II or ID genotype in hypertensive patients (Table 3).
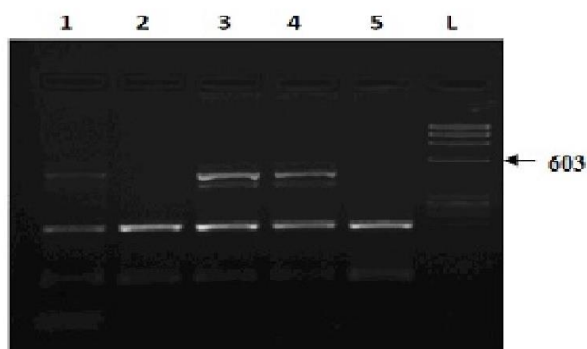

Figure 1. PCR amplification for ACE gene for some patients with ACE polymorphism. Lanes 1, 3 and 4 ACE I/D; Lanes 2 and 5 ACE D/D polymorphism.

Discussion

The renin-angiotensin-aldosterone system (RAAS) is an important system in regulating blood pressure and electrolyte balance. RAAS gene polymorphisms have been extensively studied to determine the genetic susceptibility to hypertension.[1] It also may play an important role in the degree of hypertension.

Accordingly, it was shown that plasma renin activity is an important and independent risk factor for cardiovascular complications in a barge number of patients with essential hypertension.[22] In our results, serum ACE was higher in hypertension than non-hypertensive subjects especially in severe hypertension (SBP $\geq$ 180, or DBP $\geq$ 110) where, it increased about two times than that in non-hypertensive subjects. In addition, there were a positive correlation

between serum ACE and D/D homozygous ACE gene polymorphism. Our results were agree with Ay[23] and Cardoso,[24] who found that DD genotype is associated with higher plasma ACE activity.

An increased plasma and serum ACE level is genetically determined by D/D polymorphism of the ACE gene. The D/D genotype is associated with higher ACE expression and activity and therefore might predispose individuals to hypertension.[20] Several studies of the association between DD genotype and hypertension showed conflicting results. There was no evidence to support linkage between the ACE locus and essential hypertension.[11] Several authors also did not find a significant association between I/D polymorphism and blood pressure status in subjects with high or low blood pressure and in their offspring.[12-17] Agachan,[18] Kario,[19] and Giner,[20] reported a positive association between the D allele and high blood pressure. This study reports that DD genotype and the D allele of the ACE gene are strongly associated with hypertension (specially severe hypertension) compared to healthy individuals, and they confer increased risk of hypertension.

The observed controversies may be due to ethnic and geographic differences. A study comparing Caucasians and Afro-Caribbeans showed that DD polymorphism is associated with essential hypertension in Afro-Caribbean but not in European descent.[25] Turkish population is found to have no significant association between ACE gene polymorphism and hypertension.[26] The ACE D allele is associated with higher serum ACE levels and increased conversion of angiotensin I to angiotensin II in white populations.[18] Previous studies suggest that ethnicity modulates the relationship between the ACE I/D genotype and serum ACE activity. For example, Bloem and colleagues (1996) confirmed the relationship between the number of ACE D alleles and increasing serum ACE activity in whites but found no correlation between the ACE I/D genotype and serum ACE in blacks.[27] In contrast, Forrester and colleagues 1997 reported a relationship between the ACE I/D polymorphism and serum ACE in individuals of African descent, similar to that previously reported in whites.[28]

The increased risk of hypertension with the D/D genotype may be explained by catalysis the conversion of angiotensin-I to the angiotensin II and inactivation of bradykinin, a potent vasodilator.[3] Also, angiotensin is a pro-inflammatory and pro-oxidant, thus causing cellular toxicity and apoptosis and studies have demonstrated that chronic low grade systemic inflammation can predict the future risk of hypertension (2). In the present study, the D/D genotype is not only a risk factor for hypertension but it is also associated with severe grade of hypertension. In addition, D/D genotype is associated with low serum HDL level that can explain its relation to the grade of hypertension. Cardoso reported that D allele might increase the risk of cardiovascular disease by facilitating the development of left ventricular hypertension and low HDL cholesterol, especially among men.[24]

In the present study, the D/D genotype is associated with the present of microalbuminuria in hypertensive patients. Redon and colleagues, 2000 found that the D allele in hypertensive patients poses a higher risk for

microalbuminuria and treatment with ACE inhibitors produces a greater reduction in microalbuminuria in hypertensive patients.[29]

In conclusion increased activity of the ACE (renin-angiotensin- aldosterone system) secondary to its D/D gene polymorphism might play a role in the development of target organ damage in severe essential hypertension and might have a prognostic value.

Although our study sample was relatively small as compared with other epidemiological and association studies, the result of this study supports the hypothesis that the increased activity of the ACE (renin-angiotensin-aldosterone system) secondary to its D/D gene polymorphism might play a role in the development of target organ damage in severe essential hypertension and might have a prognostic value and considered as one of risk factor of hypertension. In addition, ACE polymorphism plays an important role in the pathogenesis of hypertension. However, further studies with larger sample size are necessary to confirm the association of I/D polymorphism of the ACE gene and hypertension. In addition, further investigation is needed to understand the possible role of other polymorphisms of RAAS genes in relation to essential hypertension in Egyptians.

References

[1]Chowdhury, A. H., Zaman, M. M., Haque, K. M., Rouf, M. A., Shah, A. T., Nakayama, T., Yokoyama, T., Yoshiike, N., Tanaka, H., *Med. Res. Counc. Bull*., **1998**, *24(3)*, 55-9.

[2]Pontremoli, R., Ravera, M., Viazzi, F., Nicolella, C., Berruti, V., Leoncini, G., Giacopelli, F., Bezante, GP., Sacchi, G., Ravazzolo, R., Deferrari, G., *Kidney Int.*, **2000**, *57(2)*, 561-9.

[3]Giner, V., Poch, E., Bragulat, E., Oriola, J., González, D., Coca, A., De La Sierra, A., *Hypertension*, **2000**, *35(1 Pt 2)*, 512-7.

[4]Li, X., Li, Y., Jia, N., Guo, S., Chu, S., Niu, W., *Mol Biol Rep.* **2012**, *39(12)*, 10063-75.

[5]Nawaz, S. K., Hasnain, S. J., *Renin Angiotensin Aldosterone Syst*. **2011**, *12(4)*, 516-20

[6]Abd El-Aziz, T. A., Hussein, Y. M., Mohamed, R. H., Shalaby, S. M., *Gene*, **2012**, *498(2)*, 270-5.

[7]Mehri, S., Mahjoub, S., Hammami, S., Zaroui, A., Frih, A., Betbout, F., Mechmeche, R., Hammami, M., *Mol. Biol. Rep*., **2012**, *39(4)*, 4059-65.

[8]Huang, H. D., Lin, F. J., Li, X. J., Wang, L. R., Jiang, G. R., *Chin. Med. J. (Engl).,* **2010**, *123(22)*, 3238-42.

[9]Bawazier, L. A., Sja'bani, M., Haryana, S. M., Soesatyo, M. H., Sadewa, A. H., *Acta Med. Indones.*, **2010**, *42(4)*, 192-8.

[10]Kiss, Z., Ambrus, C., Kulcsár, I., Szegedi, J., Kiss, I. J., *Renin Angiotensin Aldosterone Syst.*, **2014**., Jul 7. pii: 1470320314535276.

[11]Jeunemaitre, X., Lifton, R. P., Hunt, S. C., Williams, R. R., Lalouel, J. M., *Nat. Genet.* **1992**, *1,* 72–75.

[12]Schmidt, S., van Hooft, I. M., Grobbee, D. E., Ganten, D., Ritz, E., *J. Hypertens*. **1993**, *11*, 345–348.

[13]Schunkert, H., Hense, H. W., Holmer, S. R., Stender, M., Perz, S., Keil, U., Lorell, B. H., Riegger, G. A., *New Engl. J. Med.,* **1994**, *330*, 1634 –1638.

[14]Iwai, N., Ohmichi, N., Nakamura, Y., Kinoshita, M. *Circulation*, **1994**, *90*, 2622–2628.

[15]Castellano, M., Glorioso, N., Cusi, D., Sarzani, R., Fabris, B., Opocher, G., Zoccali, C., Golin, R., Veglio, F., Volpe, M., Mantero, F., Fallo, F., Rossi, GP., Barlassina, C., Tizzoni, L., Filigheddu, F., Giacche, M., Rossi, F., *J. Hypertens*., **2003**, *21*, 1853–1860.

[16]Vasku, A., Soucek, M., Znojil, V., Rihacek, I., Tschoplova, S., Strelcova, L., Cidl, K., Blazkova, M., Hajek, D., Holla, L., Vacha, J., *Kidney Int.*, **1998**, *53*, 1479 –1482.

[17]Tiret, L., Blanc, H., Ruidavets, J. B., Arveiler, D., Luc, G., Jeunemaitre, X., Tichet, J., Mallet, C., Poirier, O., Plouin, P. F., Cambien, F., *J Hypertens*., **1998**, 16, 37– 44.

[18]Agachan, B., Isbir, T., Yilmaz, H., Akoglu, E., *Exp. Mol. Med.,* **2003**, *35*, 545–549.

[19]Kario, K., Hoshide, S., Umeda, Y., Sato, Y., Ikeda, U., Nishiuma, S., Matsuo, M., Shimada, K., *Hypertens. Res.,* **1999**, *22*, 95–103.

[20]Giner, V., Poch, E., Bragulat, E., Oriola, J., Gonzalez, D., Coca, A., De, La. Sierra, A., *Hypertension*, **2000**, *35*, 512–517.

[21]WHO (World Healt organization)/ ISH (International Society of Hypertension statement of mangement of hypertension; **2003**).

[22]Pontremoli, R. 1., Sofia, A., Tirotta, A., Ravera, M., Nicolella, C., Viazzi, F., Bezante, G. P., Borgia, L., Bobola, N., Ravazzolo, R., Sacchi, G., Deferrari, G., *J. Am. Soc. Nephrol.*, **1996**, *7(12)*, 2550-8.

[23]Ay, C., Bencur, P., Vormittag, R., Sailer, T., Jungbauer, C., Vukovich, T., Mannhalter, C., Pabinger, I., *Thromb. Haemost*. **2007**, *98(4)*, 777-82.

[24]Cardoso, R. L., Nogueira, A. R., Salis, L. H., Urményi, T. P., Silva, R., Moura-Neto, R. S., Pereira, B. B., Rondinelli, E., Souza, e., Silva, N. A., *Braz. J., Med. Biol. Res.,* **2008**, *41(6)*, 512-8.

[25]Atadzhanov, M., Mwaba, M. H., Mukomena, P. N., Lakhi, S., Mwaba, P., Rayaprolu, S., Meschia, J. F., Ross, O. A., *BMC Res. Notes.*, **2014**, *28*, 7:194.

[26]Gultekin, G. I., Yilmaz, S. G., Kahraman, O. T., Atasoy, H., Dalan, A. B., Attar, R., Buyukoren, A., Ucunoglu, N., Isbir, T., *Asian Pac. J. Cancer Prev.*, **2015**, *16(3)*, 1123-7.

[27]Bloem, L. J., Manatunga, A. K., Pratt, J. H., *Hypertension*, **1996**, *27(1)*, 62-6.

[28]Forrester, T., McFarlane-Anderson, N., Bennett, F. I., Wilks, R., Cooper, R., Rotimi, C., Morrison, L., Ward, R., *Am. J. Hypertens.*, **1997**, *10(5 Pt 1)*, 519-24.

[29]Redon, J., Chaves F. J., Liao Y., Pascual J. M., Rovira, E., Armengod M. E., Cooper, R. S., *Hypertension,* **2000**, *35(1 Pt 2)*, 490-5.